

POLITECNICO DI MILANO

School of Civil, Environmental and Land Management
Engineering

Department of Electronics, Information and Bioengineering

Master of Science in
Environmental and Land Planning Engineering



Effects of Climate Change on Hydrology and Hydropower Systems in the Italian Alps

Supervisor:

PROF. ANDREA CASTELLETTI

Assistant Supervisors:

DR. DANIELA ANGHILERI

PROF. PAOLO BURLANDO

Master Graduation Thesis by:

PIETRO RICHELLI
Student Id n. 799519

Academic Year 2013-2014

*Nunc age, quo pacto pluuius concrecat in altis
nubibus umor et in terras demissus ut imber
decidat, expediam. primum iam semina aquai
multa simul vincam consurgere nubibus ipsis
omnibus ex rebus pariterque ita crescere utrumque
et nubis et aquam, quae cumque in nubibus extat,
ut pariter nobis corpus cum sanguine crescit,
sudor item atque umor qui cumque est denique membris.*

*Now come, and how
the rainy moisture thickens into being
in the lofty clouds, and how upon the lands
'tis then discharged in down-pour of large showers,
I will unfold. And first triumphantly
will I persuade thee that up-rise together,
with clouds themselves, full many seeds of water
from out all things, and that they both increase-
both clouds and water which is in the clouds-
in like proportion, as our frames increase
in like proportion with our blood, as well
as sweat or any moisture in our members.*

— **Lucretius**, *De rerum natura*, 55 B.C.E.
translation by **William Ellery Leonard**

ACKNOWLEDGMENTS

First and foremost, I would like to thank my supervisor, Professor Andrea Castelletti. With his lectures he aroused my interest in water resources management and, with his valuable advices, he constantly encouraged and supported my thesis.

I would sincerely like to thank Daniela Anghileri for her incessant support and commitment to get the most out of this research. Thanks to her I learnt a lot during the last few months.

I would like to express my gratitude to Professor Paolo Burlando, who hosted me in Zurich at ETH, giving me the opportunity to work in an extremely stimulating and exciting environment.

Moreover, I would like to thank the brilliant researches that, with their help, contributed to this work: Matteo Giuliani, Simona Denaro, Yu Li, and the entire research group in Hydrology and Water Resources Management at ETH.

I am also grateful to other master students that shared with me part of the thesis: Alessia, Slaven, and Beatrice.

Besides the scientific aspects of the work, this thesis has been possible also due to the help of a bunch of wonderful classmates. Many thanks go to Mattia, Iris, Davide, Umberto, Daniele, Simone, Rebecca, and Irene.

Academic support is a necessary but not sufficient condition to achieve such a goal. In that sense I would like to thank my family for the unconditional support and encouragement across these years of university. I owe to my father, my mother, and my sister a big slice of this thesis. Moreover, special thanks go to my grandparents, who have always been an example to me.

Finally, I need to thank Maya. Besides her huge effort in correcting and revising the text of the thesis, she stayed always close to me in the past months with understanding, trust, and love.

And now, enjoy reading.

CONTENTS

Abstract	xv
Riassunto	xvii
1 INTRODUCTION	1
1.1 Setting the Context	1
1.2 Objectives of the Thesis	2
1.3 Thesis Structure	3
2 METHODS AND TOOLS	5
2.1 Methodology	5
2.2 Models and Tools	6
2.2.1 Representative Concentration Pathways and IPCC AR5	6
2.2.2 General Circulation Models and Regional Circulation Models	10
2.2.3 The Quantile Mapping Statistical Downscaling Technique	11
2.2.4 Topkapi-ETH	14
3 STUDY SITE	17
3.1 Lake Como Territory	17
3.2 Hydropower Production	17
3.2.1 A2A	17
3.2.2 Enel	22
3.2.3 Edipower	27
3.2.4 Edison	30
3.2.5 Simplifications and Notes	30
4 CLIMATE CHANGE SCENARIOS	33
4.1 The EURO-CORDEX Project	33
4.2 Selected Scenarios	34
4.3 Statistical Analysis of the EURO-CORDEX Scenarios	37
5 STATISTICAL DOWNSCALING	53
5.1 Historical Climate Observations	53
5.2 Statistical Downscaling via Quantile Mapping	53
5.3 Statistical Analysis of the Downscaled Scenarios	54
6 HYDROLOGICAL MODELLING	59
6.1 Topkapi-ETH Setup	59
6.1.1 Digital Elevation Model	59
6.1.2 Soil Map	60
6.1.3 Land Cover Map	60
6.1.4 Glacier Map	60
6.1.5 Thiessen Polygons for Temperature, Precipitation and Cloud Cover Transmissivity	60
6.1.6 Reservoirs	61
6.1.7 Groundwater Depth	61

6.2	Calibration and Validation	66
6.3	Hydrological Scenarios Analysis	69
6.3.1	Experiment Setup	69
6.3.2	Impact of Climate Change on Streamflows	69
6.3.3	Impact of Climate Change on Glaciers	78
6.3.4	Impact of Climate Change on Reservoir Inflows and Levels	81
7	UNCERTAINTY CHARACTERIZATION	87
7.1	“Cascade of Uncertainty” in Climate Change Impact Studies	87
7.1.1	Uncertainty in Radiative Forcing Modelling	90
7.1.2	Uncertainty in Global Climate Modelling	90
7.1.3	Uncertainty in Regional Climate Modelling	91
7.1.4	Uncertainty in Statistical Downscaling	91
7.1.5	Uncertainty in Hydrological Modelling	91
7.1.6	Uncertainty in Water Resources Management	92
7.2	Methods Used in the Literature to Address Uncertainty	92
7.3	Numerical Results	95
8	CONCLUSIONS	107
	Bibliography	111
A	CLIMATE SCENARIOS MASH	119
B	HYDROLOGICAL SCENARIOS MASH	139

LIST OF FIGURES

Figure 2.1	Thesis methodology	7	
Figure 2.2	RCPs IPCC AR5 trajectories	9	
Figure 2.3	GCMs 3D structure	10	
Figure 2.4	RCM of the European domain	11	
Figure 2.5	Bias correction with Quantile Mapping	13	
Figure 2.6	Qq plot for Paris area, minimum temperature		13
Figure 2.7	Topkapi-ETH structure	14	
Figure 3.1	Map of the Lake Como catchment	18	
Figure 3.2	Map of the main reservoirs of the catchment		18
Figure 3.3	A2A hydropower network	19	
Figure 3.4	Cancano reservoir	21	
Figure 3.5	San Giacomo reservoir	21	
Figure 3.6	Enel network in Valmalenco	23	
Figure 3.7	Enel network in Val Gerola	23	
Figure 3.8	Alpe Gera reservoir	24	
Figure 3.9	Campo Moro reservoir	24	
Figure 3.10	Inferno reservoir	25	
Figure 3.11	Pescegallo reservoir	25	
Figure 3.12	Trona reservoir	26	
Figure 3.13	Edipower hydropower network	28	
Figure 3.14	Montespluga reservoir	29	
Figure 3.15	Truzzo reservoir	29	
Figure 3.16	Edison hydropower network, Venina-Armisa link		30
Figure 3.17	Edison hydropower network, Ganda-Belviso link		31
Figure 3.18	Venina reservoir	31	
Figure 3.19	Belviso reservoir	32	
Figure 4.1	EUR-11 resolution over the area of interest		35
Figure 4.2	EUR-44 resolution over the area of interest		35
Figure 4.3	Boxplot climate control period	38	
Figure 4.4	Boxplot climate RCP4.5	39	
Figure 4.5	Boxplot climate RCP8.5	40	
Figure 4.6	Cluster control period	41	
Figure 4.7	Cluster RCP4.5 scenario	42	
Figure 4.8	Cluster RCP8.5 scenario	42	
Figure 4.9	RCA4/NCC temperature	44	
Figure 4.10	RCA4/NCC precipitation	45	
Figure 4.11	RCA4/NCC RR30	46	
Figure 4.12	REMO/MPI temperature	48	
Figure 4.13	REMO/MPI precipitation	49	
Figure 4.14	RACMO/ICHEC temperature	50	
Figure 4.15	RACMO/ICHEC precipitation	51	

Figure 5.1	Historical observation map	54	
Figure 5.2	Chiavenna temperature quantile-quantile plot		55
Figure 5.3	RCP4.5 downscaled scenarios	56	
Figure 5.4	RCP8.5 downscaled scenarios	56	
Figure 5.5	Temperature downscaled scenarios		57
Figure 5.6	Precipitation downscaled scenarios		58
Figure 6.1	Digital Elevation Model	62	
Figure 6.2	Soil type map	62	
Figure 6.3	Land cover map	63	
Figure 6.4	Glaciers depth	63	
Figure 6.5	Temperature Thiessen polygons		64
Figure 6.6	Precipitation Thiessen polygons		64
Figure 6.7	Reservoirs	65	
Figure 6.8	Groundwater depth	65	
Figure 6.9	Fuentes location on the catchment		67
Figure 6.10	Calibration Fuentes	70	
Figure 6.11	Boxplot streamflow Fuentes control period		71
Figure 6.12	Boxplot streamflow Fuentes RCP4.5		72
Figure 6.13	Boxplot streamflow Fuentes RCP8.5		72
Figure 6.14	Trajectories Fuentes control period		73
Figure 6.15	Trajectories Fuentes RCP4.5		73
Figure 6.16	Trajectories Fuentes RCP8.5		74
Figure 6.17	REMO/MPI Fuentes	76	
Figure 6.18	RACMO/ICHEC Fuentes	77	
Figure 6.19	Forni/Val Lia Glaciers Map	78	
Figure 6.20	Glaciers discharge REMO/MPI	79	
Figure 6.21	Glaciers discharge RACMO/ICHEC		80
Figure 6.22	REMO/MPI RCP4.5 A2A reservoir		82
Figure 6.23	REMO/MPI RCP8.5 A2A reservoir		83
Figure 6.24	RACMO/ICHEC RCP4.5 A2A reservoir		84
Figure 6.25	RACMO/ICHEC RCP8.5 A2A reservoir		85
Figure 7.1	Risk, uncertainty and ignorance scheme		88
Figure 7.2	The cascade of uncertainty	89	
Figure 7.3	The cascade of uncertainty revised		89
Figure 7.4	GCM vs RCP uncertainty	97	
Figure 7.5	RCM vs RCP uncertainty	98	
Figure 7.6	GCM vs RCM uncertainty RCP4.5		98
Figure 7.7	GCM vs RCM uncertainty RCP8.5		99
Figure 7.8	Temperature Uncertainty	100	
Figure 7.9	Precipitation Uncertainty	101	
Figure 7.10	RCP-related uncertainty in hydrology I		102
Figure 7.11	RCP-related uncertainty in hydrology II		103
Figure 7.12	GCM-related uncertainty in hydrology		104
Figure 7.13	RCM-related uncertainty in hydrology		105
Figure A.1	RCA4/MIROC temperature	120	
Figure A.2	RCA4/MIROC precipitation	121	

Figure A.3	RCA4/NCC temperature	122
Figure A.4	RCA4/NCC precipitation	123
Figure A.5	RCA4/NOAA temperature	124
Figure A.6	RCA4/NOAA precipitation	125
Figure A.7	RCA4/CCC temperature	126
Figure A.8	RCA4/CCC precipitation	127
Figure A.9	RCA4/CNRM temperature	128
Figure A.10	RCA4/CNRM precipitation	129
Figure A.11	RCA4/ICHEC temperature	130
Figure A.12	RCA4/ICHEC precipitation	131
Figure A.13	HIRHAM/ICHEC temperature	132
Figure A.14	HIRAM/ICHEC precipitation	133
Figure A.15	CCLM/ICHEC temperature	134
Figure A.16	CCLM/ICHEC precipitation	135
Figure A.17	CCLM/MPI temperature	136
Figure A.18	CCLM/MPI precipitation	137
Figure B.1	RCA4/MIROC, Fuentes	140
Figure B.2	RCA4/NCC Fuentes	141
Figure B.3	RCA4/NOAA Fuentes	142
Figure B.4	RCA4/CCC Fuentes	143
Figure B.5	RCA4/CNRM Fuentes	144
Figure B.6	RCA4/ICHEC Fuentes	145
Figure B.7	HIRHAM/ICHEC Fuentes	146
Figure B.8	CCLM/ICHEC Fuentes	147
Figure B.9	CCLM/MPI Fuentes	148

LIST OF TABLES

Table 2.1	RCPs characteristics	9
Table 3.1	Reservoirs characteristics	20
Table 4.1	EURO-CORDEX simulations characteristics	33
Table 4.2	Climate scenarios characteristics	34
Table 4.3	Combinations of EURO-CORDEX scenarios	36
Table 6.1	Calibration performance summary	69

ACRONYMS

RCM Regional Circulation Model

GCM General Circulation Model
RCP Representative Concentration Pathway
IPCC Intergovernmental Panel for Climate Change
AR₅ Fifth Assessment Report
GHGs Green House Gases
QM Quantile Mapping
SD Statistical Downscaling
ECP Extended Concentration Pathway
TE Topkapi-ETH
HWRM Hydrology and Water Resources Management
GC Grid Cell
IfU Institute of Environmental Engineering
IIASA International Institute for Applied System Analysis
NIES National Institute for Environmental Studies
JGCRI Joint Global Change Research Institute
SRES Special Report on Emission Scenarios
TAR Third Assessment Report
AR₄ Fourth Assessment Report
DEM Digital Elevation Model
WRCP World Climate Research Program
CCT Cloud Cover Transmissivity
ARPA Regional Agency for the Protection of the Environment
MASH Moving Average over Shifting Horizon
NASA National Aeronautics and Space Administration
NGA National Geospatial-Intelligence Agency
USGS United States Geological Survey
DUSAF Destinazione d'Uso dei Suoli Agricoli e Forestali
GIS Geographical Information System
SRTM Shuttle Radar Topography Mission

PPPs Policies, Plans, and Programs

ANOVA ANalysis Of VAriance

WMO World Meteorological Organization

ABSTRACT

In this study we assess the impact of climate change on the hydrological cycle of an Alpine catchment and on the management of hydropower systems. We apply the traditional climate change impact study approach, known in the literature as “scenario-based” approach, to the case study of Lake Como catchment. The “scenario-based” approach consists in employing a modelling chain, which comprises the definition of Green House Gases emission scenarios, the simulation of climate models and hydrological models, and the simulation of the impact on water resources.

We take into account an ensemble of climate scenarios, comprising two Representative Concentration Pathways (RCPs), seven General Circulation Models (GCMs) and five Regional Circulation Models (RCMs). The analysis of the climate scenarios on the domain of interest shows an increase in temperature and a seasonal shift in precipitation, causing drier summers and more rainy winters. We apply a statistical downscaling to the climate scenarios in order to match the adequate spatial resolution needed for hydrological modelling. We adopt Topkapi-ETH, a physically-based and fully distributed hydrological model, to reproduce the response of the catchment hydrology to climate change. The employment of a spatially distributed model is due to the possibility of assessing the impact of climate change on different areas of the catchment. Moreover, Topkapi-ETH allows to simulate anthropogenic infrastructures such as reservoirs and river diversions, which are widely present in the Lake Como catchment. The simulation results over the XXI century scenario show a seasonal shift in the hydrological cycle, with lower flow in summer, higher flow in winter, and an earlier snowmelt peak. This results in different patterns of storage building in the Alpine hydropower reservoirs.

Finally, we analyze the uncertainty on hydro-climatic variables associated to climate modelling. Results show that the uncertainty related to the choice of the GCM is the most critical, but comparable to the one of the RCM. The choice of the RCP is generally less crucial for short lead times, but it increases in relative terms for longer lead times.

RIASSUNTO

In questo studio viene valutato l'impatto del mutamento climatico sul ciclo idrologico di un bacino alpino e sulla gestione di sistemi idroelettrici. Il tradizionale approccio allo studio dell'impatto del mutamento climatico, noto in letteratura come "scenario-based", viene applicato ad un caso di studio nelle Alpi italiane: il bacino idrografico del lago di Como. L'approccio "scenario-based", consiste nell'utilizzo di una catena modellistica che include la definizione di scenari emissivi di gas climalteranti, la simulazione di modelli climatici e idrologici e la simulazione dell'impatto sulle risorse idriche.

Viene preso in considerazione un ensemble di scenari climatici comprendenti due Representative Concentration Pathway (RCP), sette General Circulation Model (GCM) e cinque Regional Circulation Model (RCM). L'analisi degli scenari climatici sul dominio di interesse mostra un aumento delle temperature e uno shift stagionale delle precipitazioni, che prevede estati più siccitose ed inverni con maggiori precipitazioni. Un downscaling statistico è applicato agli scenari climatici, per renderne la risoluzione spaziale adeguata alla modellazione idrologica. Al fine di comprendere la risposta idrologica al mutamento climatico viene utilizzato Topkapi-ETH, un modello fisicamente basato e spazialmente distribuito. L'utilizzo di un modello spazialmente distribuito è dovuto alla possibilità di valutare l'impatto del cambiamento climatico in diverse aree del bacino. Inoltre, Topkapi-ETH consente di implementare infrastrutture idrauliche, quali serbatoi idroelettrici e canali di gronda, largamente presenti nel bacino. I risultati della simulazione sull'orizzonte temporale del XXI secolo mostrano uno shift stagionale nel ciclo idrologico, risultante in portate minori d'estate e maggiori in inverno, oltre che in una anticipazione del picco di scioglimento nivale. Ciò comporta diverse traiettorie di invaso nei serbatoi idroelettrici.

Infine, è analizzata l'incertezza sulle variabili idroclimatiche associate alla modellazione climatica. I risultati mostrano che l'incertezza legata alla scelta del GCM è la più critica, ma confrontabile con quella legata alla scelta del RCM. La scelta del RCP è generalmente meno cruciale all'inizio, ma cresce con il passare del tempo lungo l'orizzonte temporale.

INTRODUCTION

1.1 SETTING THE CONTEXT

Climate change is considered to be a key factor in the availability of water resources during the XXI century [IPCC, 2014]. The rise of temperature and the shift in the distribution of precipitation at the global scale will affect the hydrological cycle and thus the water related human activities. The hydrology of the Alpine regions is likely to be affected more than others since they are characterized by a high presence of snow and glaciers and are more sensitive to climate conditions [Zierl and Bugmann, 2005; Beniston, 2003]. The temperature increase will cause an earlier snowmelt and a shift in temporal and spatial precipitation patterns will considerably change water availability. Furthermore, the impact of climate change on hydrology will be accentuated by the glaciers retreat [Haeberli and Beniston, 1998].

The hydropower plants installed in the Alps play a key role in the supply of electricity and, due to their flexibility compared to other electricity sources, they also provide a certain stability in the international network [Gaudard et al., 2014]. Moreover, their importance as a key resource is growing with the increase of power installed in intermittent renewable energy sources such as wind and solar power. Since the patterns of production of wind and solar power are very irregular, and other traditional sources of electricity (e.g., nuclear power and fossil fuel) are less flexible, hydropower is a strategic source for the future. Hydropower in a mountainous country like Switzerland represents 59.7% of electricity generation [Energiebundesamt, 2012], while in Italy this value decreases to 13.2% [Terna, 2012], maintaining anyhow a considerable share of the national production. The changes currently taking place in the electricity market due to the increasing share of renewable energies and the implementation of an energy stock exchange are leading to several transformations in which hydropower will be one of the main players.

In such a context, it is important to investigate the complex relationship occurring among climate, water availability, and hydropower production.

When dealing with climate change, the uncertainty related to future projection can not be neglected. Climate change impact studies are the result of a complex modelling chain, which comprises the definition of the Representative Concentration Pathway (RCP), the General Circulation Model (GCM), Regional Circulation Model (RCM), the downscaling procedure, the hydrological modelling, and the mod-

elling of the reservoirs. In recent years considerable effort has been spent in order to characterize the uncertainty related to climate and hydrology. Since an uncertainty analysis can be addressed in several different ways, a large number of approaches have been proposed in the past years, to tackle specific aspects of the problem. For example, Murphy et al. [2004] analyzed the changes in the probability density functions of some climate indicators, with a probabilistic approach. Hawkins and Sutton [2009] tried instead to quantify how the different sources of uncertainty change with the lead time of the projection. Another approach was proposed by Finger et al. [2012] that attempted, through an analysis of the variance, to quantify how different sources of uncertainty affect the climate during the twelve months of the year.

1.2 OBJECTIVES OF THE THESIS

The main objective of this thesis is to assess the impact of climate change on hydrology and hydropower production in the Italian Alps. In particular, we focus on the Lake Como catchment. We adopt the classical workflow of climate change impact studies, known in the literature as “scenario-based”. The first step is the analysis of climate change scenarios. More precisely, we consider temperature and precipitation as projected by an ensemble of climate models forced with two different Representative Concentration Pathways RCPs (4.5 and 8.5). These scenarios refer to the EURO-CORDEX project and the Intergovernmental Panel for Climate Change (IPCC) Fifth Assessment Report (AR5). The next step is to apply a statistical downscaling, since the spatial resolution of the climate scenarios is not fine enough for the hydrological modelling. Then, a fully distributed and physically-based hydrological model is calibrated and simulated. The importance of employing a spatially distributed hydrological model is related to the possibility of assessing the response of hydrology to climate change in every single part of the catchment, allowing spatial analyses on river network, glaciers, and reservoirs. The last step comprises the assessment of the impact of hydrological scenarios on the management of the reservoirs that can, thanks to the spatially distributed hydrological modelling, be jointly taken into account. Along with this workflow, an uncertainty characterization is carried out in order to assess the contribution of the single modelling components to the global uncertainty.

Ultimately, the main innovative contributions of this thesis are the following:

- The analysis of the predicted impact of climate change on the Southern Alps and on the Lake Como catchment, within the EURO-CORDEX framework.

- The employment of a fully distributed hydrological model, in order to analyze the complexity of the response of hydrology to climate change, together with the impact on the reservoirs management.
- The uncertainty characterization, carried out in order to assess, within the “scenario-based” workflow, where most of the uncertainty is located.

1.3 THESIS STRUCTURE

This thesis is structured in the following parts:

- The next chapter (2) contains a description of the methods and tools used in the thesis: the climate models, the statistical downscaling technique and the hydrological model.
- Chapter 3 provides a comprehensive description of the study area of the Lake Como catchment.
- Chapter 4 is about the impact of climate change on the study site. The IPCC AR5 is introduced and the EURO-CORDEX project with its climate models is described. Then the results of our analysis on the climate change are shown.
- Chapter 5 is intended to describe the adopted downscaling procedure, starting with the datasets used and concluding with some comparisons between historical observations and downscaled climate scenarios.
- Chapter 6 describes the application of the hydrological model Topkapi-ETH to the Lake Como catchment. At the beginning a comprehensive description of the model properties and input data for setup and calibration is given to the reader. In the second part the hydrological scenarios obtained via simulation of Topkapi-ETH on the case study are analyzed.
- Chapter 7 tackles the issues related to uncertainty. It is shown how the problem has been approached in the past and which procedure is adopted in this work to give a quantitative description of the single modelling component contribution to the global uncertainty.

METHODS AND TOOLS

2.1 METHODOLOGY

The general framework used in this thesis to assess the impact of climate change is usually addressed in literature as "top-down" or "scenario-based" approach [Wilby and Dessai, 2010]. This approach consists on the application of a cascade of models, from the demographic development to the management of a water system. Generally, in the field of water resources management this modelling cascade includes:

- The definition of a Green House Gases (GHGs) emission scenario.
- The global climate modelling via General Circulation Models (GCMs).
- The regional climate modelling via Regional Circulation Models (RCMs).
- The application of statistical downscaling in order to possibly refine even more the resolution of the climate variables.
- The employment of a hydrological model, to evaluate the stream-flow scenarios.
- The modelling of the impact on water resources management.

Another possible way to approach climate change impact studies is the so-called "bottom-up" or "vulnerability-based" approach [Wilby and Dessai, 2010]. In this different approach the perspective is reversed since it relies mainly on the observation of the current water system and less on the future scenarios. It usually implies the two following main steps:

- The identification of the current water system vulnerabilities.
- The definition of better strategies to deal with them.

The integration of the two methods is probably the best way to set a comprehensive analysis and approach policy design in climate change conditions. Nevertheless, as the main goal of this thesis is to assess the impact of the climate change on existing hydropower reservoirs, the first approach ("scenario-based") is applied. The models and tools applied to the Lake Como catchment to implement the workflow of

the scenario-based approach are graphically shown in Figure 2.1 and listed here:

- We consider two Representative Concentration Pathways in the framework of IPCC Fifth Assessment Report, they are RCP4.5 and RCP8.5.
- We take into account an ensemble of combinations of GCMs and RCMs to evaluate the effect of climate change on the variables of temperature and precipitation on the Lake Como catchment.
- As the resolution of RCMs is still too coarse for a physically-based hydrological model we apply a statistical downscaling using the Quantile Mapping technique.
- We calibrate a fully distributed and physically-based hydrological model (Topkapi-ETH) on the catchment and simulate it, fed by the downscaled scenarios, in order to assess the impact of climate change on the hydrology.
- Within Topkapi-ETH we apply an operative rule to the reservoirs in the catchment, to evaluate how changes in hydrology will reflect on the reservoirs.

2.2 MODELS AND TOOLS

In the next sections we describe the models and tools used in the thesis, namely the RCPs, the GCMs and RCMs, the statistical downscaling technique and the hydrological model.

2.2.1 Representative Concentration Pathways and IPCC AR5

The Representative Concentration Pathways are Green House Gases (GHGs) concentration trajectories adopted by the IPCC for its AR5 in 2014. They describe possible climate futures on the basis of the radiative forcing values (changes in balance between incoming and outgoing radiation to the atmosphere, caused by its composition) relative to the pre-industrial period. RCPs substitute the Special Report on Emission Scenarios (SRES) projections published in 2000, and used in IPCC Third Assessment Report (TAR) and Fourth Assessment Report (AR4). The SRES describes emission scenarios. Emission scenarios are a representation of the future discharges in the atmosphere of GHGs that provide input to climate models. To be produced they require assumptions about patterns of economic and demographic growth, technology development and future energy consumption. The SRES are complemented by socio-economic storylines, which help in their interpretation. Although they have been widely used, after over a decade of

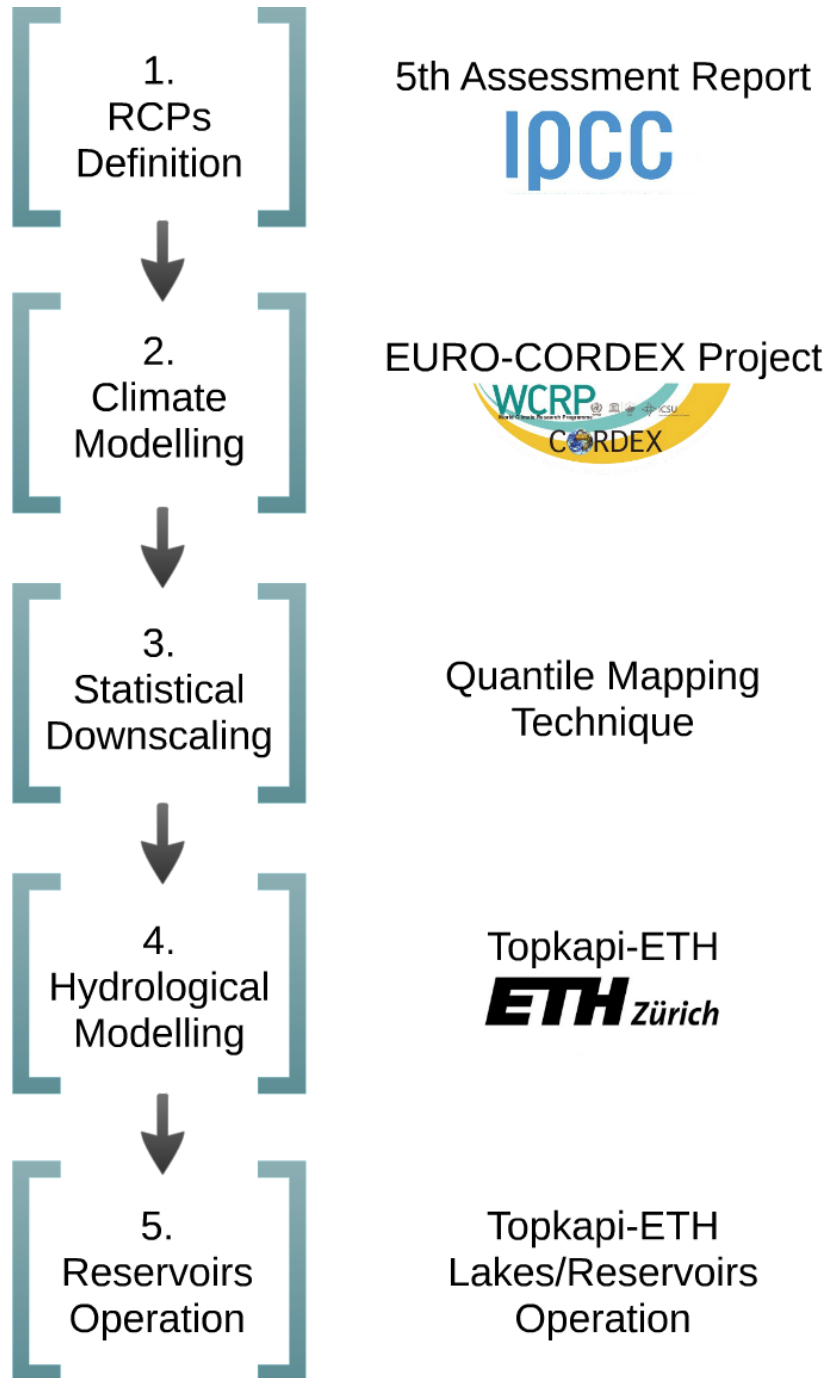


Figure 2.1: Flow chart of the main steps followed in the analysis. On the left side of the graph, are shown the traditional steps of a scenario-based workflow in water resources management. On the right side are listed the sources of the tools used in each specific step: the RCPs were considered in the framework of the IPCC AR5; the climate scenarios were retrieved from the EURO-CORDEX project; the downscaling technique used was the Quantile Mapping; the hydrological model employed was Topkapi-ETH, which comprises reservoir operative rules.

climate change studies, new economic data and technology developments, different and new scenarios were released [Moss et al., 2010]. The new scenarios, rather than using storylines, use radiative forcing trajectories, which are not associated with unique socio-economic scenarios, but can result from many combinations of demographic, economic and technology futures. Since climate models require data on concentrations of radiatively active constituents in the atmosphere, the research community identified a specific emission scenario as pathway towards achieving each radiative forcing trajectory. This step was necessary to make them usable in climate modelling and compare them with the old SRES scenarios. A selection process took place in order to identify the final RCPs, with criteria established by the research community. The main criteria adopted were: the compatibility with the complete range of emission scenarios existing in literature; a manageable and even number of scenarios (in order to avoid a central one to be taken as ‘best estimate’); a clear separation of the radiative forcing trajectories on the long term, to make them distinguishable. The IPCC Working Group III used these criteria in 2007, in order to identify first 32 potential candidates and then to make the final choice on four of them. Figure 2.2 illustrates the final chosen RCPs among the other candidates. The four RCPs selected in the IPCC AR5 (RCP2.6, RCP4.5, RCP6, RCP8.5) are named after the range of radiative forcing values at the end of the century (2100) relative to pre-industrial values (+2.6, +4.5, +6.0 and +8.5 W/m²). The main characteristics of each scenario (summarized in Table 2.1) are the following:

- RCP2.6 was developed in the Netherlands by the IMAGE modelling team. The emission path is representative of scenarios in literature that lead to very low GHGs levels, It is also known as the “peak-and-decline scenario”, reaching a maximum of radiative forcing around mid-century (+3.1 W/m²) and then declining [van Vuuren et al., 2007].
- RCP4.5 was developed in the United States by the Joint Global Change Research Institute (JGCRI). It is a stabilization scenario in which the total radiative forcing is stabilized, without overshoot (without reaching a peak), shortly after 2100 [Clarke, 2007; Smith and Wigley 2006].
- RCP6.0 was developed in Japan at the National Institute for Environmental Studies (NIES). It is again a stabilization scenario that predicts that the total radiative forcing will stabilize, without overshoot, shortly after 2100 thanks to the application of some technologies and strategies to reduce GHGs emissions. The stabilization of radiative forcing will take place like in RCP4.5, but with a higher value of GHGs concentration [Fujino, 2006; Hijioka et al. 2008].

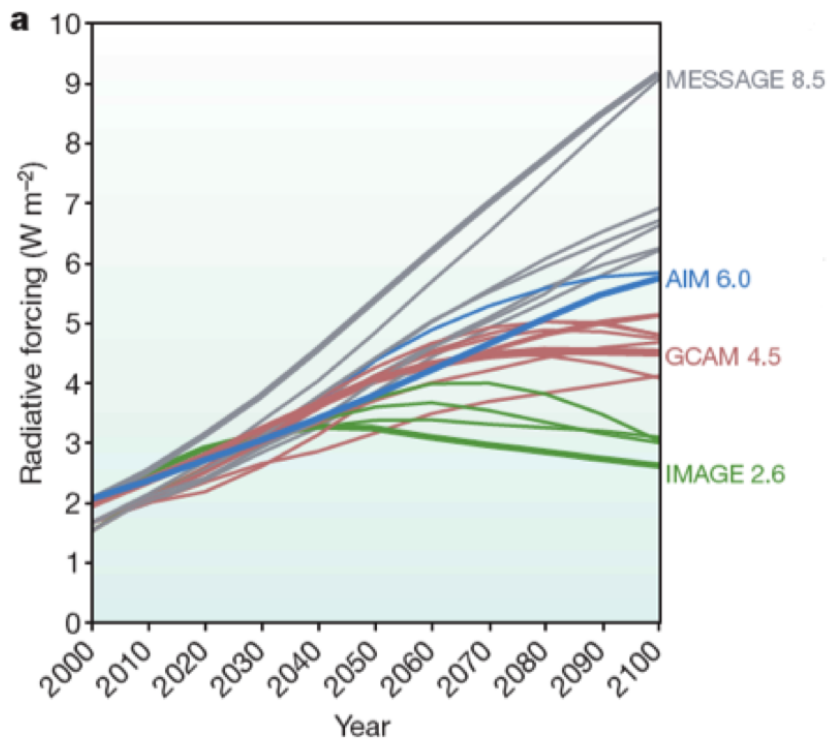


Figure 2.2: RCPs trajectories (in bold) compared to the ones of other candidates, taken from Moss et al. [2010]

- RCP8.5 was developed in Austria at the International Institute for Applied System Analysis (IIASA) using MESSAGE-MACRO, a model that incorporates energy supply with a non-linear macroeconomic model. This RCP presents increasing GHGs emissions over time and is representative of scenarios in literature that show high GHGs concentrations [Riahi et al., 2007].

Another interesting new feature of the RCPs, with regarding to the SRES, is that there was an attempt to go beyond 2100 with the projections. The Extended Concentration Pathway (ECP)s were developed extending GHGs concentrations and emissions time series. The ECPs

NAME	RADIATIVE CO2 TEMPERATURE			PATHWAY	SRES
	FORCING (W/m ²)	(PPM)	ANOMALY (°C)		EQUIVALENT
RCP8.5	8.5 W/m ²	1370	4.9	Rising	A1F1
RCP6.0	6.0 W/m ²	850	3.0	Stabilization	B2
RCP4.5	4.5 W/m ²	650	2.4	Stabilization	B1
RCP6.0	2.6 W/m ²	490	1.5	Peak and Decline	None

Table 2.1: IPCC AR5 RCPs main characteristics

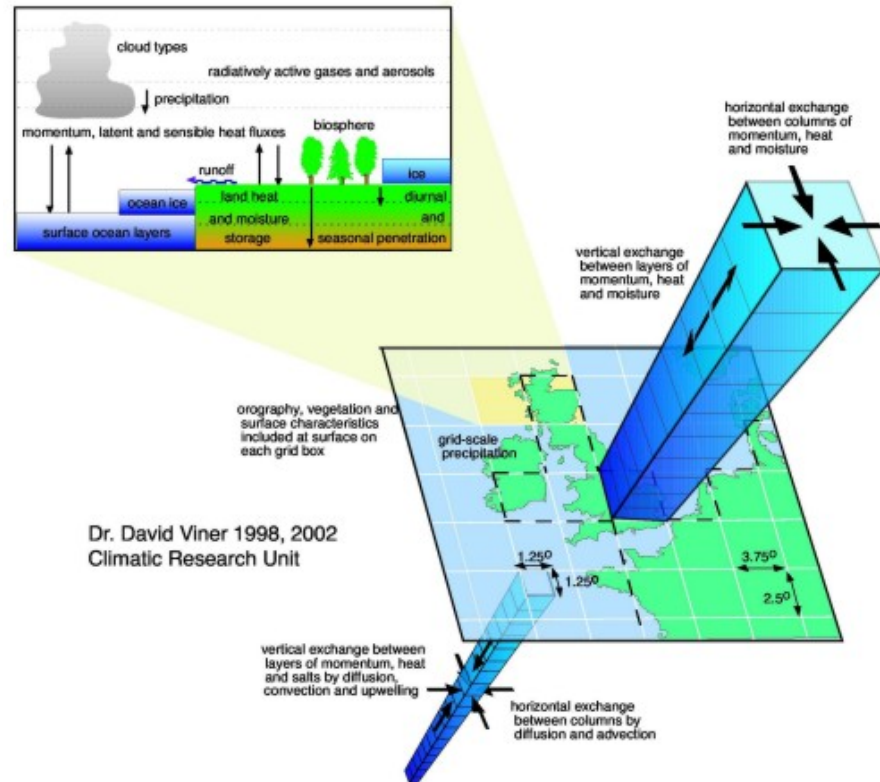


Figure 2.3: General Circulation Models 3D structure, taken from IPCC

are defined up to 2300 and are intended as a basis for longer-term simulations, compared to the traditional time frame of the XXI century. Besides the characteristics mentioned above, scenarios are used also by other scientists, non-governmental organizations, policy makers, and journalists in order to have a common framework through which they can communicate and discuss about climate change.

2.2.2 General Circulation Models and Regional Circulation Models

General Circulation Models describe the physical processes in the atmosphere, oceans, cryosphere, and land surface. At present, they are the most advanced tools to assess the response of the Earth climate to the emission of GHGs. GCMs describe a three-dimensional grid over the globe with a variable resolution (vertical and horizontal) which is rapidly increasing with the growth of computational power and the deepening of the knowledge in the physics of the atmosphere. At each time step in every grid cell the climate variables of interest (e.g., temperature, humidity and precipitation) are calculated through physically-based equations describing the fluxes of heat and mass in the atmosphere. An idea of the complexity of interactions that are described in a GCM is given by the Figure 2.3 that shows the 3D structure of the model and the coupling of differ-

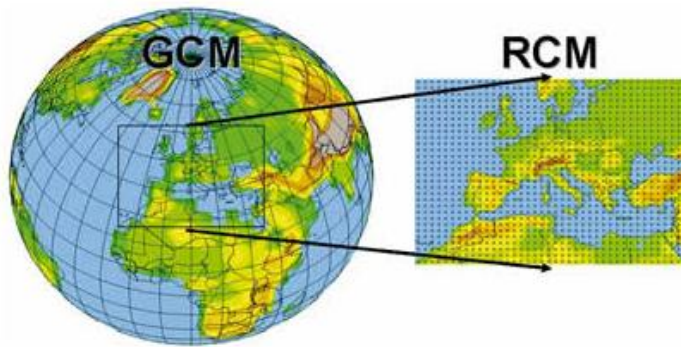


Figure 2.4: Example of RCM over the European domain, taken from WMO

ent components of the climate such as land, atmosphere, oceans and ice-sheets. Even though the resolution of GCMs has improved in the past years, it is still not fine enough to provide the accuracy needed for climate change impact studies. Further refinement of GCMs' outputs can be obtained by applying some downscaling techniques. The dynamical downscaling technique consists in nesting a Regional Circulation Model into a GCM. RCMs have the same structure of GCMs but work at a finer spatial resolution so account for more details, such as orography, land use and small-scale atmospheric features. They provide better accuracy needed in climate change impact studies with a resolution that is generally between 10 km and 50 km (Figure 2.4). The nesting procedure consists in the GCMs providing the boundary conditions for the RCM run. The dynamical downscaling is particularly attractive for mountainous [Frei et al., 2006] and coastal area, where the coarse spatial resolution of a GCM cannot describe correctly the physical processes taking place, which are usually dominated by local circulation phenomena, rather than global. Even though the reduced domain area could increase the speed of the simulation, the finer resolution makes RCMs extremely computationally intensive [Fowler and Tebaldi, 2007].

2.2.3 The Quantile Mapping Statistical Downscaling Technique

In the majority of climate change impact studies the resolution of GCMs and RCMs is not fine enough and computational limits do not allow further dynamical downscaling. In those cases the mismatch between global climate and local scale can be tackled with Statistical Downscaling (SD) techniques. SD is based on the fact that local climate is influenced by two main factors: the large-scale climate and the small-scale local features (e.g., land cover, topographic features, coasts [Von Storch, 1995]). Local climate variables are derived first determining a statistical relationship, which links the large-scale predictor to the small-scale predictand. For this part of the work, his-

torical observations of the local climate are required. After that, the estimated statistical relationship between predictor and predictand is applied to the output of the climate model, in order to obtain the local climate data [Wilby et al., 2004]. Usually predictors and predictands represent the same physical variable, but it is not strictly necessary. The SD methods are often used in climate change impact studies as they are computationally inexpensive, especially compared to dynamical downscaling techniques. Other advantages are that they can provide site-specific information, as points, typically needed in climate change impact studies [Mearns et al., 2003] and the removal of the model bias [Boe et al., 2007]. A limit is that they strongly depend on the quality of the historical observations, thus they can be used only when reliable datasets are available. Another weakness of SD methods in climate change impact studies is that they assume that the relationship between the two variables will remain the same in the future under different climate forcing which might not be true under climate change conditions. Several SD methods have been proposed, among which the most common are: delta change method [Hay et al., 2000], neural network [Olsson et al., 2001], analog method [Zorita, 1999], weather generator [Wilks and Wilby, 1999], unbiasing method [Deque, 2007] and quantile mapping [Boe et al., 2007]. In this study Quantile Mapping (QM) has been adopted, due to its simplicity and flexibility. The QM consists of generating a correction function (f) between the climate model outputs distribution and the observations distribution and its application to remove the bias. An example of bias removal is shown in Figure 2.5 [Boe et al., 2007]. As input the QM requires the historical observations, the model outputs of a control run during the same period and the forecast model outputs over the future scenario. The procedure consists in two main phases:

- CALIBRATION PHASE: the correction function (f) between the cumulative density function (cdf) of the model outputs in the control run (C) and the cdf of the observations (O) is calibrated. An example is shown in Figure 2.6, for the minimum temperature in the Paris area [Deque, 2007].

$$O = f'(C)$$

- PROJECTION PHASE: the calibrated correction function (f') is and applied to the variables from the forecast (F), removing the bias. A linear interpolation is applied between two percentiles. The result of the operation is the downscaled time series (F').

$$F' = f'(F)$$

In the QM algorithm used in this work, if a forecast value exceeds the quantiles computed (which might happen under climate change conditions) a constant correction equal to the 99th or 1st quantile is applied. The calibration phase can be done yearly, seasonally or monthly, as the model error might differ during the year.

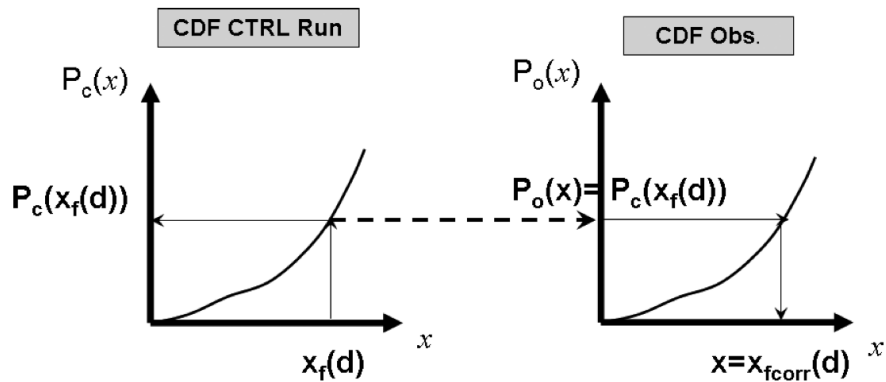


Figure 2.5: Scheme of bias correction using Quantile Mapping. cdf stands for Cumulative Distribution Function. The subscript o, f, c stand for the historical observation, the climate scenario model output and the control simulation respectively. For the value $x_f(d)$ of the variable x in the day d in the climate scenario, the corresponding seasonal cumulative frequency $P_c(x_f(d))$ where $P(x) = P_r(X \leq x)$ is searched in the calculated cdf of the climate control simulation. After that, the value of x such as $P_o(x) = P_c(x_f(d))$ is searched on the cdf of the historical observations. This final value ($x_{fcorr}(d)$), is used as the corrected value of $x_f(d)$ [Boe et al., 2007].

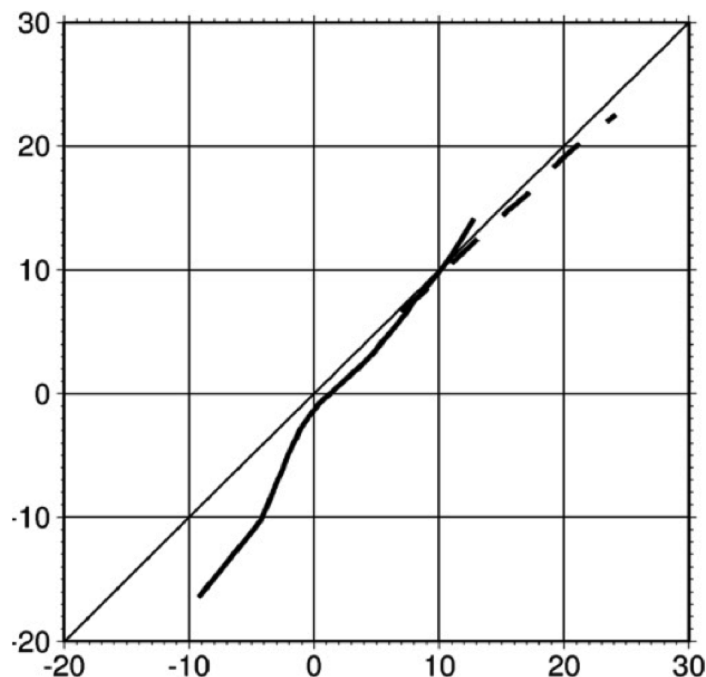


Figure 2.6: Quantile-quantile plot for model outputs (x -axis) versus historical observations (y -axis) of the minimum temperature ($^{\circ}\text{C}$) in the Paris area during the period 1961-1990. Solid line represents winter values, while dash line summer values [Deque, 2007].

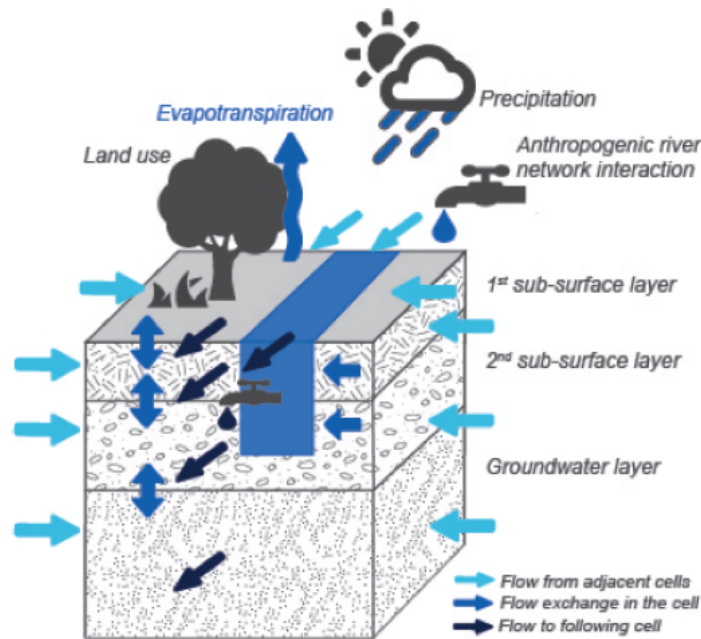


Figure 2.7: Topkapi-ETH Structure. The arrows represent the flows taking place in a grid cell.

2.2.4 *Topkapi-ETH*

When dealing with climate change, it is very important to correctly describe the physical processes occurring in the hydrological cycle, in order to assess how changes in climate affect the hydrological regimes. Therefore, it is highly preferable to employ physically-based model, rather than empirical and conceptual ones. The model adopted in this thesis is Topkapi-ETH (Topographic Kinematic Approximation and Integration model), originally developed by Todini and others [Ciarapica and E., 2002; Liu and Todini, 2002; Liu and Todini, 2006]. After some enhancements at the department of Hydrology and Water Resources Management (HWRM), in the Institute of Environmental Engineering (IfU) of the Federal Institute of Technology in Zurich, it took the current name, Topkapi-ETH (TE).

Topkapi-ETH presents a regular grid in which the smallest computational element is the single Grid Cell (GC). Flow directions are defined as shown in Figure 2.7 with a single outflow direction (one downstream GC) and up to three upstream cells. The model uses a vertical discretization of belowground in three layers. The deepest layer mimics the behavior of slow components such as fractured or porous rock aquifers, while the first two layers represents deep and shallow soil as non-linear reservoir. GCs are connected to the surface and subsurface according to topographic gradients. The potential infiltration rate is calculated with an empirical formula and runoff can result from saturation excess or infiltration processes. The topographic effects on

radiation (particularly significant in mountainous terrains) are regulated as described in Corripio [2003]. The evapotranspiration is regulated by the Priestly Taylor equation [Priestley and Taylor, 1972] and a monthly correction is applied to distinguish between different land uses. Snow and ice-melt are calculated with an empirical temperature index model, which is fed only by shortwave radiation and air temperature [Pellicciotti et al., 2005; Carenzo et al., 2009]. Topkapi-ETH compared to other physically-based state-of-art hydrological models does not represent the rigorousness and richness of hydrological processes [Fatichi et al., 2013], but it is a reasonable trade-off between hydrological representation and computational time for large catchment considering also the long time horizons and the large number of simulation required by the different climate change scenarios considered in this analysis. Moreover the latest upgrade of the model, done by HWRM at ETH Zurich gives the possibility to take into account some anthropogenic infrastructures such as reservoirs, river diversions and water abstractions. The reservoirs are described by their technical features such as maximum outflow, spillway definition, volume-level curves, and environmental flows and some simple operational rules are implemented. Other artificial facilities such as diversion channels and water abstractions can be included in the model setup.

In Topkapi-ETH, the values of air temperature, cloud cover transmissivity and precipitation for each GC at the temporal and spatial resolution selected for the model simulation are the meteorological inputs required. Furthermore, Topkapi-ETH requires a series of spatial inputs for the model setup: a digital elevation map of the catchment, a soil map, a land use map, and a map of the glaciers. For the grid cells time series the available outputs are: water volume in upper subsurface layer, effective saturation in upper subsurface layer, effective saturation in lower subsurface layer, effective saturation in groundwater aquifer, channel flow, flow in upper subsurface layer, flow in lower subsurface layer, flow in groundwater aquifer, and snow water equivalent.

STUDY SITE

3.1 LAKE COMO TERRITORY

The Lake Como, also known with its traditional Latin name “Lario” is a natural lake with glacial origins (Figure 3.1). With its 140 meters of depth is the fifth deepest European lake (after four Norwegian lakes) and with its 145 km² of surface it is the third largest Italian lake after Lake Garda and Lake Maggiore. The lake is surrounded by mountains and receives water by 37 tributaries (Mera and Adda being the main ones). The River Adda, the only emissary of the lake, flows through the Lombardy territory until it reaches the River Po. The Lake Como is regulated by the Olginate dam, located near Lecco. The catchment of River Adda, closed at the Olginate dam, has an area of 4762 km² of which 90% is Italian and the remaining 10% is Swiss. The Swiss part of the basin is composed by the territory of Val Bregaglia and Val Poschiavo. The River Spoel, which naturally flows into the Danube catchment, is partly diverted into the Lake of San Giacomo. At the bottom of the Valtellina, the River Adda flows at Fuentes into the Lake Como, with an average discharge of 88m³/s [Giacomelli et al., 2008]. A snowmelt peak in late spring and a secondary peak in autumn characterize the hydrological year, while in winter average streamflows are considerably lower.

3.2 HYDROPOWER PRODUCTION

Since the beginning of the past century the area upstream the Lake Como has been exploited with the construction of many dams and artificial lakes. Today it is a complex hydropower system, with several big reservoirs, run by four main energy companies: A2A, Enel, Edison and Edipower. Figure 3.2 shows the location of the main reservoirs, while Table 3.1 illustrates their main characteristics.

3.2.1 A2A

A2A (previously named AEM, Azienda Elettrica Milanese) owns a widespread and extensive hydraulic network in Valtellina (Figure 3.3). The two main artificial lakes are Cancano and San Giacomo (Figures 3.4 and 3.5), which feed a dense network of power plants headed by the main one of Premadio. They are two contiguous reservoirs, located in the municipality of Valdidentro, in the Fraele Valley. The first lake, San Giacomo was built in 1950, has an altitude measured

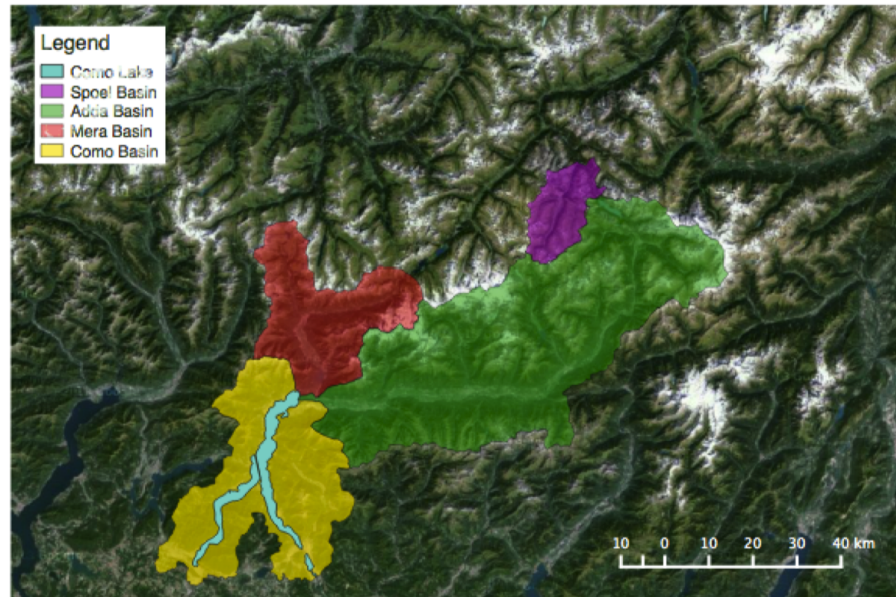


Figure 3.1: Map of the Lake Como catchment. It is possible to distinguish the four main sub-catchments: the River Adda, the River Mera, the catchment of the Lake Como and the catchment of the Spoel, which naturally would be a tributary of the Danube, but it is artificially diverted to the Cancano reservoir.

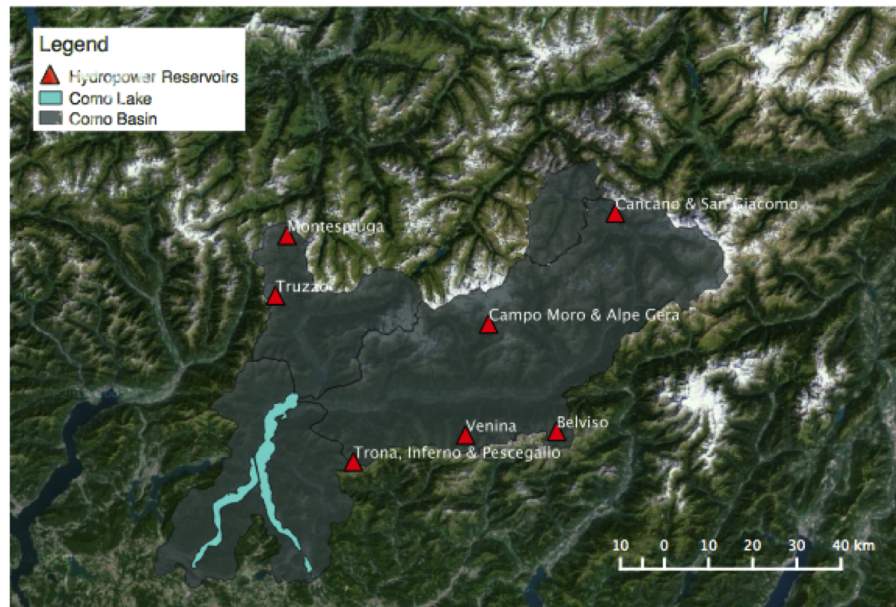


Figure 3.2: Map of the main reservoirs of the catchment. It is possible to see how some reservoirs were conceptually merged together for the analysis: Cancano and San Giacomo, Alpe Gera and Campo Moro and Trona, Inferno and Pescegallo.



Figure 3.3: A2A hydropower network in Valtellina, adapted from A2A

NAME	NATURAL		CONNECTED	DAM	COMPANY
	STORAGE Mm ³	BASIN Km ²	BASIN Km ²	ALTITUDE m a.s.l	
San Giacomo	64.0	18.7	322.3	1952	A2A
Cancano	124.0	36.0	322.3	1902	A2A
Alpe Gera	68.1	39.9	50.9	2128	Enel
Campo Moro	10.8	39.9	50.9	1969	Enel
Inferno	4.2	1.1	0.3	2088	Enel
Trona	5.4	2.6	11.5	1805	Enel
Pescegallo	1.1	0.9	1.0	1863	Enel
Montespluga	32.6	24.0	2.9	1904	Edipower
Truzzo	20.0	10.0	5.5	2088	Edipower
Venina	11.2	8.3	11.8	1824	Edison
Belviso	50.1	27.3	20.1	1486	Edison

Table 3.1: Characteristics of the main reservoirs existing in Valtellina and Valchiavenna

at the top of its dam of 1951.5 m and a maximum storage of 64 Mm³. It is fed by the channel Spoel and the streams Gravia, Frodolfo, Alpe, Zebrù, Forcola, and Braulio together with the River Adda. The Lake Cancano, located directly next to San Giacomo, has a capacity of 124 Mm³ and a dam, built in 1956, located at 1902 m a.s.l.. The reservoir is fed directly by Lake San Giacomo and the channel Viola. The entire catchment has an area of 36 Km², but considering the connected basin it goes up to 322.3 Km². The power plant of Premadio, located downstream the two big reservoirs, has a total installed capacity of 226 MW, thanks to six Pelton turbines. The maximum streamflow in the power plant is 39 m³/s.



Figure 3.4: Cancano reservoir, source: ARPA Lombardia



Figure 3.5: San Giacomo reservoir, source: ARPA Lombardia

3.2.2 *Enel*

Enel is the second biggest producer of electricity in terms of power in Valtellina and it manages reservoirs both on the right and on the left hydrographic side of River Adda. The lakes Alpe Gera and Campo Moro are located on the right hydrographic side and are then connected to the power plant of Lanzada (Figure 3.6). On the left side instead there are the lakes of Pescegallo, Inferno and Trona, connected first to the power plant of Trona and afterwards to the main one of Gerola Alta (Figure 3.7). The power plant of Lanzada and Gerola Alta have an installed capacity of 188 MW and 13.8 MW respectively. Alpe Gera and Campo Moro are fed by the Fellaria glacier through the Lanterna stream. Alpe Gera is the reservoir located upstream and its dam, built in 1964, is situated 2128 m a.s.l., whereas downstream the Lake Campo Moro is located at an altitude of 1969 m. Together the two lakes have a catchment area of 39.9 Km², and a connected area of 50.9 Km². The maximum storage is respectively of 68.1 Mm³ and 10.8 Mm³, representing, after the system Cancano and S. Giacomo, the biggest reservoirs in the study area. Also these two dams, like the majority of big dams in the north of Italy were built between the '50s and '60s (Alpe Gera in 1964 and Campo Moro in 1959, shown in Figures 3.8 and 3.9 respectively). Pescegallo, Inferno, and Trona represent a minor part of the Enel network in Valtellina, they have a smaller catchment area and they are located at a lower altitude (Figure 3.7). Lake Inferno is located at the southeast corner of the catchment, has a maximum storage of 4.17 Mm³ and an altitude of 2088 m (Figure 3.10). The Lake Pescegallo, with storage of only 1.1 Mm³, is the smallest reservoir considered in this thesis and it is located at an altitude of 1863 m (Figure 3.11). The natural and connected basin together do not reach the surface of 2 Km². Lake Trona is located 1802 m above sea level, has a maximum storage of 5.35 Mm³ and presents a catchment area of 2.62 Km² and a connected basin of 11.5 Km² (Figure 3.12). This reservoir was originally a natural lake of glacial origins and the construction of the dam in 1942 increased its capacity.



Figure 3.6: Enel network in Valmalenco, where the dams of Campo Moro and Alpe Gera are located, source: Enel



Figure 3.7: Enel network in Val Gerola, where the dams of Trona and Inferno and Pescegallo are located, source: Enel



Figure 3.8: Alpe Gera reservoir, source: [ARPA Lombardia](#)



Figure 3.9: Campo Moro reservoir, source: [ARPA Lombardia](#)



Figure 3.10: Inferno reservoir, source: [ARPA Lombardia](#)



Figure 3.11: Pescegallo reservoir, source: [ARPA Lombardia](#)



Figure 3.12: Trona reservoir, source: [ARPA Lombardia](#)

3.2.3 *Edipower*

The reservoirs belonging to Edipower are located in Valchiavenna, along the rivers Liro and Mera (Figure 3.13). River Mera's source is located over 2800 m above the sea level in Switzerland and it reaches the Italian territory in Castesegna. Liro's source is located near the Spluga pass and after roughly 25 Km it flows into the Mera near the town of Chiavenna. Due to particular climatic conditions this area located north of the Lake Como is characterized by humid winds and frequent and intense precipitation events. Downstream the two reservoirs, it is built a dense hydropower network, whose biggest plant is the one of Mese, having an installed capacity of 170 MW. Lake Montespluga is located between the Spluga pass and Madesimo, it has a maximum storage of 32.6 Mm³ and an altitude of 1903.5 m. It is closed by two dams, Cardanello and Stuetta, both built in 1932 and it has a catchment area of 24 Km² and a connected basin of 2.85 Km² (Figure 3.14). Lake Truzzo is located in a valley perpendicular to Valchiavenna (Valle del Drogo) and has a maximum storage of 20 Mm³. After the one of the Alpe Gera, it is the highest among the ones considered in this analysis (2088 m a.s.l.). It has a catchment area of 10 Km² and a connected basin of 5.5 Km² (Figure 3.15).

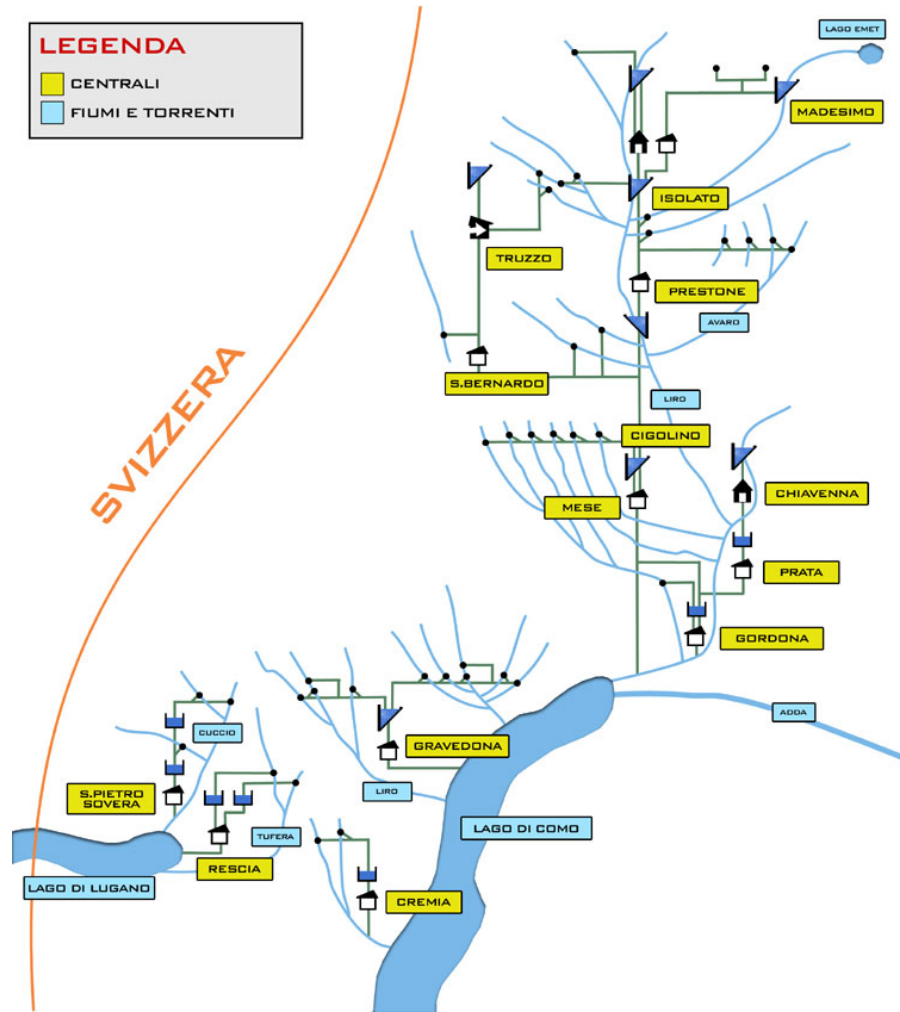


Figure 3.13: Edipower hydropower network in Valchiavenna, source: Edipower



Figure 3.14: Montespluga reservoir, source: [ARPA Lombardia](#)



Figure 3.15: Truzzo reservoir, source: [ARPA Lombardia](#)

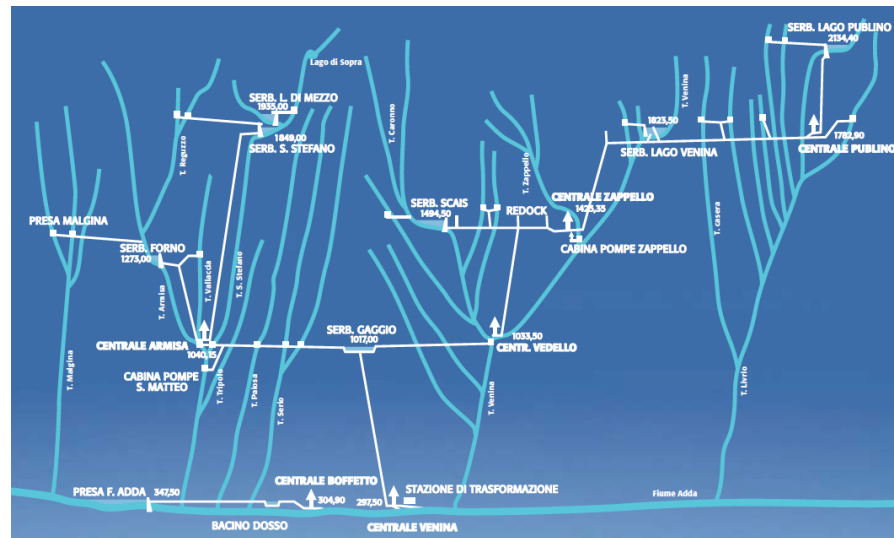


Figure 3.16: Edison hydropower network in the area of the Lake Venina, source: Edison

3.2.4 *Edison*

The facilities of Edison in the area of Valtellina were built by Falck steelworks between the '20s and the '60s and they consist of two hydraulic links: the link Venina-Armisa (Figure 3.16) and the link Ganda-Belviso (Figure 3.17). Lake Venina is fed mainly by the homonymous river and it is closed downstream by a dam located 1824 m above the sea level. It has a maximum storage of 11.2 Mm³ and a natural catchment area of 8.3 Km², while the connected basin is 11.8 Km² wide. Lake Venina feeds the homonymous plant, which has a total capacity of 67 MW (Figure 3.18). Lake Belviso owes its name to the River Belviso by which it is fed and it was born with the construction of the Frera dam (1486 m a.s.l). Due to the strategic location next to several valleys it has a catchment area of 27.3 Km² and 20.1 Km² of connected basin. With a maximum storage of 50.1 Mm³, Lake Belviso is the fourth biggest lake among the ones described here (Figure 3.19). Lake Belviso feeds with its water the two main plants of the link: Ganda and Belviso, which have both a capacity of 66 MW and a streamflow concession of 14 m³/s.

3.2.5 *Simplifications and Notes*

As already mentioned, not the whole river catchment of Adda is in the Italian territory. The part of the catchment in the Helvetic territory is anyhow exploited with hydropower reservoirs and plants, but in this analysis we have to exclude the Swiss reservoirs due the scarcity of data that would mislead the analysis. These excluded lakes are: Lake White, Lake Poschiavo, Lake Pirola, Lake Palù, and Lake Al-

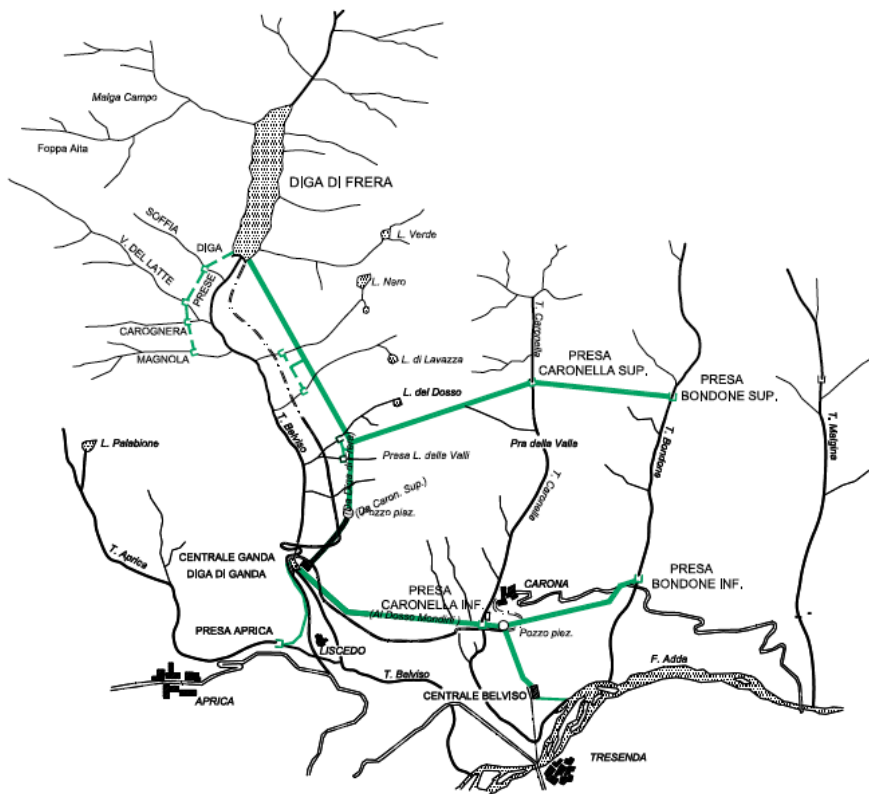


Figure 3.17: Edison hydropower network in the area of the Lake Belviso, source: Edison



Figure 3.18: Venina reservoir, source: ARPA Lombardia



Figure 3.19: Belviso reservoir, source: [ARPA Lombardia](#)

bigna. Lake Albigna is the biggest among the reservoirs excluded from the analysis and its maximum storage is 70.6 Mm^3 . The other reservoirs excluded are smaller and together the Swiss reservoirs account for approximately one fifth of the total water storage in the Lake Como catchment.

CLIMATE CHANGE SCENARIOS

4.1 THE EURO-CORDEX PROJECT

The EURO-CORDEX Project is the European branch of the CORDEX initiative, an international program, sponsored by the World Climate Research Program (WRCP), which aims at creating a framework to produce advanced regional climate change projections. It is the direct descendant of the projects Prudence and Ensembles, which ended in 2004 and 2009, respectively. EURO-CORDEX provides regional climate change projections over the European domain within the framework of the IPCC Fifth Assessment Report [Jacob et al., 2014]. The project started in 2009, when the WRCP established a Task Force for Regional Climate Downscaling that created the CORDEX initiative with the major goals of providing a climate projection and model evaluation framework as well as an interface to the researchers in climate change impact, adaptation and mitigation studies [Giorgi et al., 2009]. Because of the projects Ensembles and Prudence, Europe was already the object of high spatial resolution regional climate change simulation. The improvements brought with EURO-CORDEX are the increased spatial resolution (12.5 Km, 0.11 degree) and the use of the new RCPs. Some extra simulations are anyhow conducted with the standard resolution of 50 Km (0.44 degree), as shown in Table 4.1. The simulations considered in the EURO-CORDEX project are based on the following Representative Concentration Pathways described in the AR5:

- RCP8.5: rising radiative forcing crossing 8.5 W/m² at the end of the 21st century [Riahi et al., 2007].
- RCP4.5: stabilization of radiative forcing after the 21st century at 4.5 W/m² [Clarke, 2007; Smith and Wigley 2006].
- RCP2.6: peaking radiative forcing within the 21st century at 3.0 W/m² and declining afterwards [van Vuuren et al., 2007].

Region	27N-72N, 22W-45E
Control Period	1951-2005
Scenario	2006-2100
Spatial Resolution	EUR-11 (0.11 degree) / EUR-44 (0.44 degree)

Table 4.1: EURO-CORDEX simulations characteristics

SCENARIO	RCM	GCM	RESOLUTION
RCA4/MIROC	RCA4	MIROC-MIROC5	0.44 degree
RCA4/NCC	RCA4	NCC-NorESM1-M	0.44 degree
RCA4/NOAA	RCA4	NOAA-GFSL-GFDL-ESM2M	0.44 degree
RCA4/CCC	RCA4	CCCma-CanESM2	0.44 degree
RCA4/CNRM	RCA4	CNRM-CERFACS-CNRM-CM5	0.11 degree
RCA4/ICHEC	RCA4	ICHEC-EC-EARTH	0.11 degree
RACMO/ICHEC	RACMO22E	ICHEC-EC-EARTH	0.11 degree
HIRHAM/ICHEC	HIRHAM5	ICHEC-EC-EARTH	0.11 degree
CCLM/ICHEC	CCLM 4-8-17	ICHEC-EC-EARTH	0.11 degree
CCLM/MPI	CCLM 4-8-17	MPI-M-MPI-ESM-LR	0.11 degree
REMO/MPI	REMO2009	MPI-M-MPI-ESM-LR	0.11 degree

Table 4.2: Climate scenarios characteristics

4.2 SELECTED SCENARIOS

We retrieve the climate scenarios trying to consider the highest possible number of **GCMs** and **RCMs** combinations and **RCPs** in order to better represent the climate scenario uncertainty. Out of the three available **RCPs** considered in the EURO-CORDEX project, only two (**RCP4.5** and **RCP8.5**) are taken into account whereas the so-called “peak-and-decline” scenario (**RCP2.6**) was not available in a sufficient number of simulations and thus not comparable with the former two. We select a daily time resolution and the two variables of interest: precipitation and temperature. We download in total twenty-two scenarios and consider them in the analysis. They include two different Representative Concentration Pathways, five Regional Circulation Models (REMO, RCA4, RACMO, HIRHAM, CCLM) and seven General Circulation Models (MPI, NOAA, NCC, CCC, ICHEC, MPI, MIROC) as shown in Table 4.2. The original European domain is cut over the region of interest, the Lake Como catchment and the surrounding areas as shown in Figure 4.1 and Figure 4.2. Regarding the length of the time horizon, we take into account the complete EURO-CORDEX scenario, which begins in 2006 and ends in 2100, and use it through the entire analysis.

Table 4.3 shows the available climate scenarios, represented as combinations of **GCM** and **RCM**. The columns represent the **RCMs** and the rows indicate the **GCMs**, while in the single cells is written the spatial resolution of the simulation, if available. The large number of empty cells in the table shows that the most of the possible combinations between **GCM** and **RCM** are not available. This aspect has a negative impact on the uncertainty characterization carried out in Chapter 7, limiting the analysis that can be done.

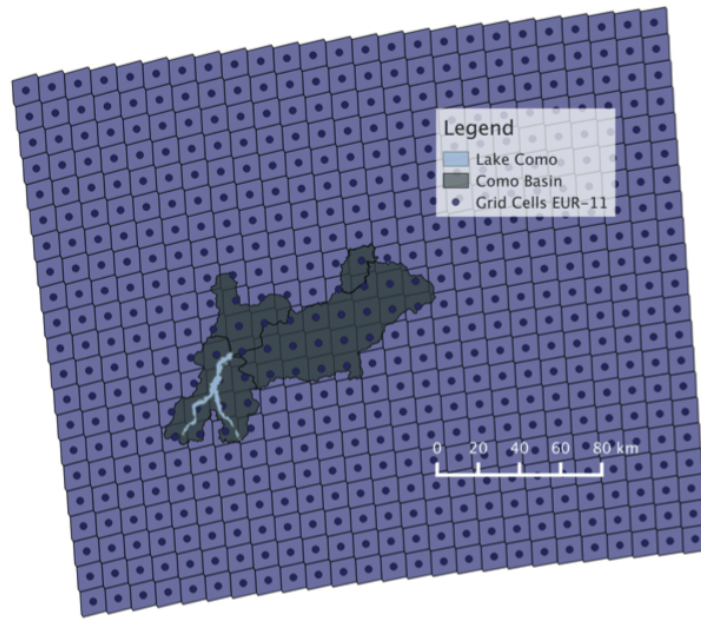


Figure 4.1: EUR-11 resolution over the area of interest

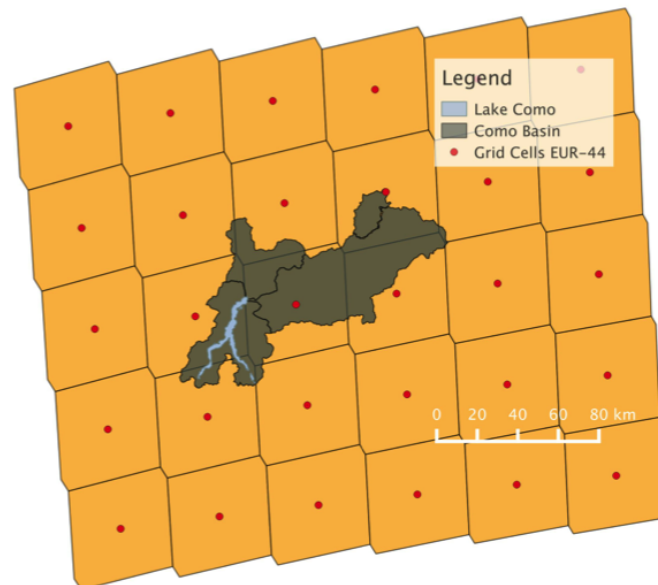


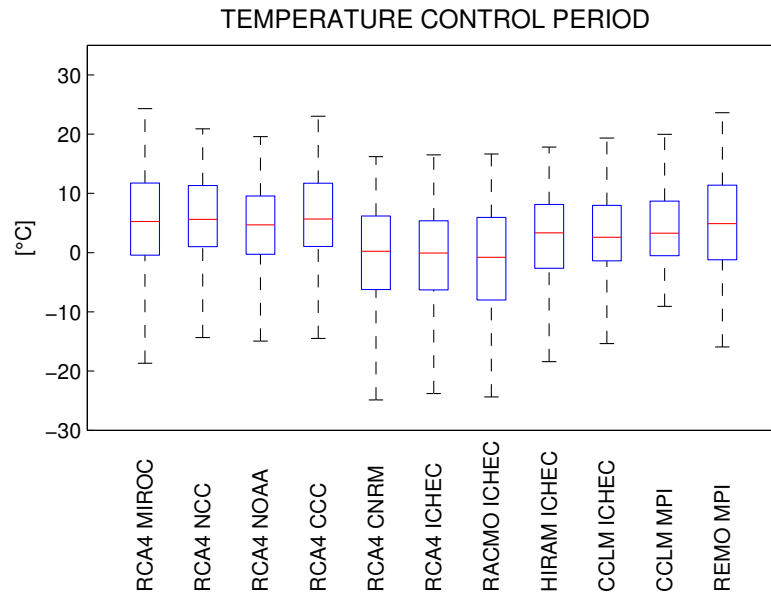
Figure 4.2: EUR-44 resolution over the area of interest

	RCA4	CCLM	HIRHAM	RACMO	REMO
MIROC	0.44	-	-	-	-
NCC	0.44	-	-	-	-
NOAA	0.44	-	-	-	-
CCC	0.44	-	-	-	-
CNRM	0.11	-	-	-	-
ICHEC	0.11	0.11	0.11	0.11	-
MPI	-	0.11	-	-	0.11

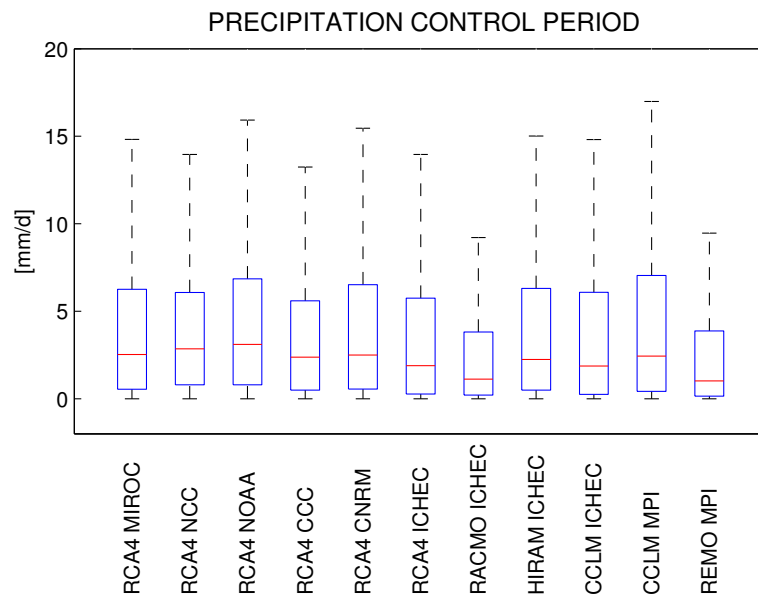
Table 4.3: Combinations of EURO-CORDEX climate scenarios. The RCMs are shown in the first row, while the GCMs are represented in the first column. All the climate scenarios listed here are available in both RCP4.5 and RCP8.5.

4.3 STATISTICAL ANALYSIS OF THE EURO-CORDEX SCENARIOS

We conduct a statistical analysis on the climate scenarios in order to characterize the predicted changes in temperature and precipitation over the area of interest. The main objective of this analysis is the understanding of the differences between current climate and future scenarios, predicted by the different climate models. In order to do that we carry out an analysis on the temperature and precipitation time series, together with spatial and interannual plots. First we calculate some statistics, summarizing them in boxplots, and analyze similarities and eventual clusters among the climate models. Then some spatial plots are analyzed in order to gain some more information on the spatial distribution of the climate change over the domain of interest. In order to do so, we plot the map of the Lake Como catchment over a raster plot representing the cells of the climate models considered in the analysis. Finally the focus is moved to the seasonal behaviour, calculating a cyclostationary average with a tool named Moving Average over Shifting Horizon ([MASH](#)) [[Anghileri et al., 2014](#)], which facilitates the detection of trends in the two climate variables within the year. The [MASH](#) tool is helpful for the analysis of changes in the seasonal pattern of precipitation and temperature. The first clear aspect that we see is a high variability within the different climate model scenarios for both the variables, even when considering only the control period. The variability among the different models can be seen in the boxplots in [Figures 4.3, 4.4, and 4.5](#), which show the statistics computed over the entire period simulated by each scenario. All the models agree in predicting a rise in the mean of temperature and its first and third quantiles. Specifically, the mean temperature over the scenario horizon is expected to increase between 1°C and 4°C . When looking at main statistics only, it is harder to detect changes in precipitation ([Figures 4.4b and 4.5b](#)). Most of the scenarios show a slight increase in the mean annual precipitation, but the rest predicts lower values.

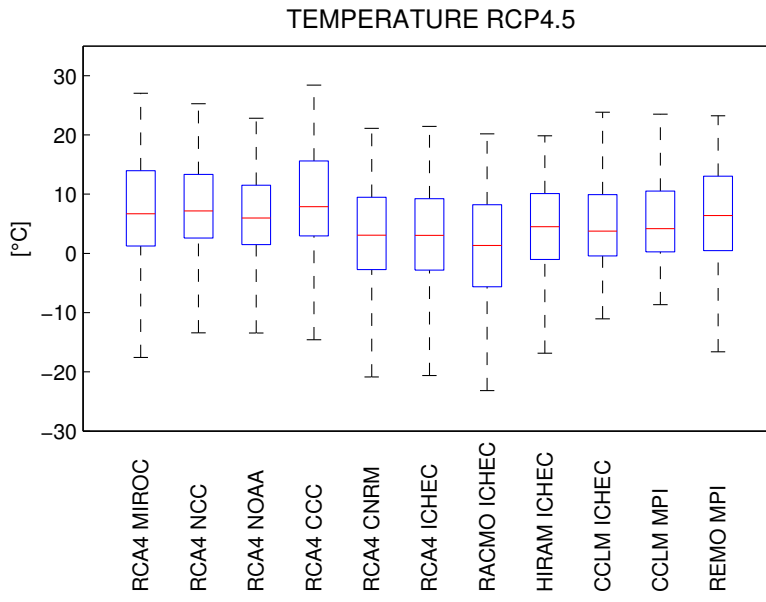


(a)

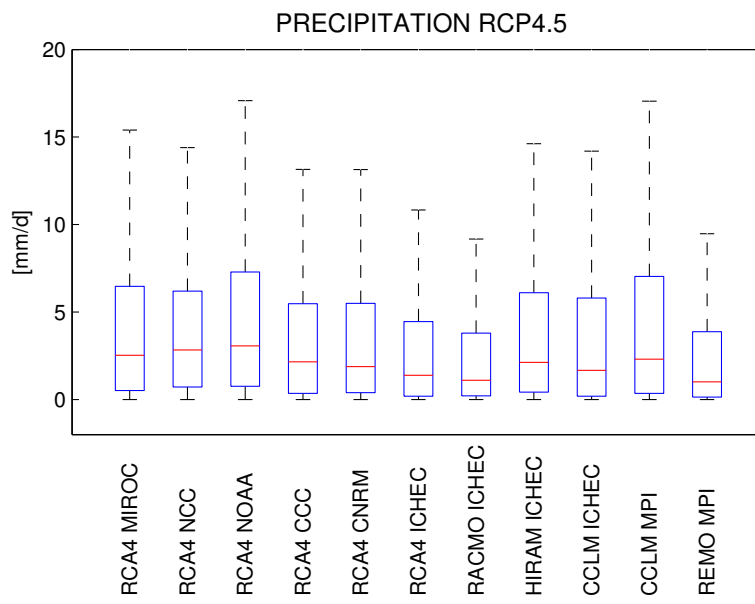


(b)

Figure 4.3: Boxplot temperature and precipitation control period

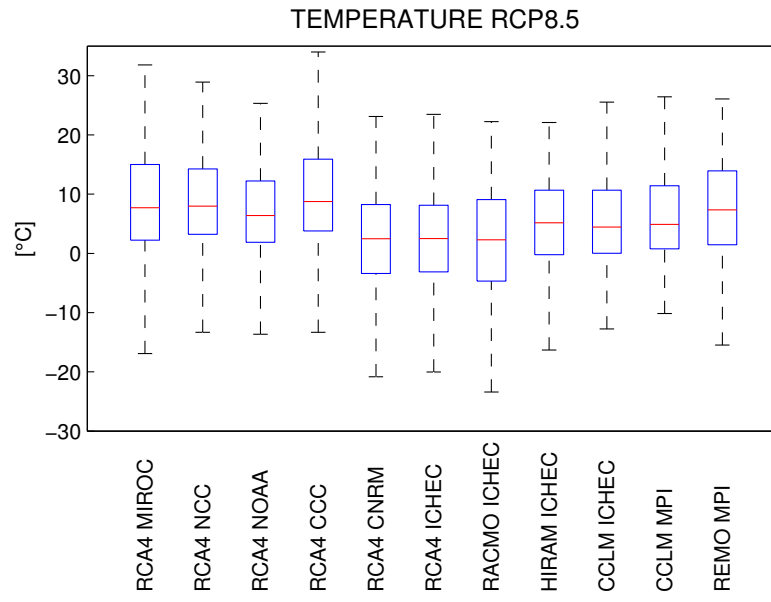


(a)

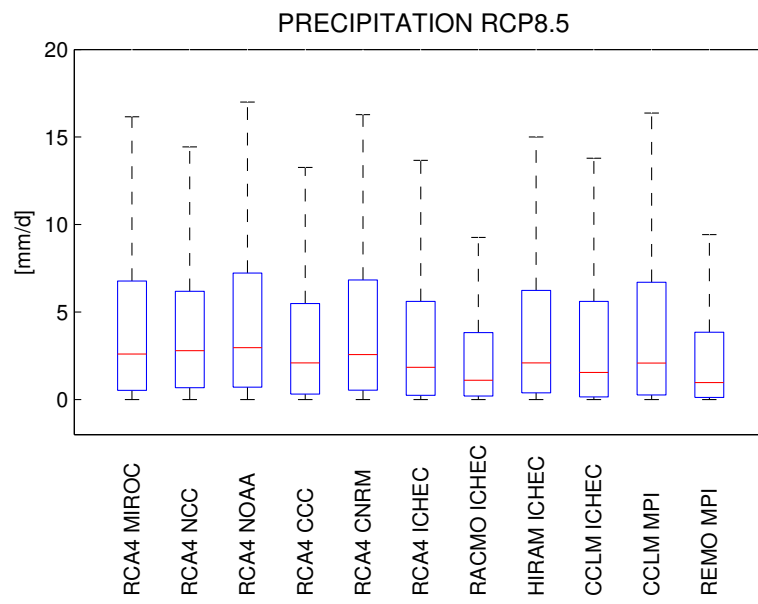


(b)

Figure 4.4: Boxplot temperature and precipitation RCP4.5



(a)



(b)

Figure 4.5: Boxplot temperature and precipitation RCP8.5

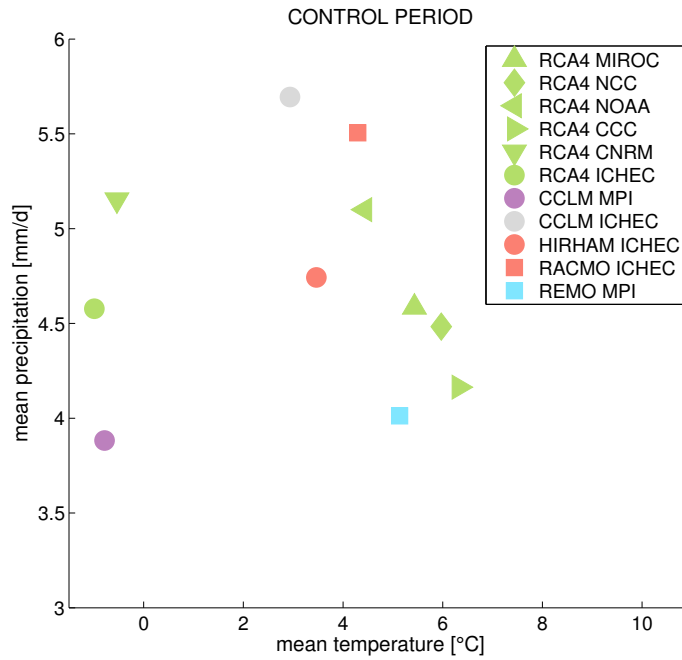


Figure 4.6: Climate models mean precipitation and temperature over the control period. Different GCMs are represented by different symbols, while different RCMs are represented by different colors.

We plot also the mean values of temperature and precipitation in order to assess the existence of clusters of scenarios having a similar behavior. The plots in Figures 4.6, 4.7, and 4.8 allow to identify warmer or colder and drier or wetter scenarios. The scenarios are equally spread over the graph, suggesting that there are no clearly distinguishable clusters. However, looking at the single dots, we can identify the models predicting the extreme scenarios. For instance, the scenarios REMO/MPI and RCA₄/CCC predict under both RCPs, drier and warmer climates, while the scenario RCA₄/CNRM predicts wetter and colder ones. Conversely, the scenario RACMO/ICHEC indicates always a drier and colder climate compared to the other ones.

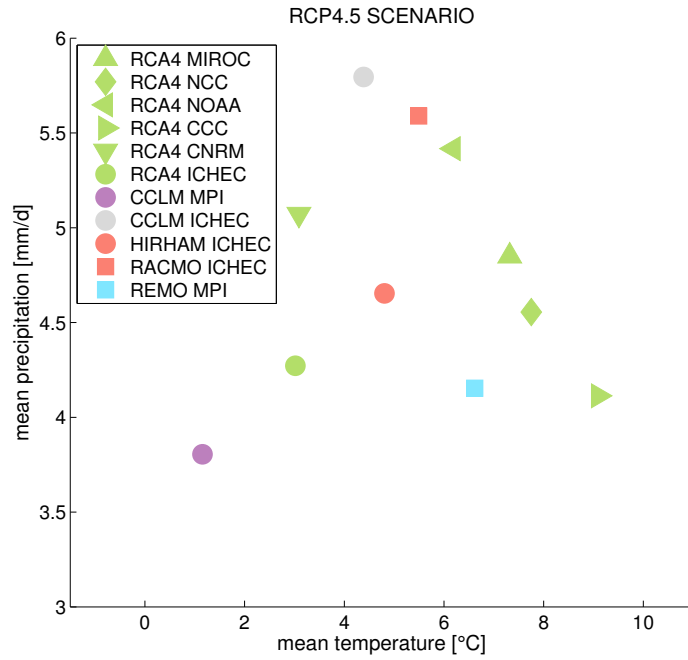


Figure 4.7: Climate models mean precipitation and temperature over the RCP4.5 Scenario (2006-2100). Different GCMs are represented by different symbols, while different RCMs are represented by different colors.

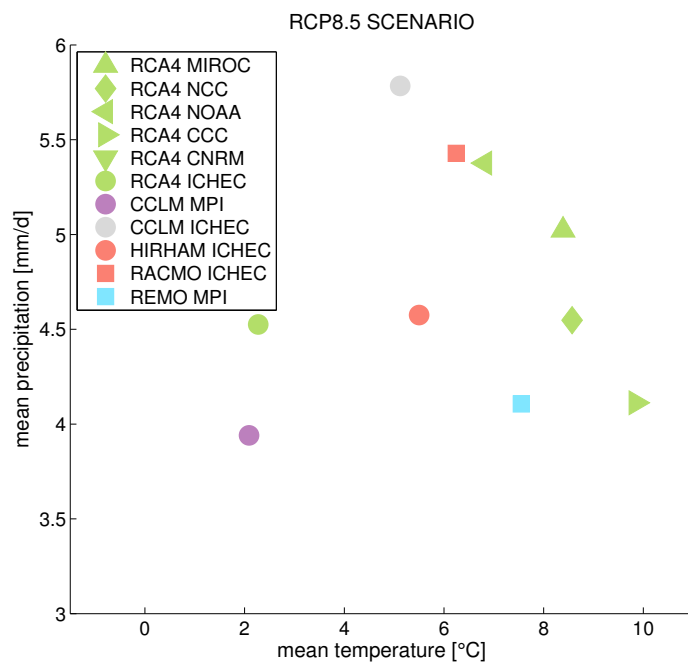


Figure 4.8: Climate models mean precipitation and temperature over the RCP8.5 Scenario (2006-2100). Different GCMs are represented by different symbols, while different RCMs are represented by different colors.

The spatial variability of the climate change within the area of interest is assessed through some raster plots, where the climate variables are plotted over the domain in different color shades. We separate the scenario's horizon in four sub-periods of twenty years starting from 2021 (2021-2040, 2041-2060, 2061-2080, and 2081-2100). In Figure 4.9 the differences in mean temperature between the sub-periods and the control period (1951-2005) for the scenario RCA4/NCC (taken as an example for the entire ensemble) are plotted, forced by both the RCPs. Figure 4.9 shows that the temperature's increasing trend is visible on the entire domain and that under the RCP8.5 this tendency has a higher intensity. Regarding the mean precipitation, the relative difference $((x_{scen} - x_{ctrl})/x_{ctrl})$, with x representing the mean daily precipitation, is calculated and plotted over the domain. Figure 4.10 shows a slight increase in precipitation over most of the cells compared to the control period. However, precipitation is predicted to decrease in other cells of the domain. Unlike temperature, with precipitation we can not detect a clear trend, and the RCP8.5 is not an intensification of the RCP4.5, but predicts different temporal evolutions. An indicator describing changes in the frequency of heavy precipitation events is RR30 [Frei et al., 1998]. The RR30 index represents the frequency of days with a precipitation over 30 mm of rain

$$RR30 = \text{Ndays}_{(\text{rain} > 30\text{mm})} / \text{Ndays}$$

where Ndays is the total number of days and $\text{Ndays}_{(\text{rain} > 30\text{mm})}$ is the number of days in which the precipitation exceeds 30 mm. In Figure 4.11 the relative difference of the indicator RR30 is plotted over the domain during the four sub-periods already described. We can see that an increase of approximately 20% in heavy precipitation events is expected over the domain of interest in the majority of the cells for the model RCA4/NCC fed by the RCP4.5 scenario, while for the RCP8.5 scenario this increase goes up to 30%. The two RCPs are concordant in predicting an increase of heavy precipitation events and the RCP8.5 shows a more intense rise compared to the RCP4.5.

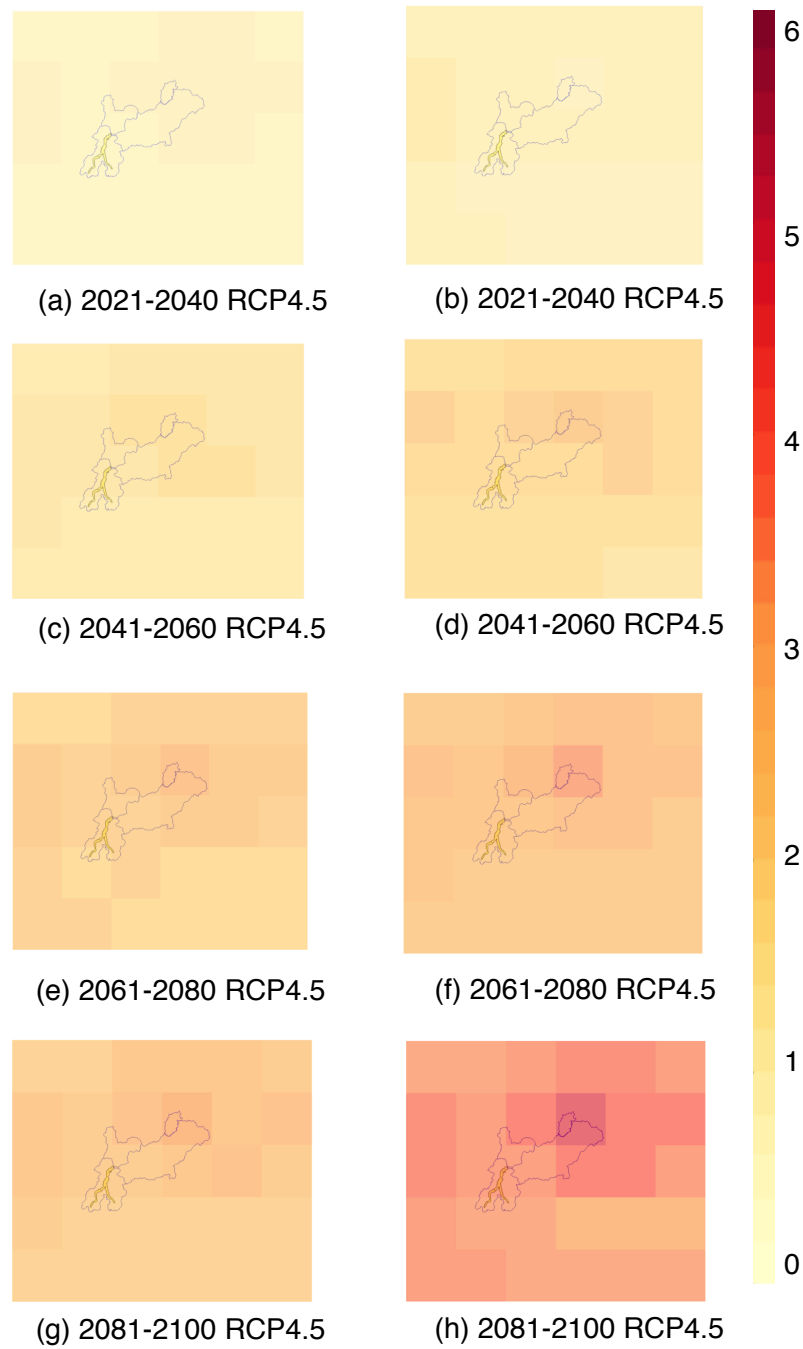


Figure 4.9: Changes in mean temperature ($^{\circ}$ C) of RCA₄/NCC between control period and future scenario.

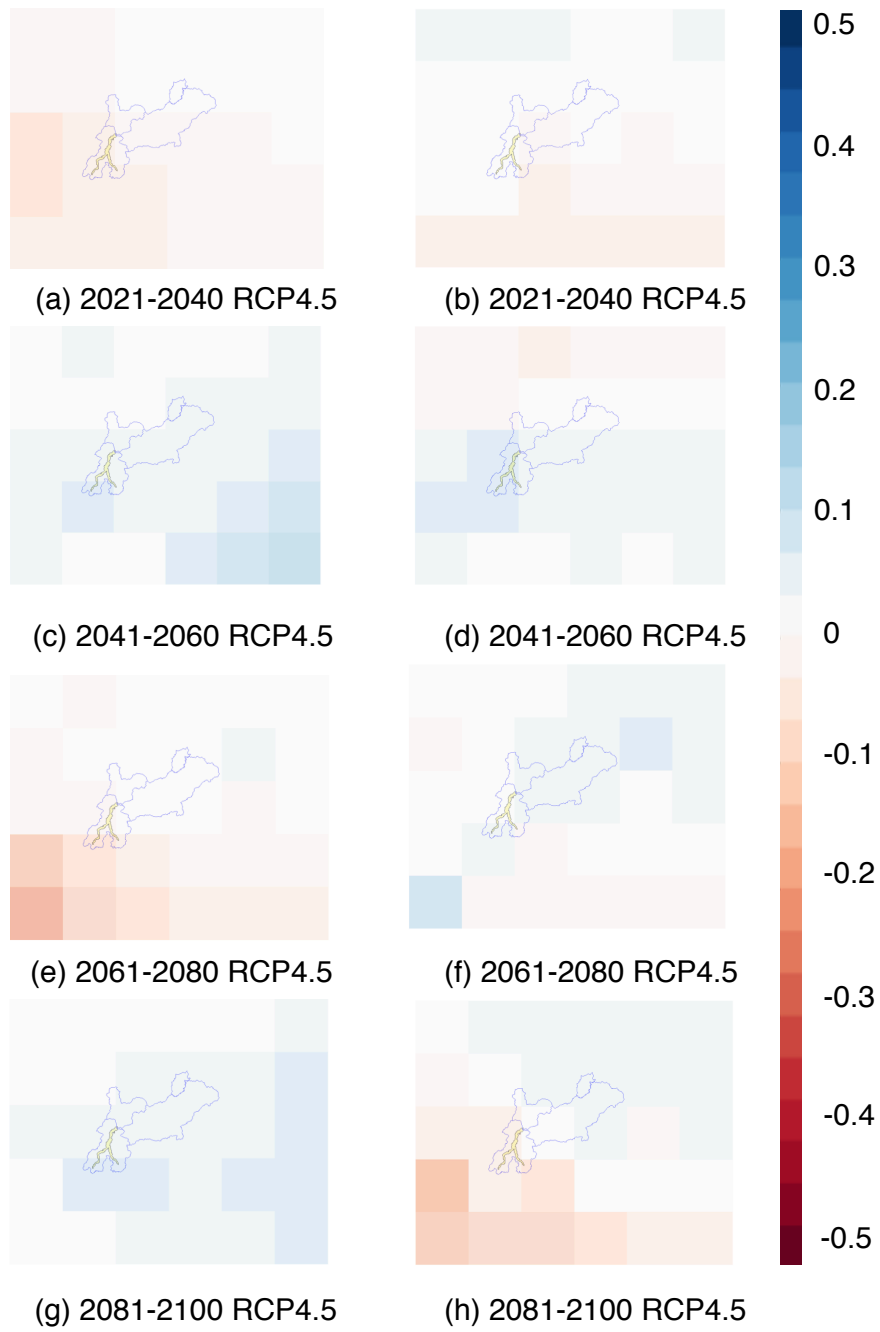


Figure 4.10: Relative difference in mean precipitation (-) for RCA₄/NCC between control period and future scenario.

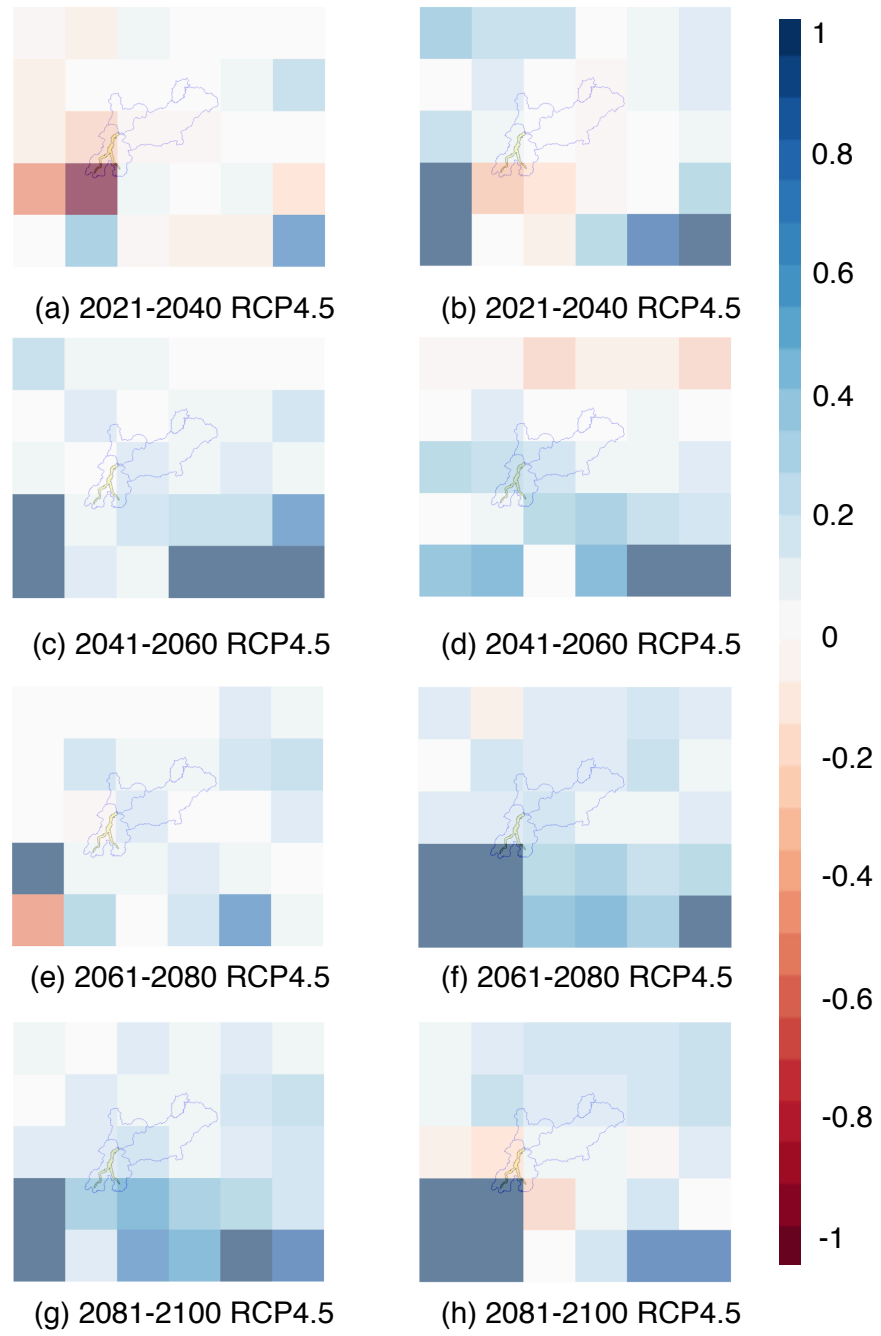


Figure 4.11: Relative difference in RR30 for RCA4/NCC between control period and future scenario.

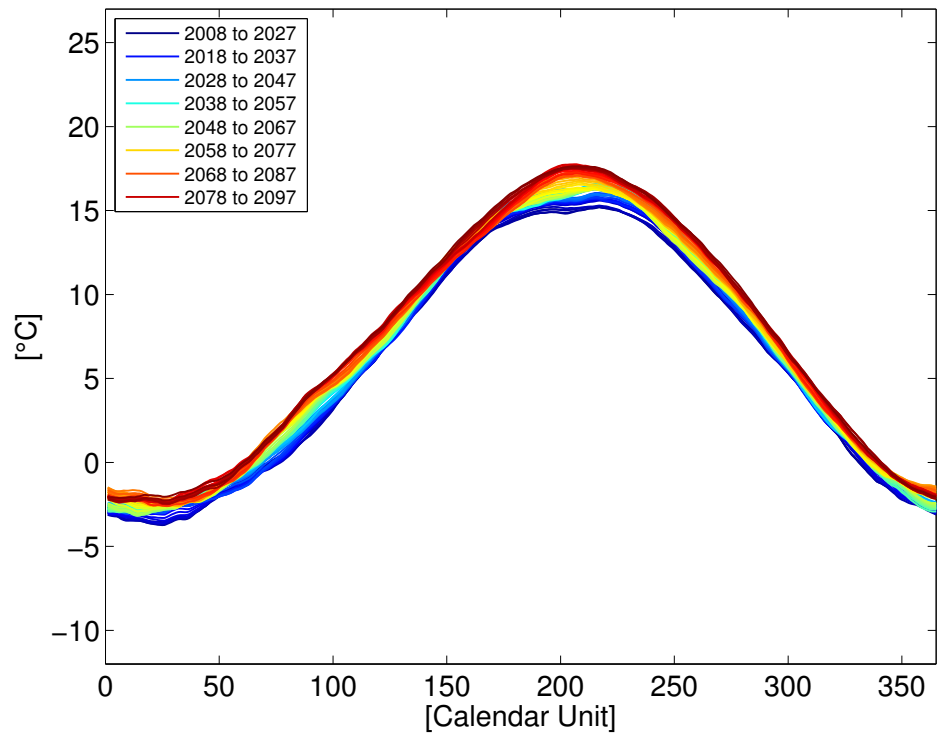
In this thesis, among the several analysis methods, we use the **MASH** tool [Anghileri et al., 2014]. The **MASH** is a novel visual method, which allows detecting trends in climate and hydrological variables, showing changes in seasonal patterns. The **MASH** consists of averaging the daily values over consecutive days in the same year (considering always 365 days per year) and over the same days for consecutive years, shifting progressively the horizon. The **MASH** can therefore be considered as the following matrix

$$\text{MASH} = \begin{bmatrix} \mu_{1,1} & \mu_{1,2} & \dots & \mu_{1,N_h} \\ \mu_{2,1} & \mu_{2,2} & \dots & \mu_{2,N_h} \\ \dots & \dots & \dots & \dots \\ \mu_{365,1} & \mu_{365,2} & \dots & \mu_{365,N_h} \end{bmatrix}$$

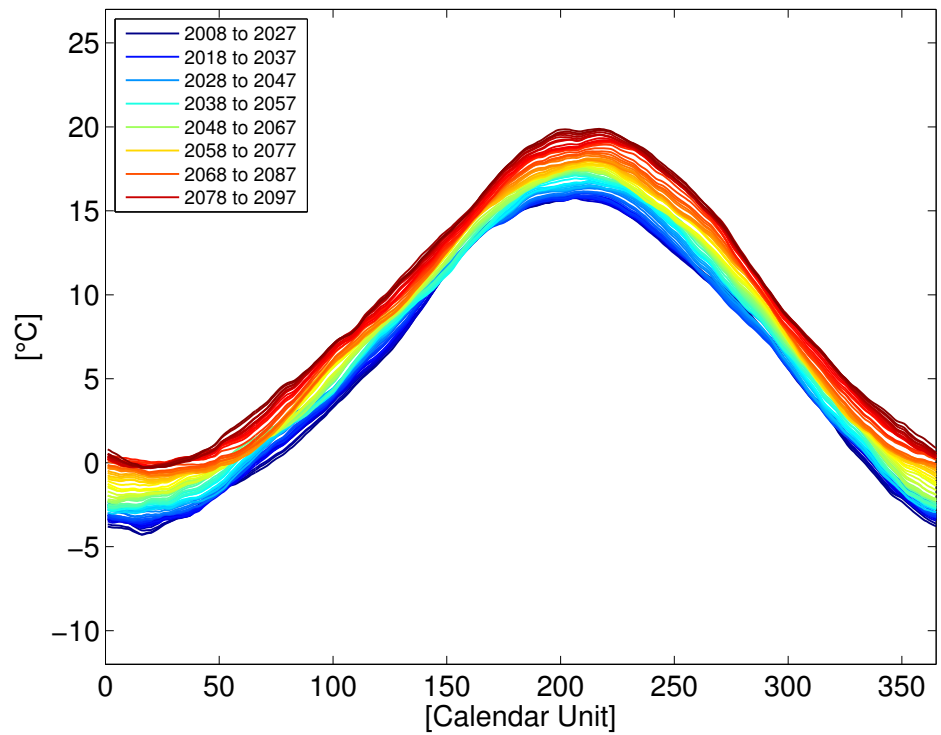
where each element is the average daily flow on the t^{th} day of the year over the h^{th} horizon, calculated as follows

$$\mu_{t,h} = \underset{y \in [h, h+Y-1]}{\text{mean}} \left[\underset{d \in [t-w, t+w]}{\text{mean}} X_{d,y} \right]$$

where $X_{d,y}$ is the value of the variable of interest at day d and year y . Y is a parameter representing the number of years averaged together, in the formula from year h to year $h + Y - 1$. w is the parameter related to the day-to-day variability and total number of days averaged together is $2 * w + 1$ (from day $t - w$ to day $t + w$, as shown in the formula). In our analysis we set the parameters Y to 20, considered to be large enough to filter out the natural climate variability. The parameter w , related to the daily variability, was set to 15 (namely averaging over 31 days), considered to be a good compromise between filtering the day-to-day variability and preserving the natural seasonal patterns. Figures 4.12, 4.13, 4.14, and 4.15 show the **MASH** plots for two climate scenarios of the variables of temperature and precipitation under the RCP4.5 and RCP8.5 over the XXI century time horizon. The two scenarios REMO/MPI and RACMO/ICHEC are chosen as representative of the entire ensemble. The graphs of the remaining scenarios are reported in Appendix A. Within the scenario time horizon, we see the increase in temperature, which has a positive sign in all seasons and is always higher in graphs related to the RCP8.5 (Figures 4.12b and 4.14b). Regarding the precipitation, most of the scenarios analyzed show a decrease in the summer months and an increase in winter, as shown in Figures 4.13a to 4.15b for the representative scenarios REMO/MPI and RACMO/ICHEC. The intensity of this seasonal shift is higher for the RCP8.5, as shown for instance in Figure 4.13b for the scenario REMO/MPI. Similar changes were already detected in other works on the Alpine region, for example in Gobiet et al. [2014].

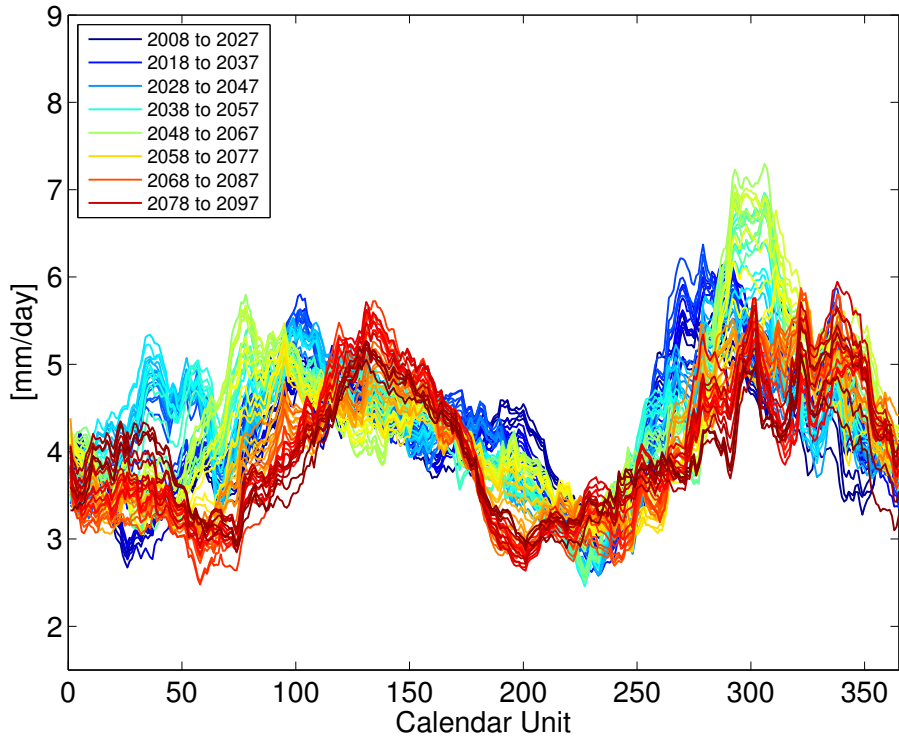


(a) RCP4.5

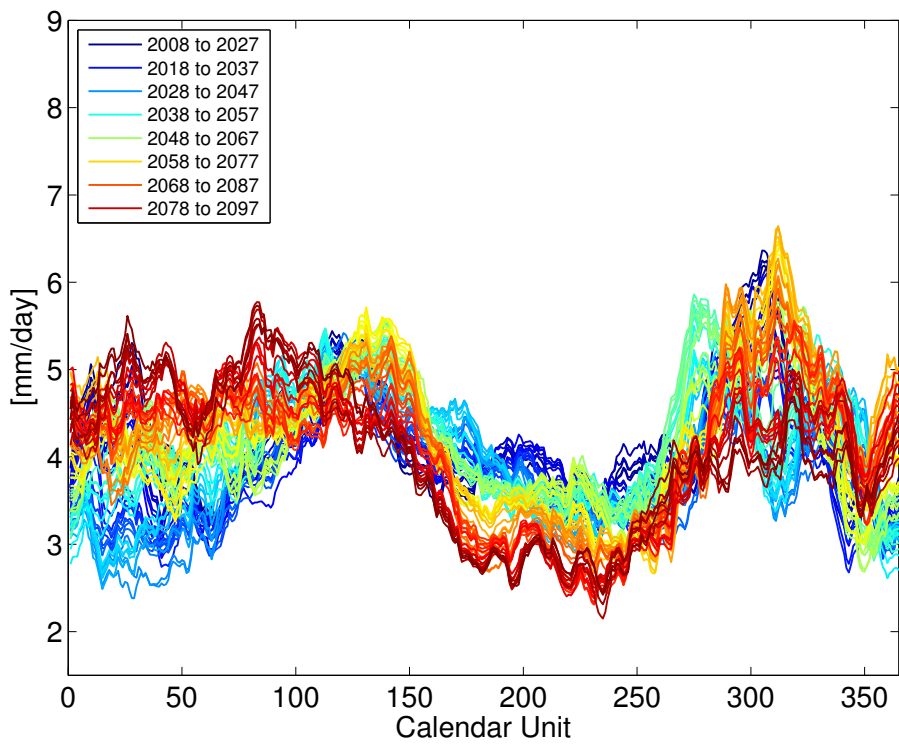


(b) RCP8.5

Figure 4.12: Temperature MASH of REMO/MPI

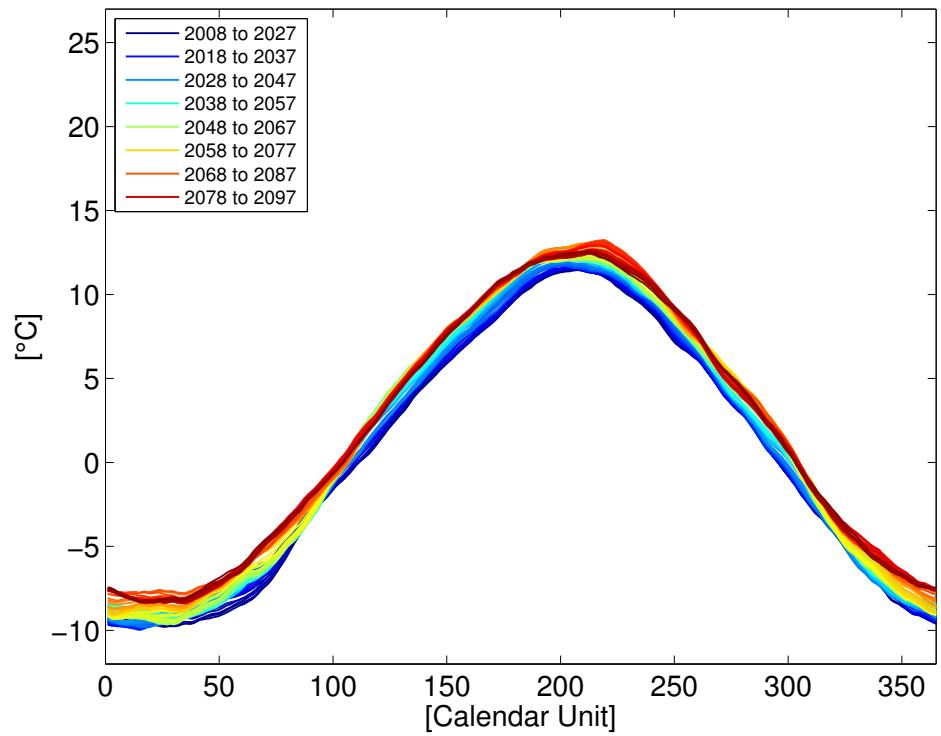


(a) RCP4.5

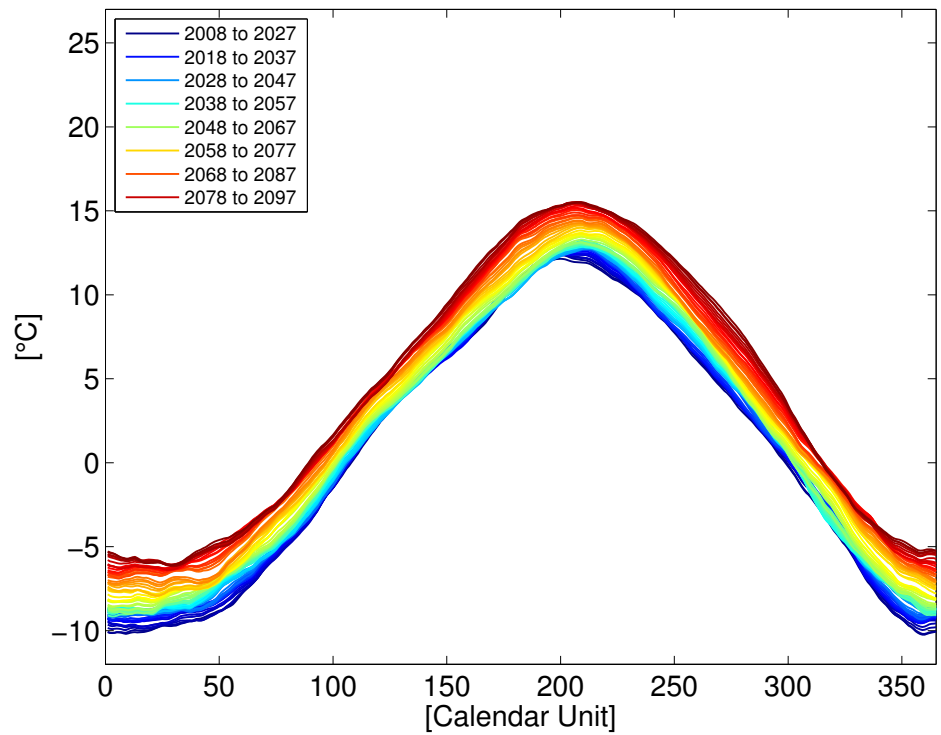


(b) RCP8.5

Figure 4.13: Precipitation *MASH* of REMO/MPI

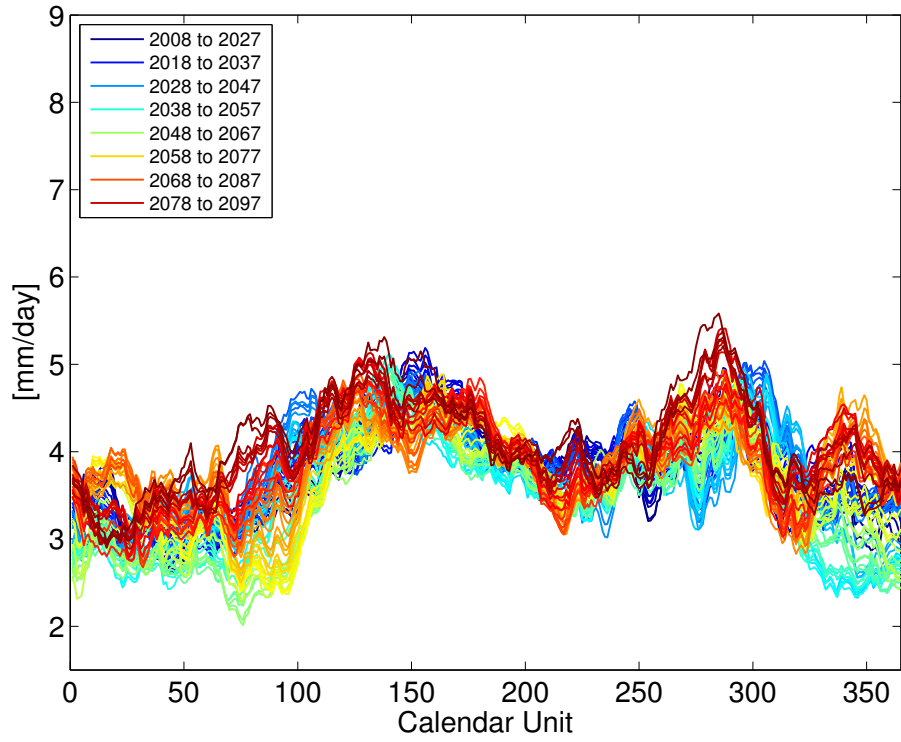


(a) RCP4.5

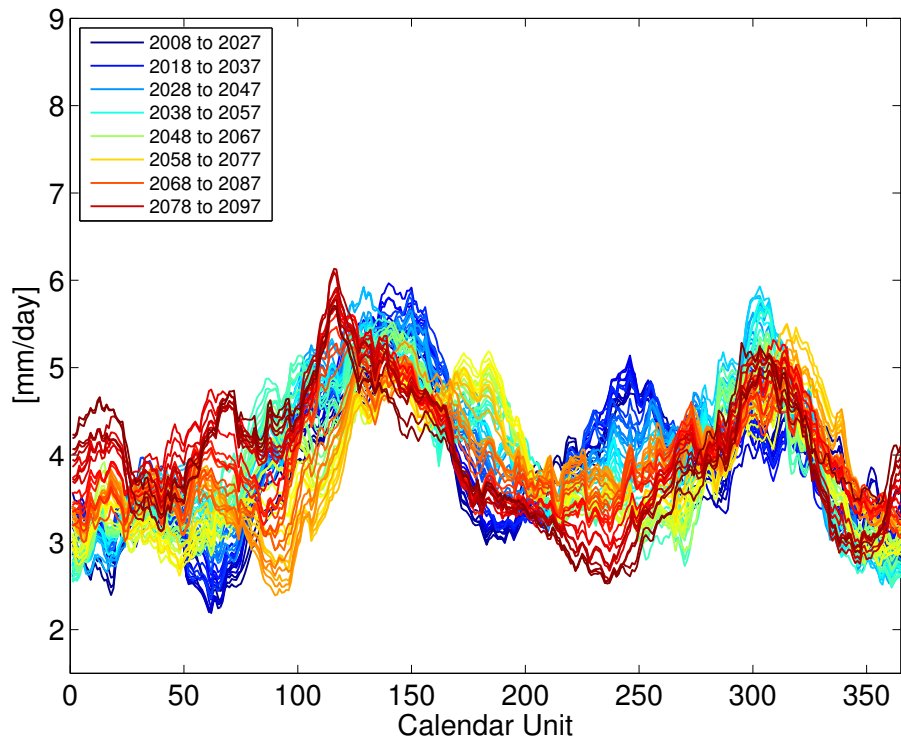


(b) RCP8.5

Figure 4.14: Temperature MASH of RACMO/ICHEC



(a) RCP4.5



(b) RCP8.5

Figure 4.15: Precipitation MASH of RACMO/ICHEC

STATISTICAL DOWNSCALING

5.1 HISTORICAL CLIMATE OBSERVATIONS

As described in Chapter 2, in order to downscale the climate change scenarios we need historical climate observations on a sufficiently long time horizon. The historical observations used in this analysis are taken from the temperature stations belonging to ARPA and from a high-resolution grid precipitation dataset distributed by the Swiss Federal Office of Meteorology and Climatology, MeteoSwiss (Figure 5.1). The ARPA meteorological network consists of several stations with daily and hourly time resolution located in Lombardia. We choose the stations with a long time series and with a good record quality. The results of this selection are the time series of mean daily temperature from 1988 to 2001 recorded in Sondrio, Chiavenna, Scais and Santa Caterina (Figure 5.1). The precipitation grid dataset is the result of a trans-national analysis that has been carried out collecting information from precipitation gauges over the Alpine area in seven countries (Italy, Switzerland, Austria, Germany, France, Slovenia, and Croatia) with approximately 5500 measurements per day from 1971 to 2008 [Isotta et al., 2014]. The result is a high-resolution grid (5 Km), over a domain that encompasses approximately 1200 km from France to Austria and over 700 km from southern Germany to northern Italy, including parts of the territory of Slovenia and Croatia. The grid cells that intersect the Lake Como catchment are 247 (Figure 5.1).

5.2 STATISTICAL DOWNSCALING VIA QUANTILE MAPPING

We adopt a simple and efficient procedure to carry out the downscaling of the climate model outputs. We associate the closest EURO-CORDEX cell to every single ARPA weather stations and grid cell of the Alpine dataset. We carry out this assignment twice, once with EURO-CORDEX coarser resolution (0.44 degree) and once with the finer one (0.11 degree). We perform the assignment in order to be able to carry out the downscaling of the climate model on every point of the Alpine precipitation grid and on every temperature gauge. After assigning a predictor (large-scale output of the climate models) to every predictand (small scale variable of the climate observations), the Quantile Mapping method is applied, computing the quantile curves. As an example, Figure 5.2 shows the quantile-quantile plot of the EURO-CORDEX cell in the EUR-44 resolution over the period 1988-2001 (model RCA4/MIROC) and the temperature time series of

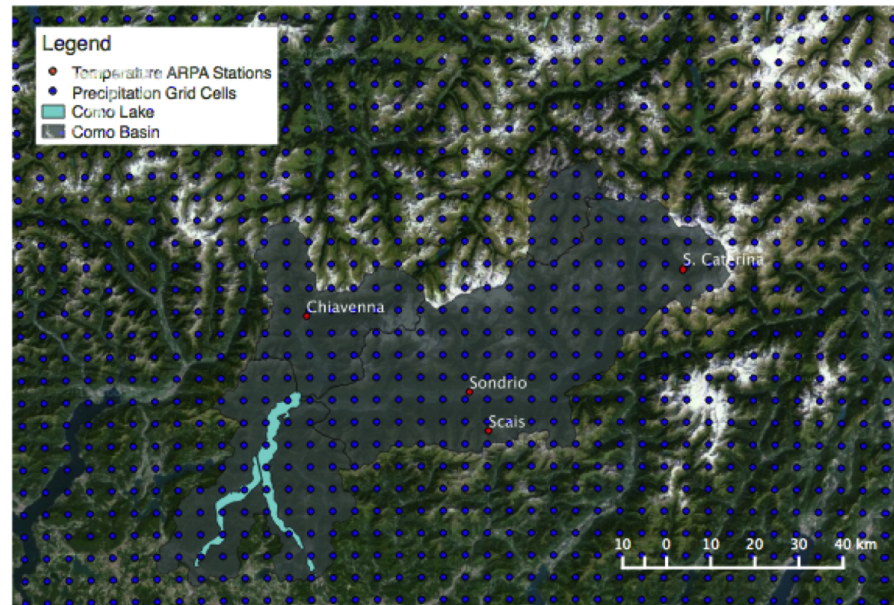


Figure 5.1: Precipitation Grid Cells and ARPA Temperature stations

the nearest weather station (Chiavenna). We see that, in this case, the climate model underestimates the observations and it does it more intensely for low temperature.

5.3 STATISTICAL ANALYSIS OF THE DOWNSCALED SCENARIOS

After the downscaling phase a brief statistical analysis is carried out. The goal of this part of the work is to examine if the downscaled scenarios are consistent with the original climate model outputs and if the expected effects of the bias removal are observed. The bias removal should reduce the differences in the average behaviour among the model scenarios in the control period and consequently also in the future scenarios, if we suppose that the model errors of the GCM/RCM are constant over the past and over the future. This effect can be seen in Figures 5.3 and 5.4, where the mean precipitation and the mean temperature of all the model scenarios are plotted on a graph. Compared to what shown in Chapter 4, we see that the behaviour of the different models over the future scenario, even considering both the RCPs, is less spread (w.r.t. Figures 4.7 and 4.8) and contained in a smaller region of the graph with mean temperature between 7°C and 10°C . The same range for mean daily precipitation varies approximately from 3.35 to 4.25 mm/d, corresponding to yearly precipitation values between 1200 and 1550 mm/y.

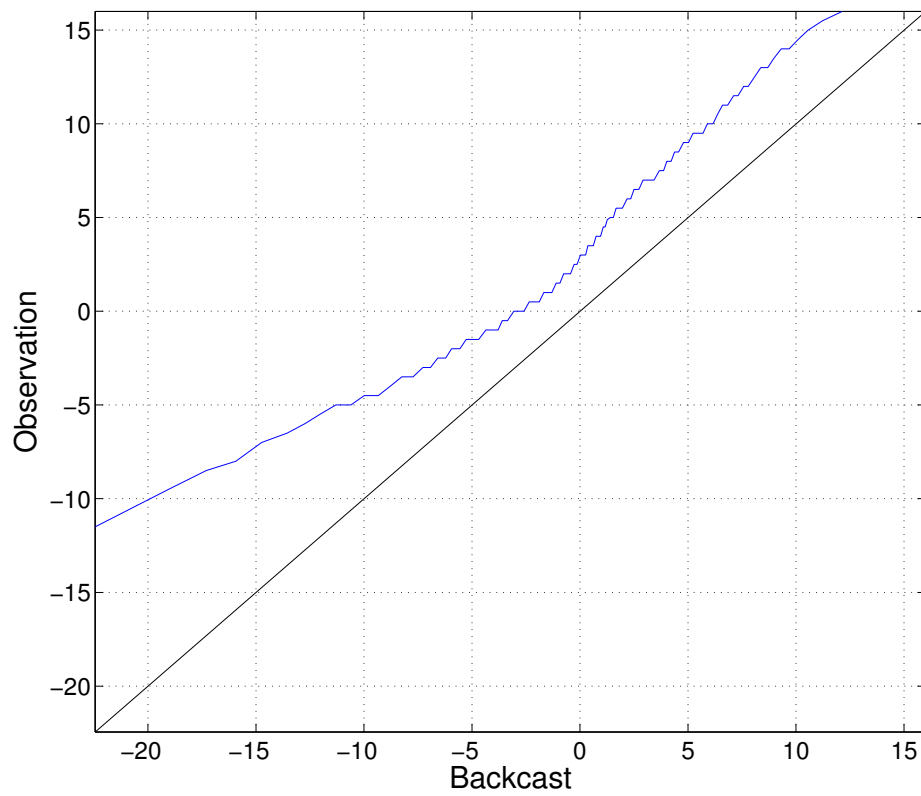


Figure 5.2: Quantile-quantile plot of the Chiavenna temperature station and its predictor for the model RCA4/MIROC forced by the RCP4.5

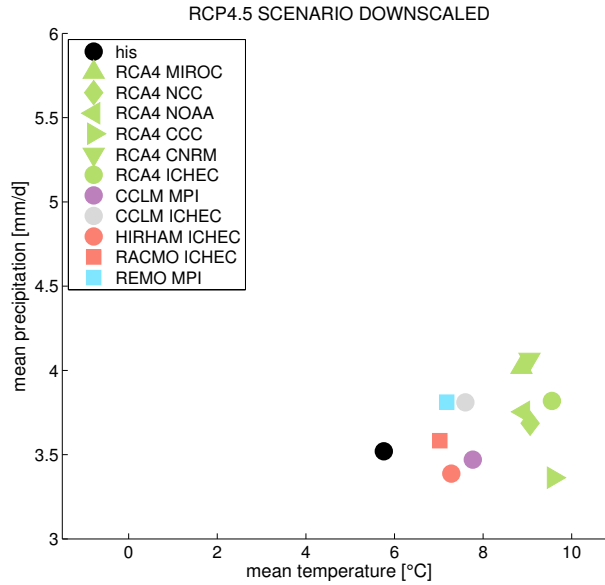


Figure 5.3: Mean values of temperature (x-axis) and precipitation (y-axis) for all the downscaled scenarios fed by the RCP4.5 over the time horizon 2006-2100. Different GCMs are represented by different symbols, while different RCMs are represented by different colors.

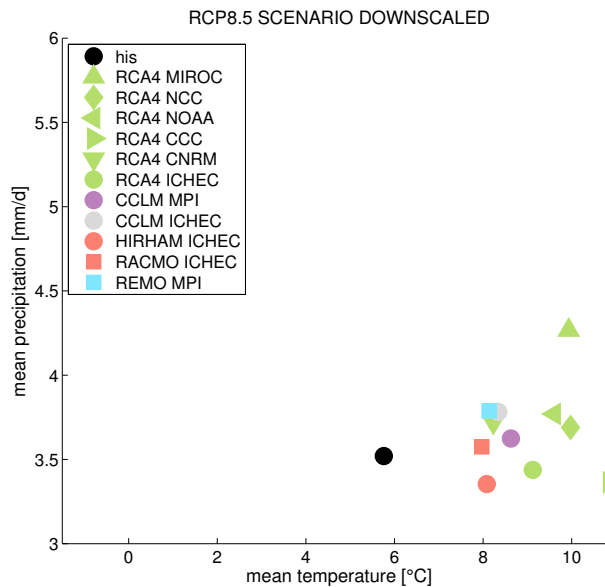


Figure 5.4: Mean values of temperature (x-axis) and precipitation (y-axis) for all the downscaled scenarios fed by the RCP8.5 over the time horizon 2006-2100. Different GCMs are represented by different symbols, while different RCMs are represented by different colors.

The raster plot shown in Figure 5.5 shows clearly the increasing trend in temperature, while for the precipitation indicated in Figure 5.6 it is more difficult to detect a trend in the average yearly behaviour. A further detail that can be clearly seen, both in the temperature raster plot and in the Figures 5.3 and 5.4, is how the Regional Circulation Model RCA₄, which is the one with the largest number of simulations available, is also the one that predicts the highest increase in temperature.

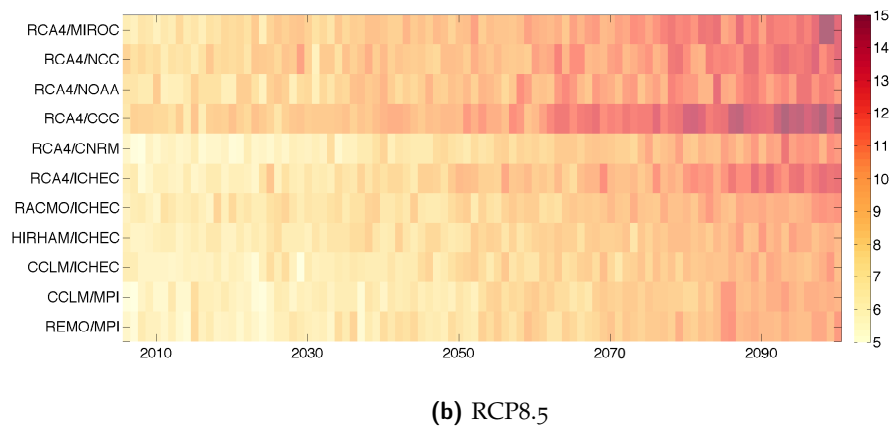
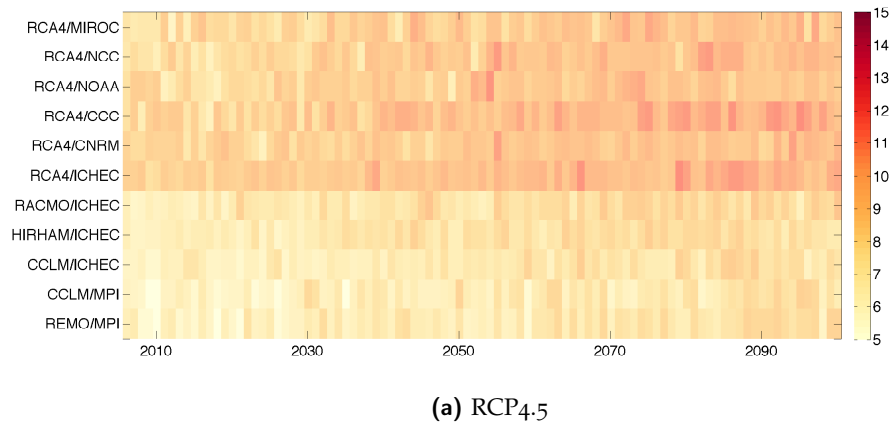
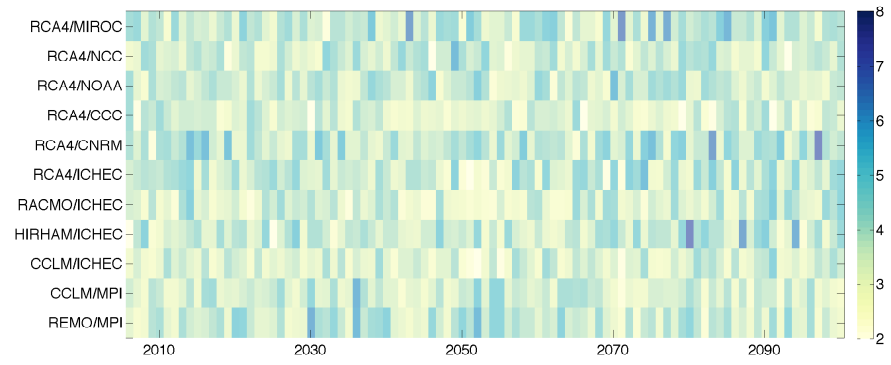
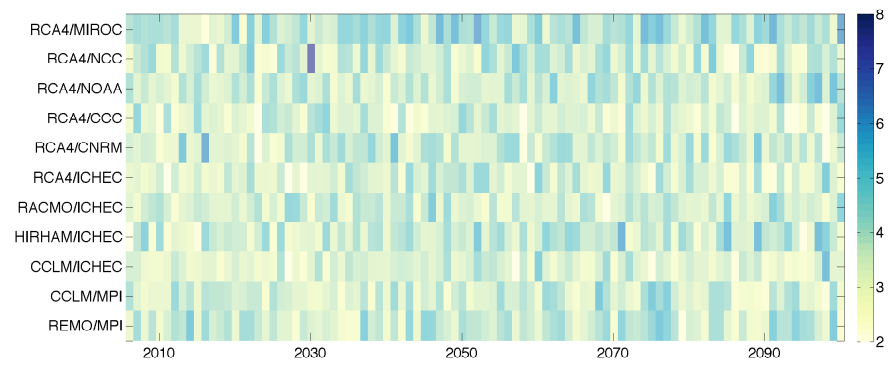


Figure 5.5: Annual mean values of temperature calculated for the down-scaled scenarios [$^{\circ}$ C]



(a) RCP4.5



(b) RCP8.5

Figure 5.6: Annual mean values of precipitation calculated for the down-scaled scenarios [mm/d]

6.1 TOPKAPI-ETH SETUP

The following step of the thesis involves the understanding of the climate change impact on the hydrology of the Lake Como catchment. As already shown in Chapter 2, in order to fully understand the relationship between changes in climate and hydrological regime, it is necessary to consider a model that describes the physical processes affecting the hydrological cycle in an Alpine environment (e.g., evapotranspiration, snowmelt, and glacier dynamics). We use Topkapi-ETH (TE), a physically-based and fully distributed hydrological model that provides the possibility to account for anthropogenic infrastructures such as reservoirs and river diversions, which play a key role in the study site. The importance of employing a spatially distributed model is due to the possibility of assessing the hydrological response to climate change in every single area of the catchment, allowing spatial analyses on river network, glaciers, and hydropower reservoirs. Moreover, the spatial analysis could be extended to the assessment of mitigation measures on other water-related activities, for instance flood protection, ecosystem conservation, and agriculture. TE represents a good trade-off between computational time, required to run the model, and a thorough description of hydrological processes. We implement the model on a spatial grid of 250 m, which represents a good compromise between a reasonable computational time (given the large number of climate scenarios which has to be simulated) and an accurate topographic description of the complex Alpine terrain. The model requires a description of several spatial characteristics of the catchment: a Digital Elevation Model (DEM), a soil map, a land cover map, a glaciers map, a glaciers depth map, and the maps of the Thiessen polygons of the weather stations of temperature, precipitation, and cloud cover transmissivity.

6.1.1 *Digital Elevation Model*

The Digital Elevation Model is obtained from the Shuttle Radar Topography Mission (SRTM), a space mission coordinated by National Aeronautics and Space Administration (NASA) and National Geospatial-Intelligence Agency (NGA). The data has an original resolution of 1 arc-second (approximately 30 m) and was retrieved in GeoTIFF format from the United States Geological Survey (USGS) website, see Fig-

ure 6.1. A DEM is required in Topkapi-ETH to extract information about the catchment area, the flow direction, and the river network.

6.1.2 Soil Map

Considering the location of the basin, which extends over two countries, the information concerning soil is obtained from two different sources and then merged together within a Geographical Information System (GIS). For the Italian part of the domain, the soil map is provided by the local ARPA. For the Swiss part we retrieve the Bodeneignuskarte from the Swiss Federal Agriculture Office (Bundesamt für Landwirtschaft), see Figure 6.2. To every soil class are associated the parameters regarding thickness and hydraulic properties (see Section 6.2).

6.1.3 Land Cover Map

Also for the land cover, we obtain the information from two different sources. For the Italian part of the basin, the used land cover map is the Destinazione d'Uso dei Suoli Agricoli e Forestali (DUSAF), a product developed by the local ARPA. For the Swiss part of the domain the Corine Land Cover, a European land cover map less detailed than DUSAF, is the best information available, see Figure 6.3. Parameters as the Manning coefficients and the monthly evapotranspiration coefficients are associated in Topkapi-ETH to every class of the land cover map (see Section 6.2).

6.1.4 Glacier Map

A glaciers map is provided by the local ARPA. Since there is no available information on the glaciers' ice thickness across the whole domain, this data is estimated from the area, with an empirical formula and assuming a uniform ice thickness, as follows [Fatichi et al., 2013; Farinotti et al., 2009]

$$h_{ice} = 33A^{0.36}$$

where $A[\text{km}^2]$ is the area of the single glacier and $h_{ice}[\text{m}]$ represents its ice thickness. This assumption on the initial ice thickness is necessary to evaluate the potential glacier retreat due to melting, see Figure 6.4.

6.1.5 Thiessen Polygons for Temperature, Precipitation and Cloud Cover Transmissivity

Since Topkapi-ETH requires spatial inputs, we transform the temperature, precipitation, and Cloud Cover Transmissivity time series from

points to maps using the Thiessen polygons. As already shown in Chapter 5, the temperature time series are taken from the historical ARPA stations and the Thiessen polygons are computed in a GIS environment, see Figure 6.5. Figure 6.6 shows the map obtained transforming with Thiessen polygons the points of the Alpine precipitation grid. The best available information on Cloud Cover Transmissivity is provided by a single station, at the Samedan Airport, which is located slightly outside the catchment. We thus consider only one Thiessen polygon over the entire domain.

6.1.6 *Reservoirs*

Figure 6.7 shows the hydropower reservoirs included in the analysis as well as the Lake Como. Besides the location and the spatial extent for each reservoir, Topkapi-ETH further requires a level/storage and a level/max-outflow curve. Moreover, Topkapi-ETH allows including simple reservoir operational rules, which can be defined separately for each artificial lake.

6.1.7 *Groundwater Depth*

The groundwater depth is an optional input in Topkapi-ETH that simulates the groundwater flow with an approach described in Liu et al. [2005], accounting for percolation to deep soil layers and groundwater flows. In our analysis we define two groundwater classes, one, 8 meters deep, at lower altitudes along the river network and one, 2 meters deep, for the rest of the catchment, as shown in Figure 6.8.

Elevation [m a.s.l.]

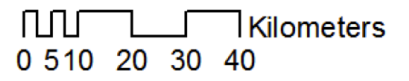


Figure 6.1: DEM of the catchment obtained with Topkapi-ETH

Legend

-  Reservoir
-  Glacier
-  Medium Loam
-  Clay
-  Clay Loam
-  Loamy sand
-  Sandy Loam
-  Silty Loam

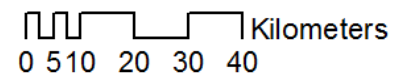
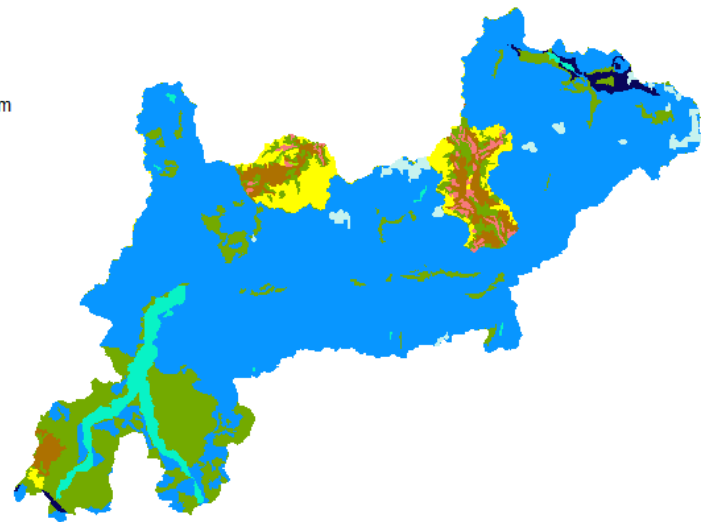


Figure 6.2: Soil Type Map

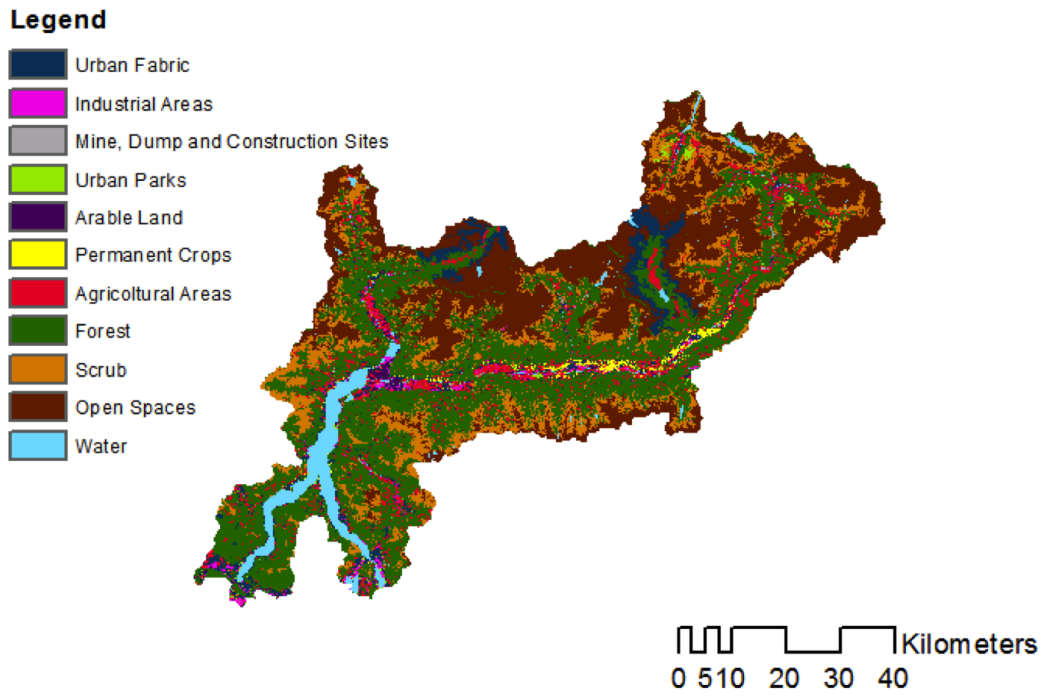


Figure 6.3: Land Cover Map

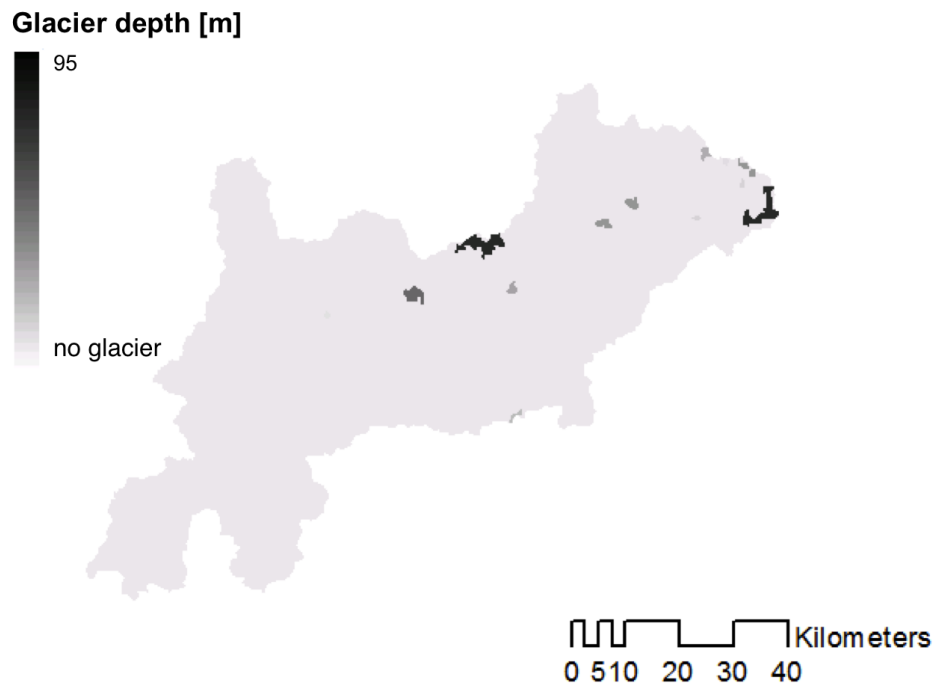
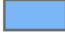





Figure 6.4: Glaciers Depth Map

Legend

-  Scais
-  Chiavenna
-  Sondrio
-  Santa Caterina

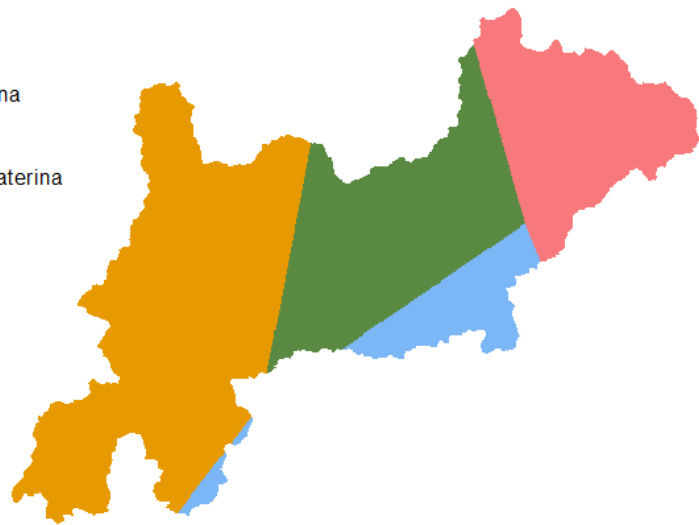



Figure 6.5: Temperature Thiessen Polygons Map

Legend

-  Precipitation IDs

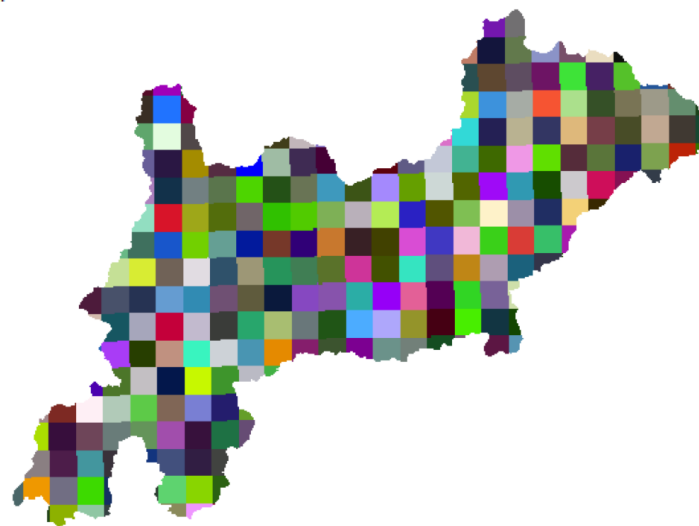


Figure 6.6: Precipitation Thiessen Polygons Map

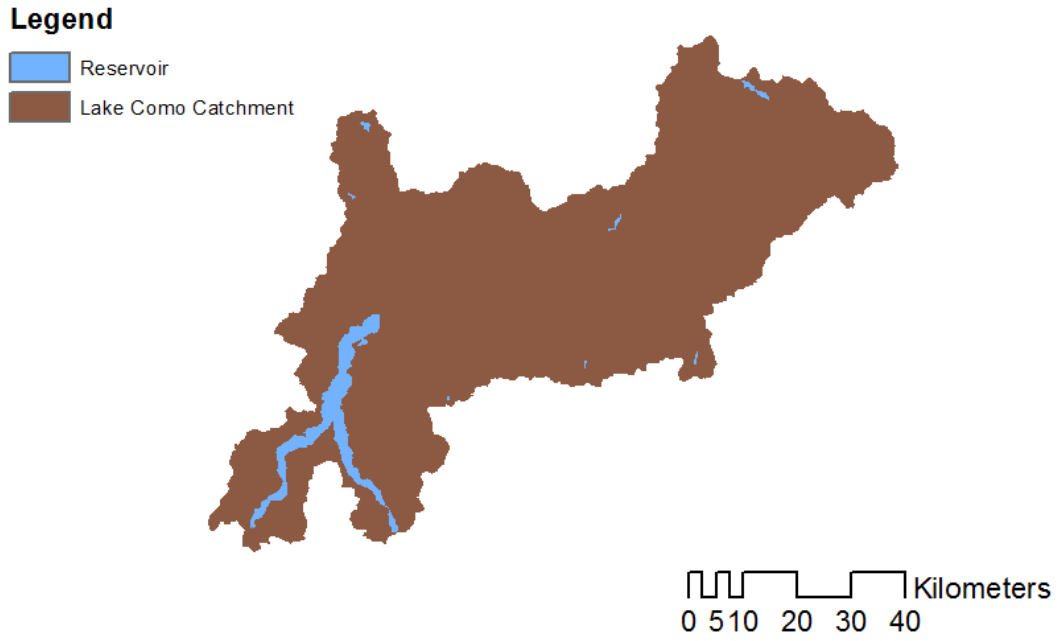


Figure 6.7: Reservoirs map

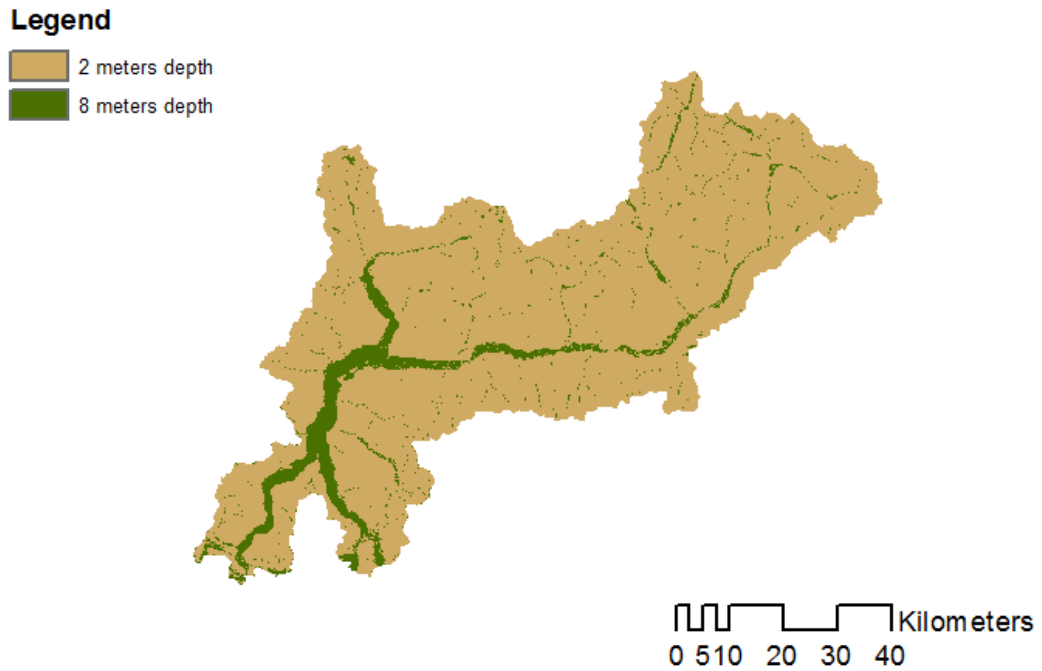


Figure 6.8: Groundwater Depth Map

6.2 CALIBRATION AND VALIDATION

As described in Chapter 2, Topkapi-ETH requires as input time series of precipitation, temperature and cloud cover transmissivity. As already said, we retrieve the former two from the Alpine precipitation grid distributed by MeteoSwiss [Isotta et al., 2014] and the ARPA temperature gauges. Cloud Cover Transmissivity (CCT) is obtained by the solar radiation collected in Samedan, located approximately 25 Km outside the catchment.

Topkapi-ETH can simulate the reservoirs operation defining a “rule curve”, i.e., a reference trajectory that can be defined as the trajectory of the storage during a normal hydrological year [Soncini-Sessa et al., 2007]. In Topkapi-ETH the “rule curve” is implemented setting the reservoir outflow to zero, when the storage is lower than the reference trajectory, and to the maximum value allowed, when the storage is bigger than the reference trajectory. This simple operative rule is far from correctly describing the behaviour of the reservoir manager, whose decisions are based on other factors (e.g., day of the week, forecasted inflow, and electricity price). Nevertheless, the employment of a “rule curve” can reproduce the general effect of the reservoirs on the hydrology, which is basically moving water volumes among seasons. The annual reference trajectory for each reservoir is calculated from the historical observations of storages for the period 2006-2012. We compute a cyclostationary mean across the 2006-2012 time horizon, smoothing the values with a mobile window of 11 days.

We consider the section of Fuentes, located on the River Adda at the mouth to the Lake Como for the calibration and validation of the hydrological model (Figure 6.9). Observations at Fuentes gauge station are the most reliable observations of streamflow across the catchment. The time series used for the calibration is provided by ARPA, comprising a period of 41 years (1971-2011). The calibration of Topkapi-ETH is initially performed using literature values for the parameters referring to soil and land use properties. In fact, all its parameters have a physical meaning and are associated to particular classes. For example, the physical properties of the soil, such as hydraulic conductivity, can vary depending on its composition. This initial parameter set is then slightly adjusted to improve the performances of the model with regard to the available streamflow time series. More precisely, we perform a manual calibration of the following parameters:

- Manning coefficient:
it is the surface roughness coefficient and depends on the land cover types, defining the resistance to flows.
- Monthly evapotranspiration coefficients:
they represent the evapotranspiration factors for each land cover

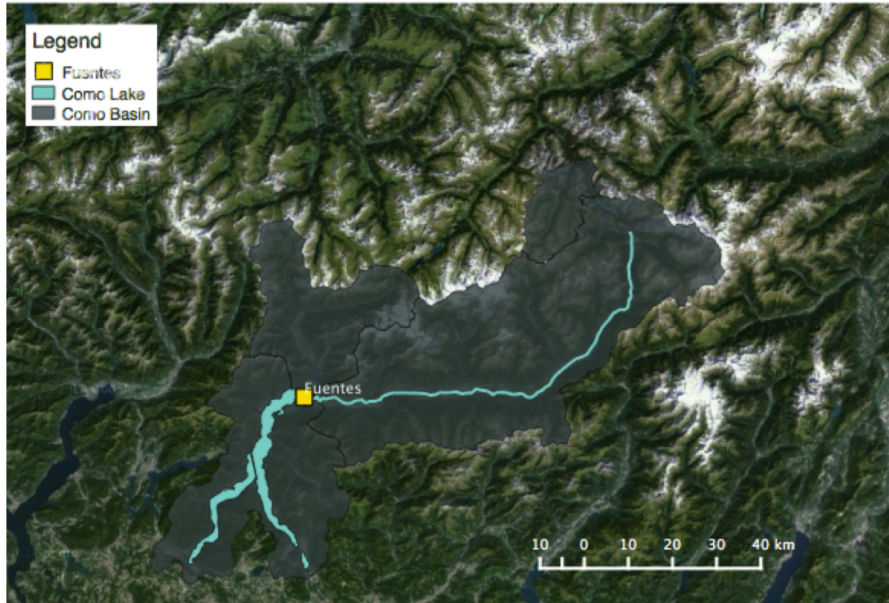


Figure 6.9: Fuentes location on the catchment. The Figure shows the river section of Fuentes, where we did the calibration, the Lake Como and the River Adda.

type and month. The values are generally lower in the cold months and higher in spring and summer.

- **Soil Depth:**
it represents the soil thickness of the two layers defined in Topkapi-ETH.
- **Residual water content ratio (Θ_{aR}) and water content ratio at saturation (Θ_{aS}):**
they represent the water content characteristics of the two soil layers.
- **Horizontal (K_{sH}) and vertical (K_{sV}) hydraulic conductivity:**
they are a measure of saturated soil ability to transmit water when subjected to a hydraulic gradient. These parameters vary within a wide range of orders of magnitude, depending on the soil type. For instance, clay has a lower hydraulic conductivity at saturation than sand.

The calibration is performed w.r.t. three performance indices: The coefficient of determination (R^2), the root of the mean square error (RMSE), and Kling-Gupta Efficiency (KGE). R^2 represents the portion of the total variance of the observed data that can be explained by the model

$$R^2 = 1 - \frac{\text{var}(y_{\text{obs},t} - y_{\text{mod},t})}{\text{var}(y_{\text{obs},t})}$$

where $y_{obs,t}$ and $y_{mod,t}$ are the observed and modelled time series respectively. As known, R^2 is very sensitive to outliers and not sensitive to proportional and additive variations, so it might be misleading, for instance, when dealing with systematic underestimations or overestimation of the streamflow [Legates and McCabe, 1999].

RMSE represents the standard deviation of the difference between observed and predicted values and it is widely used in hydrological modelling [Legates and McCabe, 1999]

$$RMSE = \sqrt{\frac{\sum_{t=1}^N (y_{obs,t} - y_{mod,t})^2}{N}}$$

where $y_{obs,t}$ and $y_{mod,t}$ are the observed and modelled values at time t respectively.

KGE is an alternative measure of performance for hydrological models which aims to overcome the traditional problems associated with calibration, for instance variability underestimation and low sensitivity to proportional and additive variations [Gupta et al., 2009]

$$\alpha = \frac{\sigma_{mod}}{\sigma_{obs}}, \beta = \frac{\mu_{mod}}{\mu_{obs}}, r = \sqrt{R^2}$$

$$ED = \sqrt{(r-1)^2 + (\alpha-1)^2 + (\beta-1)^2}$$

$$KGE = 1 - ED$$

where σ_{obs} and σ_{mod} are the standard deviations of observed and modelled time series, while μ_{obs} and μ_{mod} are the two means.

We calibrate the model on the period 1988-1994, considering the first two years as warm-up period, and we validate it on the period 1997-1999. The final performance values of the calibration are: $R^2 = 0.72$, $RMSE = 103.30 \text{ m}^3/\text{s}$, and $KGE = 0.74$ (Table 6.1). Figure 6.10 shows the comparison between modelled and observed time series over the period 1990-1994 (Figure 6.10a) and over the year 1992 (Figure 6.10b). These values are acceptable considering the wide domain, the daily time step, and the spatial time resolution adopted (250 m). As visible especially in the zoom-in over the year 1992 (Figure 6.10b), there are weekly fluctuations caused by the operations of the reservoirs that release smaller volumes of water during the weekends. Those fluctuations are visible especially in the winter months as the natural streamflow is lower. In order to filter the extra variability caused by the hydropower operations, we calculate the performance metrics on the weekly average streamflow, instead of on the daily one (Table 6.1). As expected, all the metrics improve when computed on a weekly basis.

	Calib. Daily	Valid. Daily	Calib. Weekly	Valid. Weekly
$R^2[-]$	0.72	0.69	0.79	0.79
RMSE[m ³ /s]	103.30	59.82	37.18	49.94
KGE[-]	0.74	0.77	0.81	0.84

Table 6.1: Calibration performance summary: R^2 , RMSE, and KGE over the calibration and validation periods

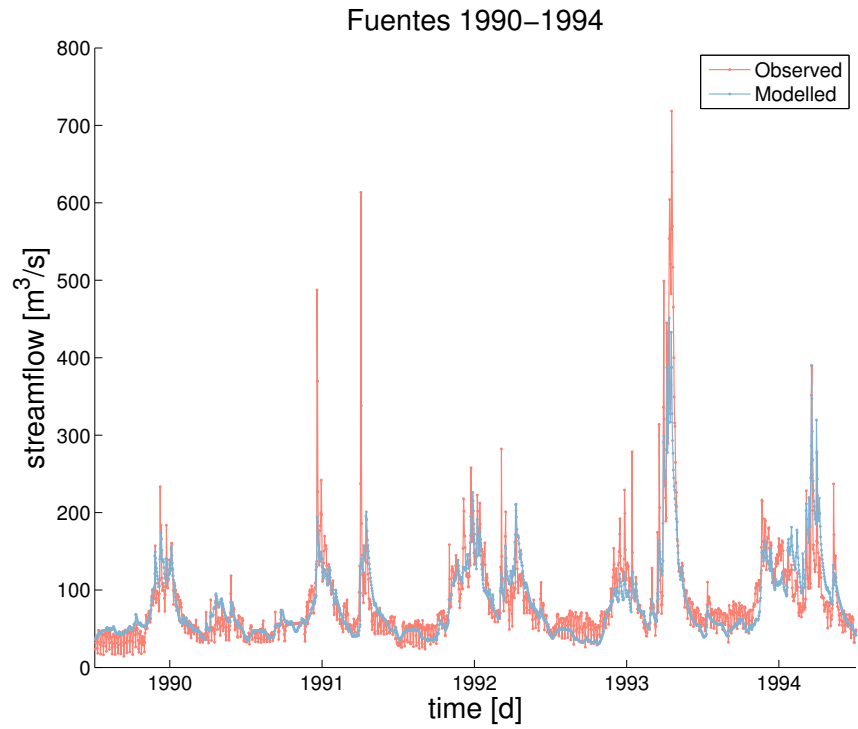
6.3 HYDROLOGICAL SCENARIOS ANALYSIS

6.3.1 Experiment Setup

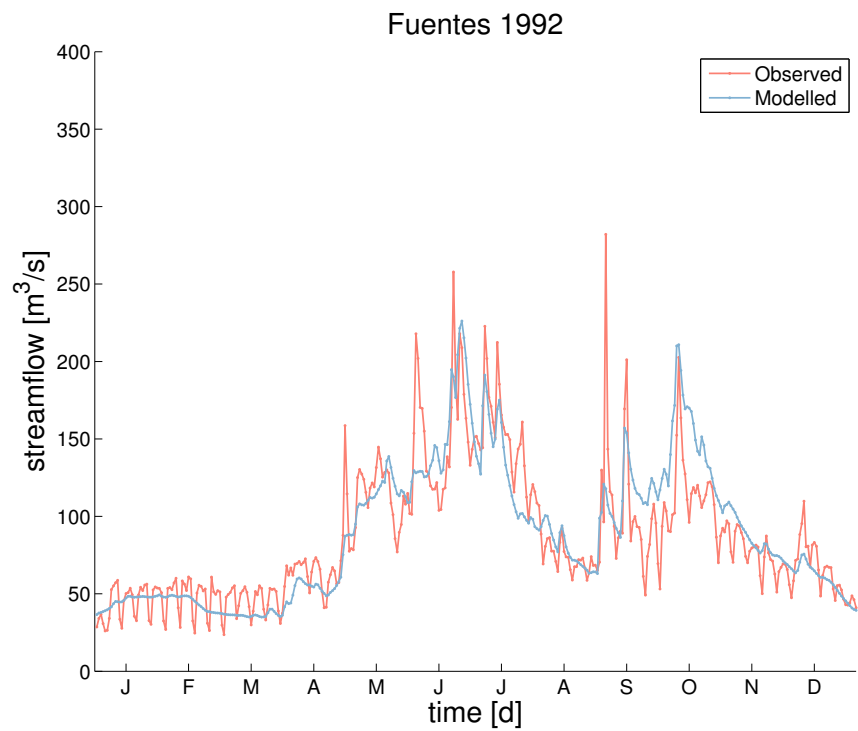
In order to assess the impact of climate change on the hydrology of the catchment, we carry out the simulations of Topkapi-ETH fed by the downscaled time series of temperature and precipitation retrieved from the EURO-CORDEX scenarios. As already discussed in Chapter 4, we consider combinations of five RCMs (REMO, RCA₄, RACMO, HIRHAM, and CCLM) and seven GCMs (MPI, NOAA, NCC, ICHEC, MIROC, CCC, and CNRM) forced by two Representative Concentration Pathways (RCP_{4.5} and RCP_{8.5}), for a total of 22 scenarios over the period 2006-2100 (not all the combinations are available). Aside the 22 simulations of the future scenarios, we also carry out 11 simulations fed by the downscaled variables over the control period, in order to simulate the current hydrology. The total computational time is approximately 90 hours. As for the reservoir operation, we perform a business-as-usual analysis, supposing that the rule curves will remain the historical ones also in the future.

6.3.2 Impact of Climate Change on Streamflows

We carry out a statistical analysis of the hydrological model output, in order to assess how the predicted changes in temperature and precipitation reflect on the streamflows in the catchment. As already done for the climate scenarios, we use boxplots to summarize the main statistics (Figures 6.11, 6.12, and 6.13). After that, we calculate the cyclostationary mean of all the scenarios over the CORDEX time-horizon. Finally, we compute MASH plots of all the hydrological scenarios. In this Chapter we present only the results relative to the scenarios REMO/MPI and RACMO/ICHEC, considered representative of the entire ensemble (for the MASH of the other scenarios see Appendix B).



(a) 1990–1994



(b) Zoom-in 1992

Figure 6.10: Observed and modelled streamflows at the river section of Fuentes

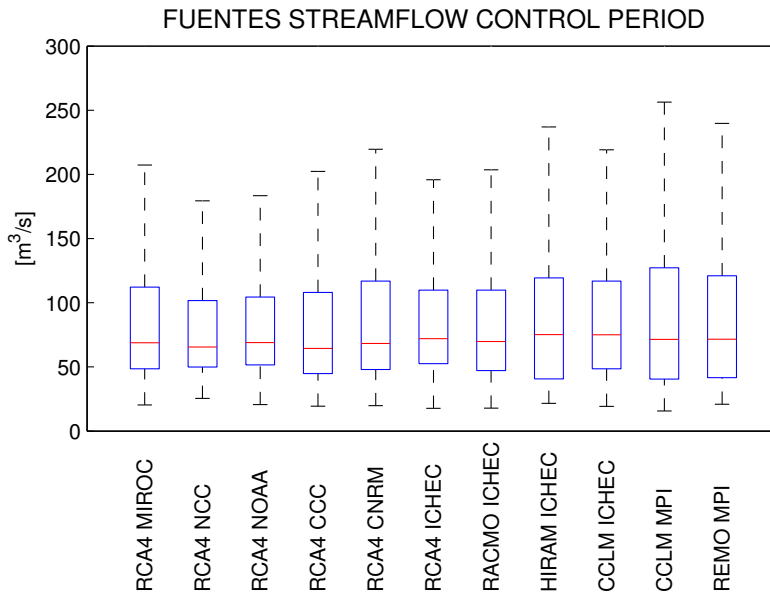


Figure 6.11: Boxplot Streamflow Fuentes Control Period

As already seen with the climate variables, looking only at the standard statistics shown in the boxplots, it is difficult to determine concordant changes in hydrology between the control period and the future scenarios (Boxplots 6.11 to 6.13). Figure 6.11 shows that all the scenarios have similar statistics, besides the CCLM/MPI, which shows a slightly higher variability. Figure 6.14, 6.15, and 6.16 show the cyclostationary averages of the streamflows at Fuentes, computed over the control period and then over the future horizon for all the climate scenarios forced by RCP4.5 and 8.5 respectively. Looking at the scattered distribution of the lines on the graphs we perceive the high uncertainty related to the climate models that reflects on the hydrological scenarios. Over the control period the climate scenarios having CCLM as RCM, show a different pattern with a late snowmelt peak and lower intensity in the autumn flows. The cyclostationary mean of the simulation outputs over the future scenarios (Figures 6.15 and 6.16) show a high variability, among the different models, both in winter and summer streamflows and in the time of the snowmelt peak.

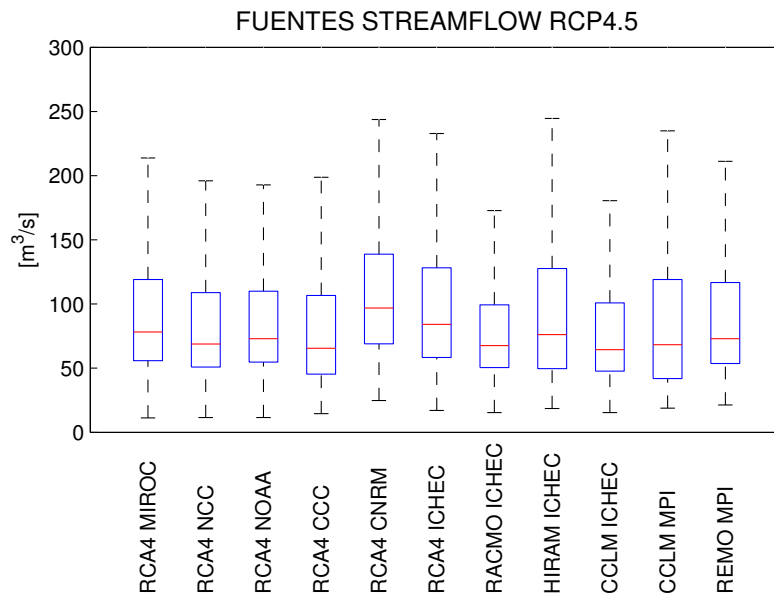


Figure 6.12: Boxplot Streamflow Fuentes RCP4.5

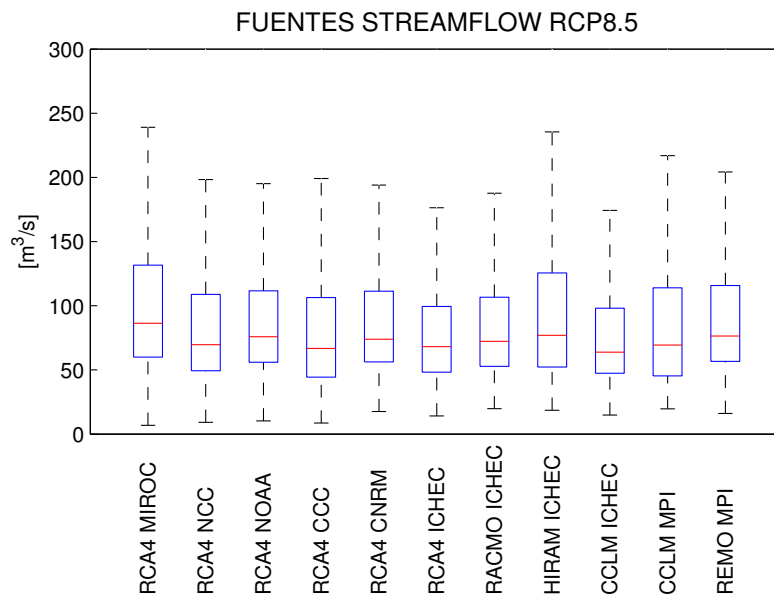


Figure 6.13: Boxplot Streamflow Fuentes RCP8.5

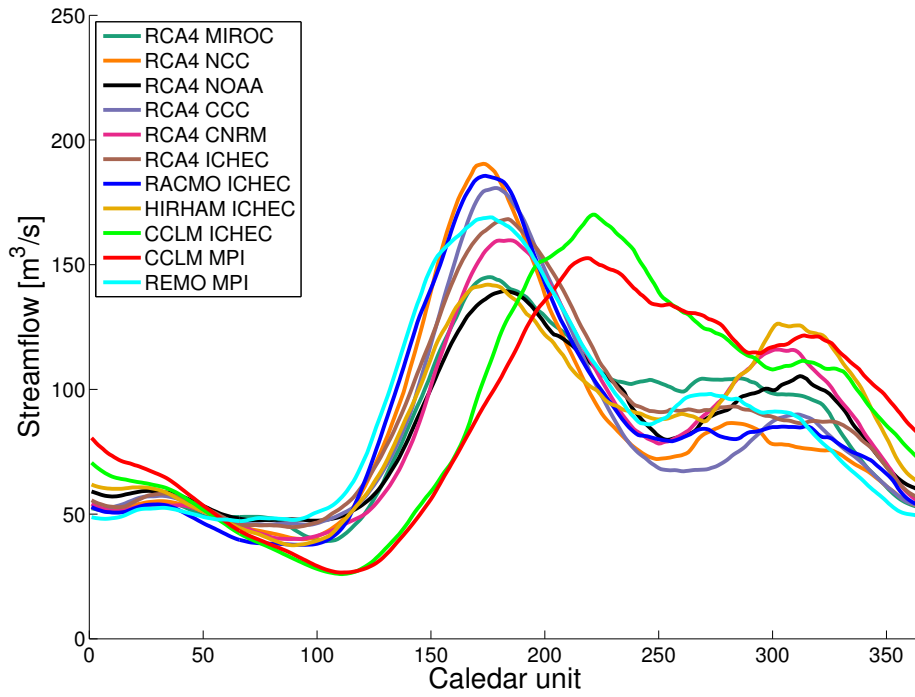


Figure 6.14: Trajectories Fuentes Control Period

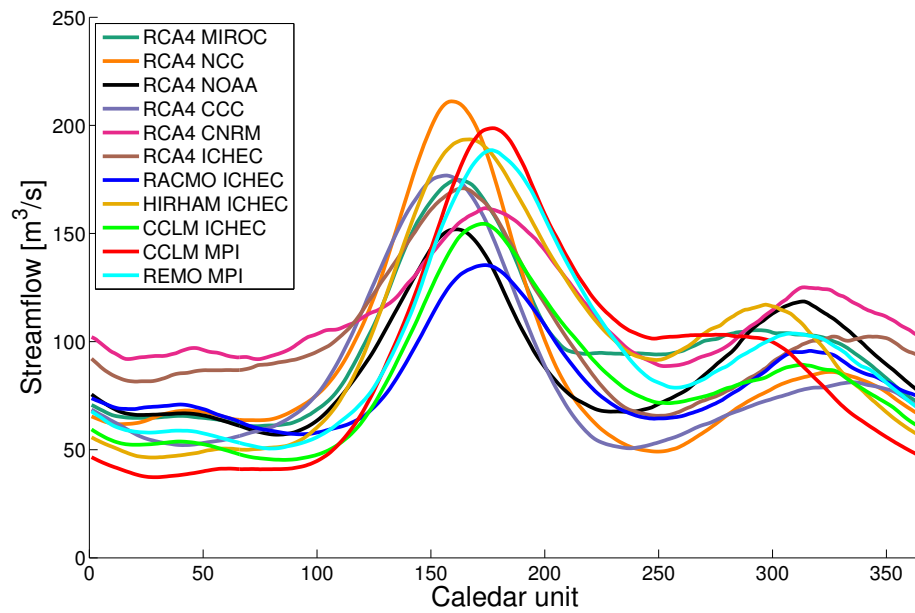


Figure 6.15: Trajectories Fuentes RCP4.5

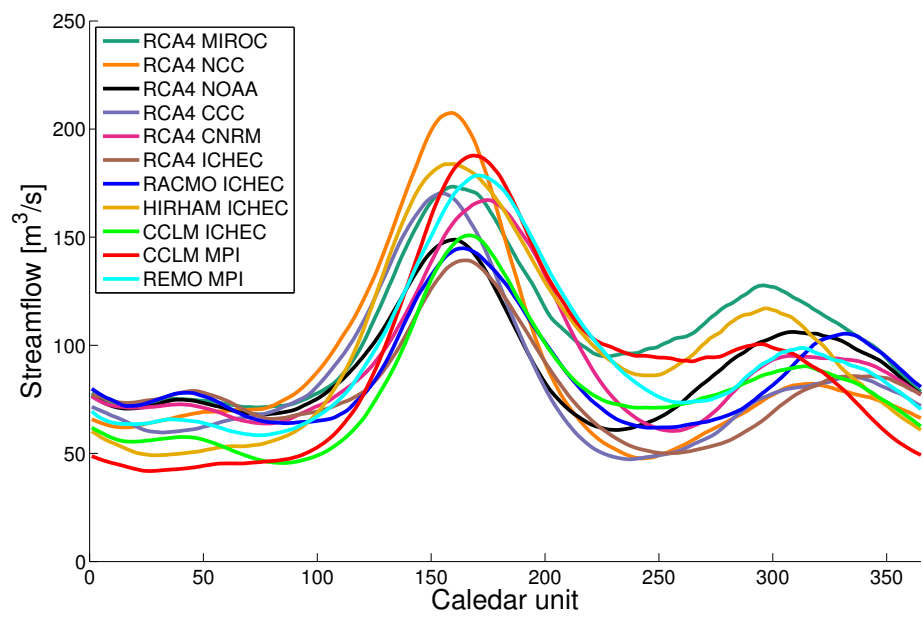
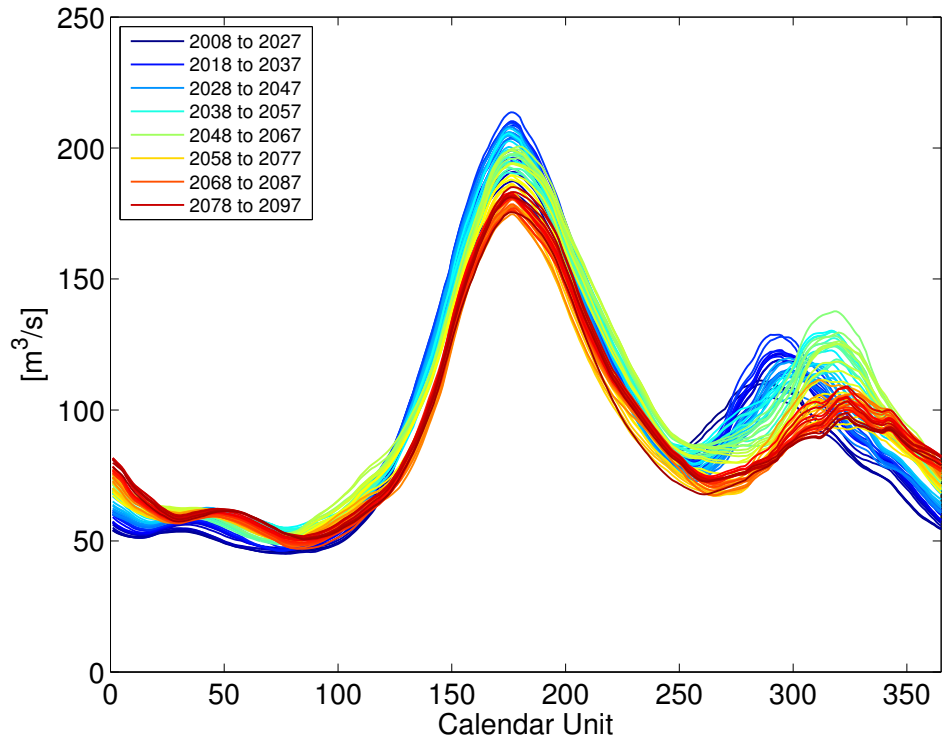
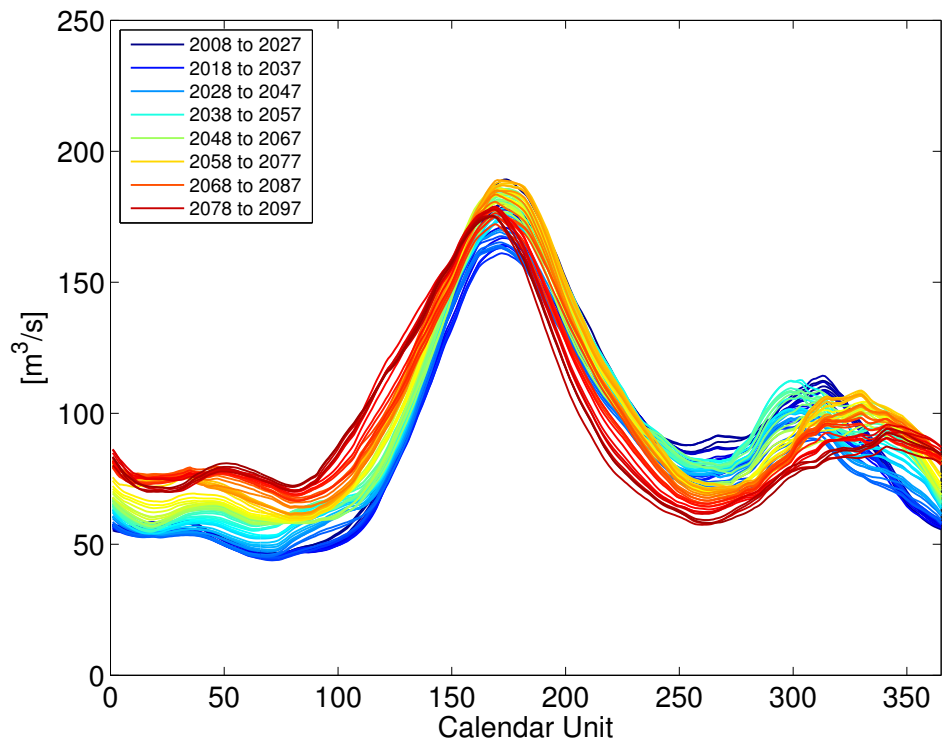


Figure 6.16: Trajectories Fuentes RCP8.5

As already done in Chapter 4 for the climate variables, we apply the **MASH** tool also to the hydrological scenarios, to detect changes in the seasonal pattern of streamflow over the century. In order to be consistent with the previous analysis, the parameters used are $Y = 20$ and $w = 15$. As already mentioned for the climate variables, these values represent a good trade-off between filtering out the daily variability and preserving seasonal patterns. In this section we show the **MASH** relative to the scenarios REMO/MPI and RACMO/ICHEC, taken as representative of the whole ensemble (the graphs related to the other scenarios are fully shown in Appendix B). The main trends visible in Figures 6.17 and 6.18 are an increase in winter streamflow and a decrease in summer streamflow. Other aspects observed in most of the scenarios are a shift towards an earlier snowmelt peak and a delayed secondary autumn peak. Figure 6.17 shows the **MASH** for the REMO/MPI scenario, where the mean rise in winter streamflow between the first and last two decades of simulation (2008-2027 and 2081-2100) amounts to 26.6% for RCP4.5 and to 43.14% for RCP8.5. On the contrary there is a mean summer decrease of 7.3% and 23.1% respectively. The changes detected in the RACMO/ICHEC scenario are 19.6% and 31.6% of winter increase for RCPs 4.5 and 8.5, and reductions of 5.5% and 14.9% during the summer months (Figure 6.18). The snowmelt peak is expected up to one month earlier for the RCP8.5 in some scenarios, while this anticipation is lower for the RCP4.5. The shift towards a later autumn peak can be seen under both the RCPs, as shown in Figure 6.17, representing the outputs of the model REMO/MPI fed by RCP4.5 and RCP8.5.

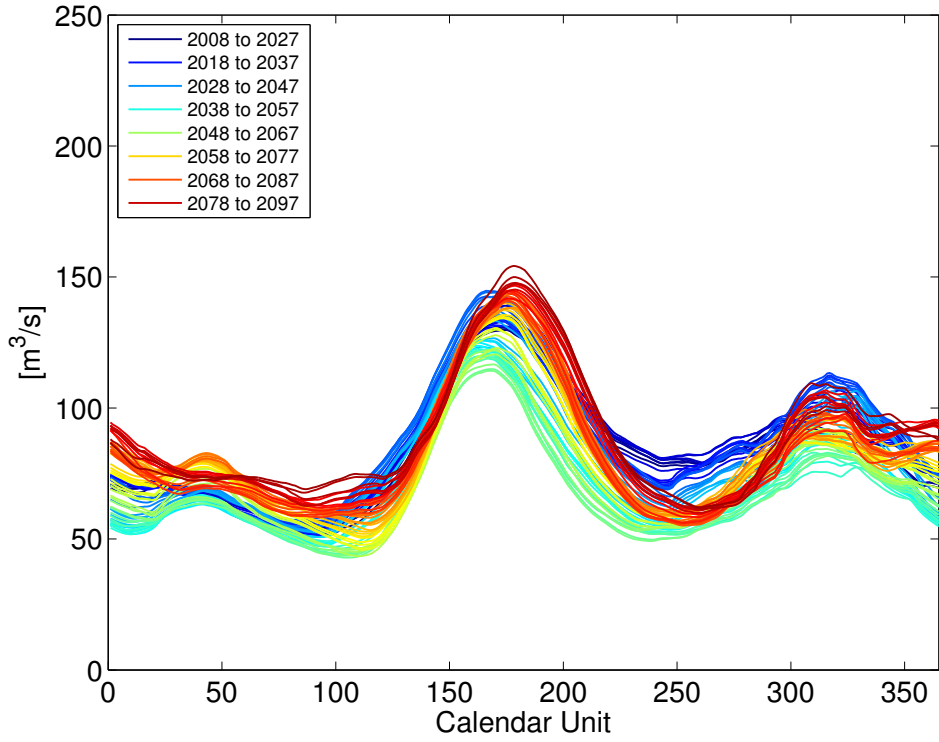


(a) RCP4.5

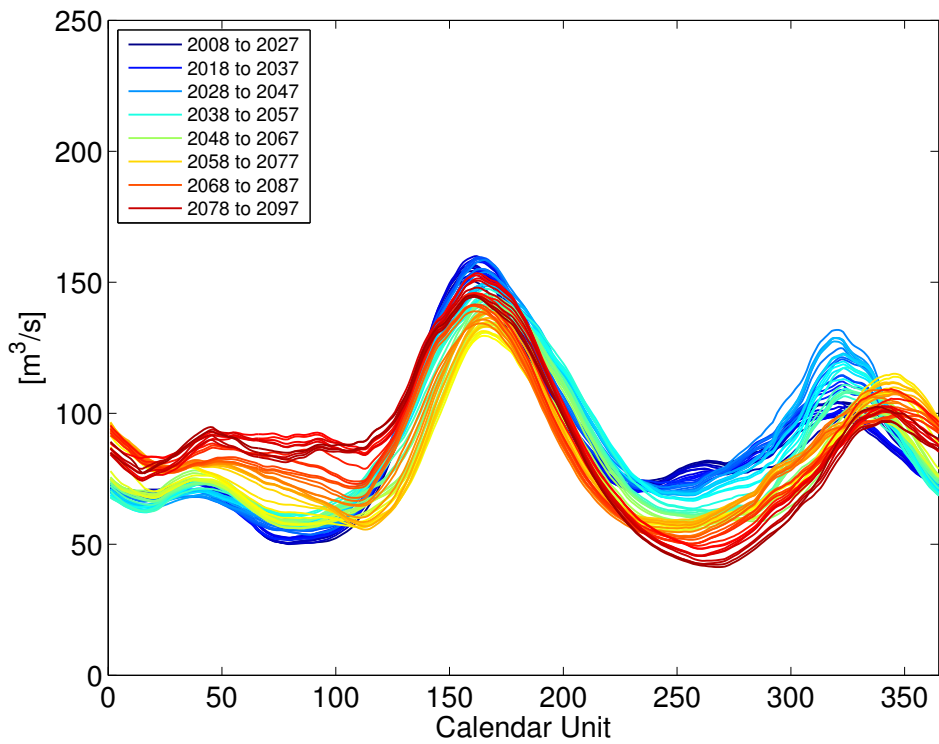


(b) RCP8.5

Figure 6.17: REMO/MPI, Fuentes streamflow



(a) RCP4.5



(b) RCP8.5

Figure 6.18: RACMO/ICHEC, Fuentes streamflow

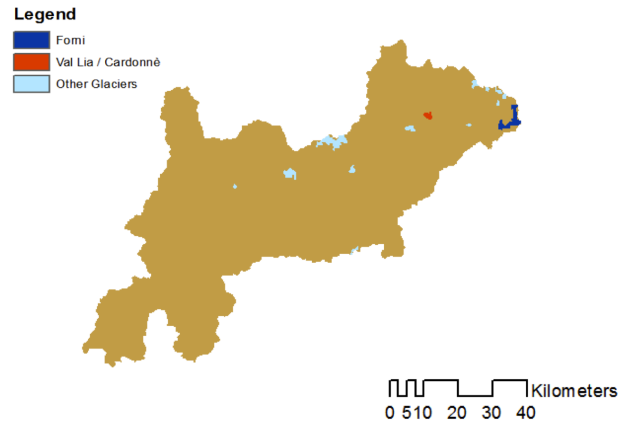
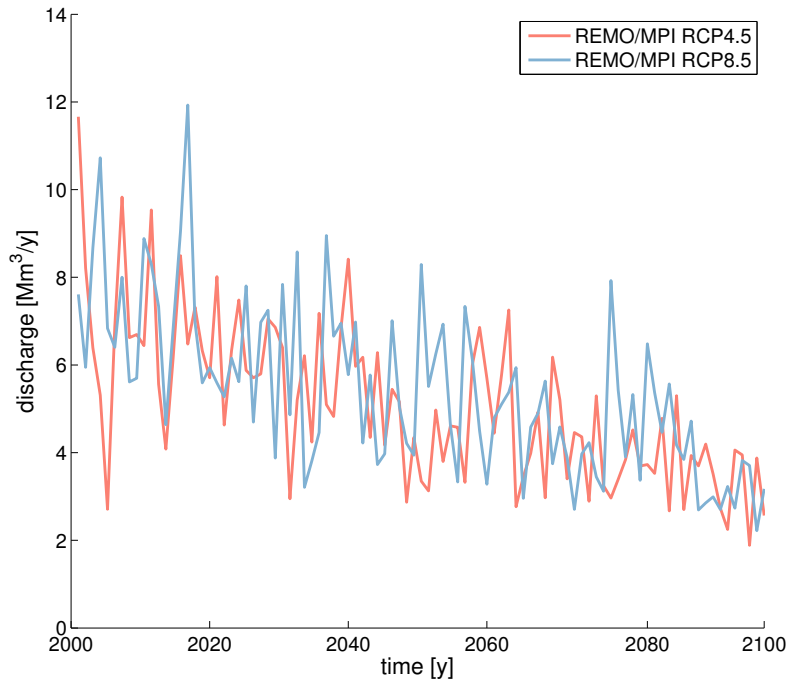


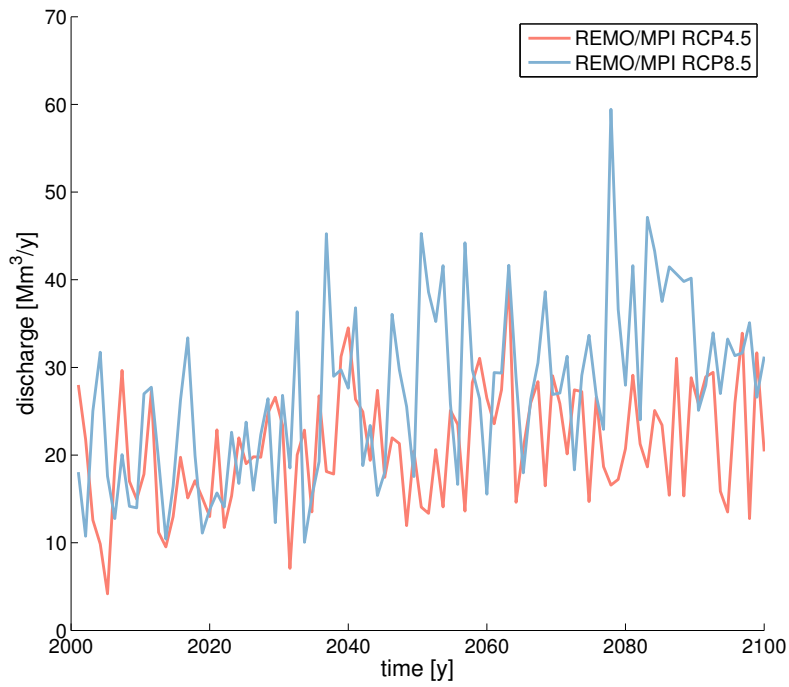
Figure 6.19: Glacier Map of the catchment with highlighted the Forni Glacier (in blue) and the Val Lia / Cardonnè Glacier (in red).

6.3.3 Impact of Climate Change on Glaciers

Glaciers retreat strongly affects the hydrology in high-elevation catchments [Fatichi et al., 2013]. In the Lake Como basin the glaciers surface is only 1.4% of the total area, considering the catchment closed at Olginate, but this value considerably increases if taking into account only the areas nearby the Alpine reservoirs. San Giacomo and Cancano reservoirs, for instance, are fed by highly glacierized areas through artificial channels. As an example, we analyzed the Forni Glacier, the Val Lia, and the Cardonnè Glaciers. The Forni Glacier is the biggest glacier in the Italian Alps and it is located in the Orties–Cevedale Group at an average altitude of 3096 m a.s.l. Contrarily, the Val Lia and Cardonnè Glaciers are considerably smaller and located on average at 2800 m a.s.l. (Figure 6.19). Monitoring the output of the two representative scenarios (REMO/MPI and RACMO/ICHEC) we see that the smaller and lower glacier shows a considerable decrease in yearly discharge (Figures 6.20a and 6.21a). On the contrary the glacier of Forni, located at a higher altitude, does not show relevant signs of retreat in the two climate models, forced by the RCP4.5 (Figures 6.20b and 6.21b). When forced by the RCP8.5, the model REMO/MPI shows instead an increase in the discharge of the Forni Glacier, during the last decades of the century (Figure 6.20b, blue line), which might be caused by the initial retreat, which usually produces higher discharges [Jansson et al., 2003]. Similar results on the elevation dependent glacier response to climate change were obtained by Fatichi et al. [2013]. The sum of the discharges from all the glaciers considered in the catchment shows a decrease of 20% for RCP4.5 and of 32.7% for RCP8.5 comparing the last part of the century (2071-2100) to the control period, when taking into account all the 22 scenarios of the analysis.

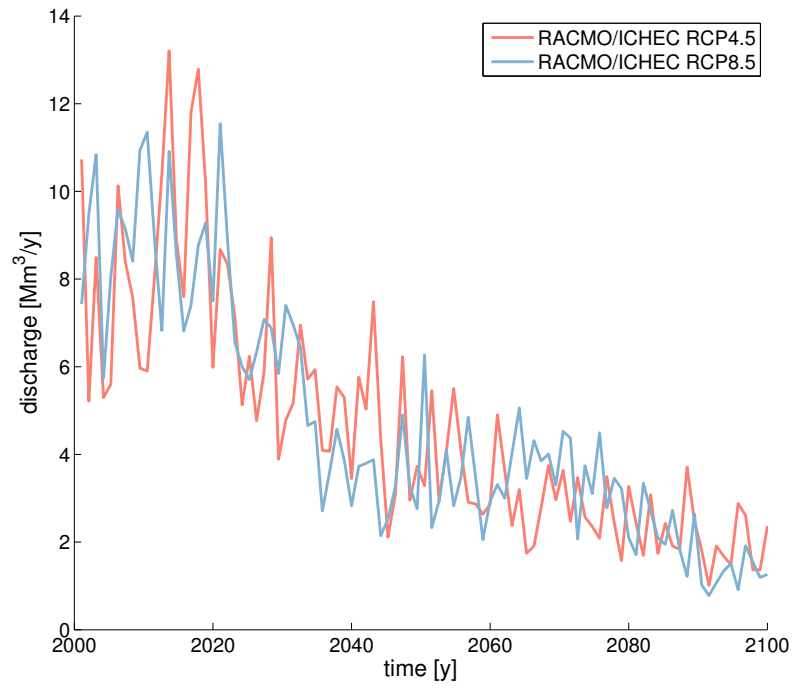


(a) Val Lia / Cardonnè

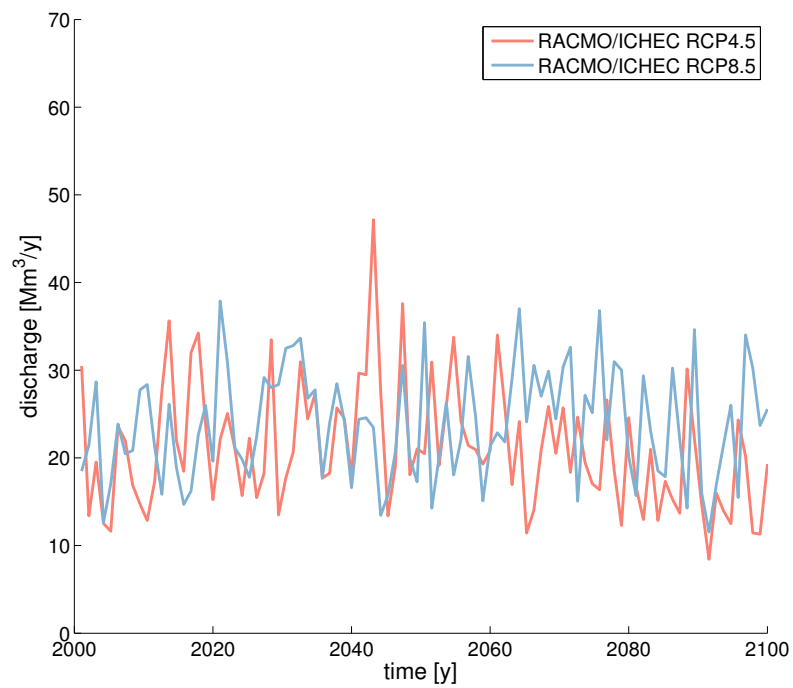


(b) Forni

Figure 6.20: Discharge of glacier Forni and Val Lia / Cardonnè under the scenarios REMO/MPI



(a) Val Lia / Cardonnè



(b) Forni

Figure 6.21: Discharge of glacier Forni and Val Lia / Cardonnè under the scenarios RACMO/ICHEC

6.3.4 *Impact of Climate Change on Reservoir Inflows and Levels*

The last objective of our analysis is the understanding of the impact of climate change on the inflow to the reservoirs and the resulting effects on their management. We focus on the biggest reservoirs in the catchment, i.e., San Giacomo and Cancano reservoirs. Topkapi-ETH allows monitoring the inflow to the reservoir from its tributaries, lake banks, precipitation, and redistributed snow. The operative rule used during the simulation is the one employing a “rule curve”, calculated with the historical level observations, as already discussed in Section 6.2. The MASH tool is adopted also to analyze the reservoir levels, and to compare it to the target level of the “rule curve”. Figures 6.22a and 6.23a show the MASH for the REMO/MPI scenario, indicating a 9.8% rise in winter streamflow for RCP4.5 between the first and last two decades of simulation (2008-2027 and 2081-2100) and 20% for RCP8.5. The summer decrease amounts to 8.9% and 22.8% respectively. Figures 6.24a and 6.25a show the changes detected in the RACMO/ICHEC scenario that amount to 12.8% and 18.5% of winter increase for RCPs 4.5 and 8.5, and reductions of 1% and 11% respectively during the summer. Figures 6.22b, 6.23b, 6.24b, and 6.25b show the water level of the reservoir during the simulations forced by the reference scenarios. They demonstrate how the hydrological shift would affect the levels and the storages of the reservoir. The red lines are the cyclostationary mean calculated over the last decades of the century. They show a decrease during summer and autumn in the water level compared to the blue lines, which are the means calculated at the beginning of the simulation horizon. A 7 cm gap in the level, shown in Figure 6.23b between the target level and the means computed by the MASH over the last decades of simulation (shades of red), indicates approximately 300,000 m³ less storage. The shift towards an earlier snowmelt peak in the REMO/MPI scenario has an impact on the storage pattern of the reservoir, which tends to be filled earlier. Figures 6.22b and 6.23b show the respective shift in the level pattern, where the red lines in the months of May, June, and July show higher values than the blue ones. Regarding the scenario RACMO/ICHEC, forced by the RCP4.5, Figure 6.24b shows that, after an initial decrease, in the last part of the century (red lines), the storage of the reservoir seems to get closer to the target level. On the other hand, the same model forced by the RCP8.5 shows a clear decrease in the reservoir storage, caused by an intense reduction in summer and autumn inflow (Figure 6.25b). The results shown in this Chapter demonstrate that the current storage seasonal patterns can not be reproduced in the future under climate change conditions. The impossibility of following the current seasonal patterns, due to lower summer inflows and a seasonal hydrological shift, will very likely induce hydropower companies to change their strategy.

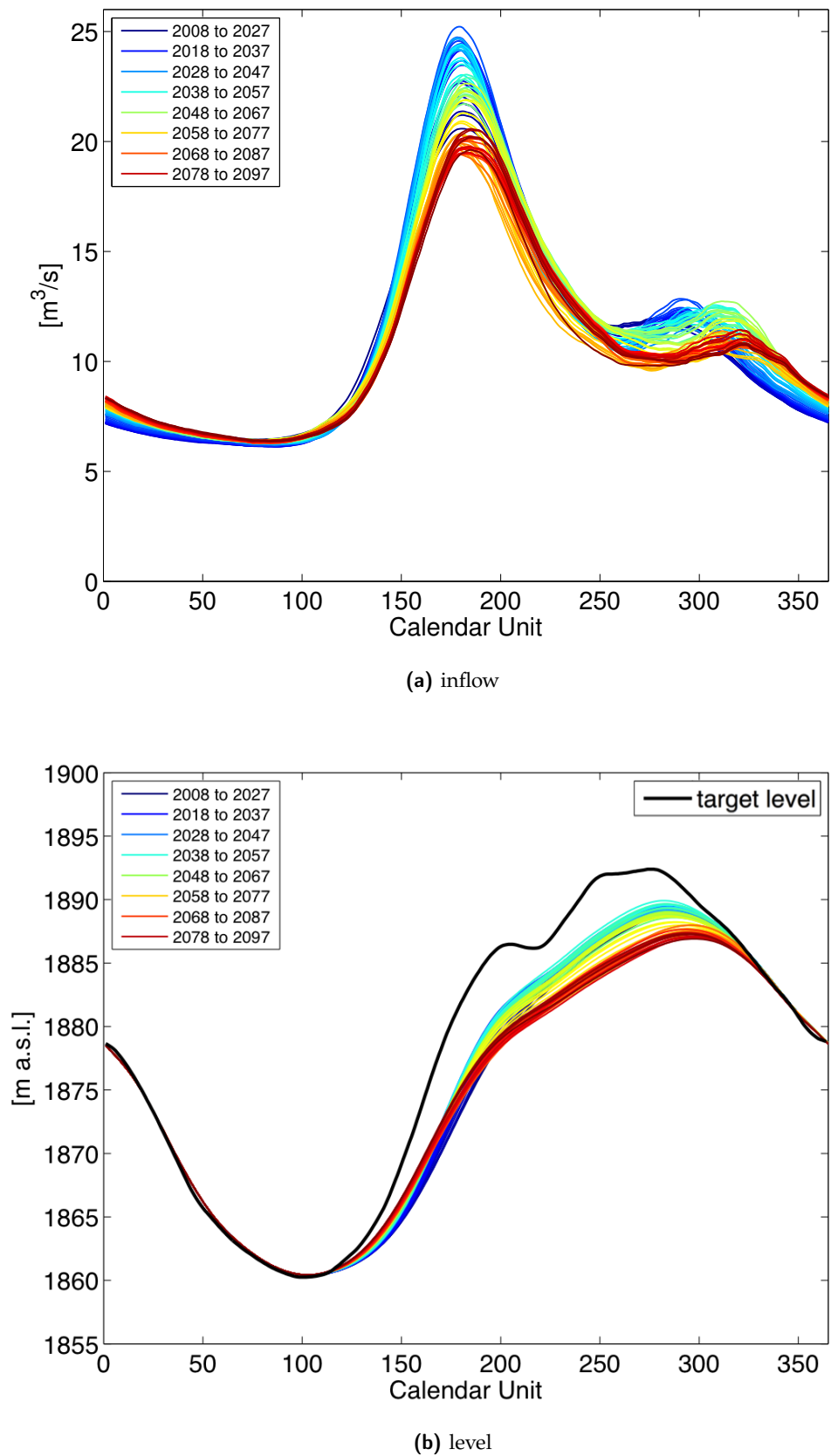


Figure 6.22: REMO/MPI RCP4.5. MASH of the A2A reservoir inflow and level. The target level adopted in the simulation is represented with a black line.

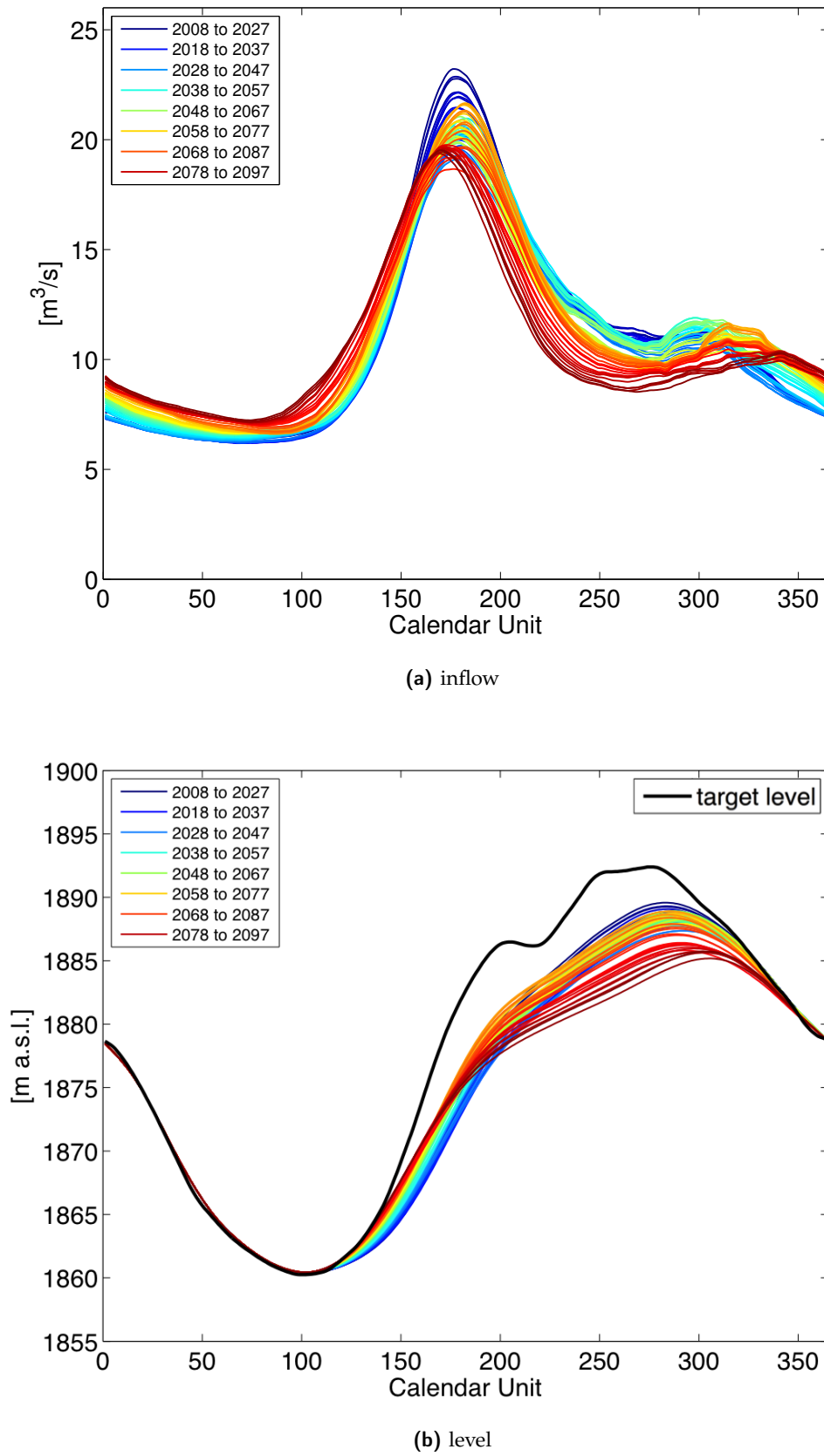


Figure 6.23: REMO/MPI RCP8.5. MASH of the A2A reservoir inflow and level. The target level adopted in the simulation is represented with a black line.

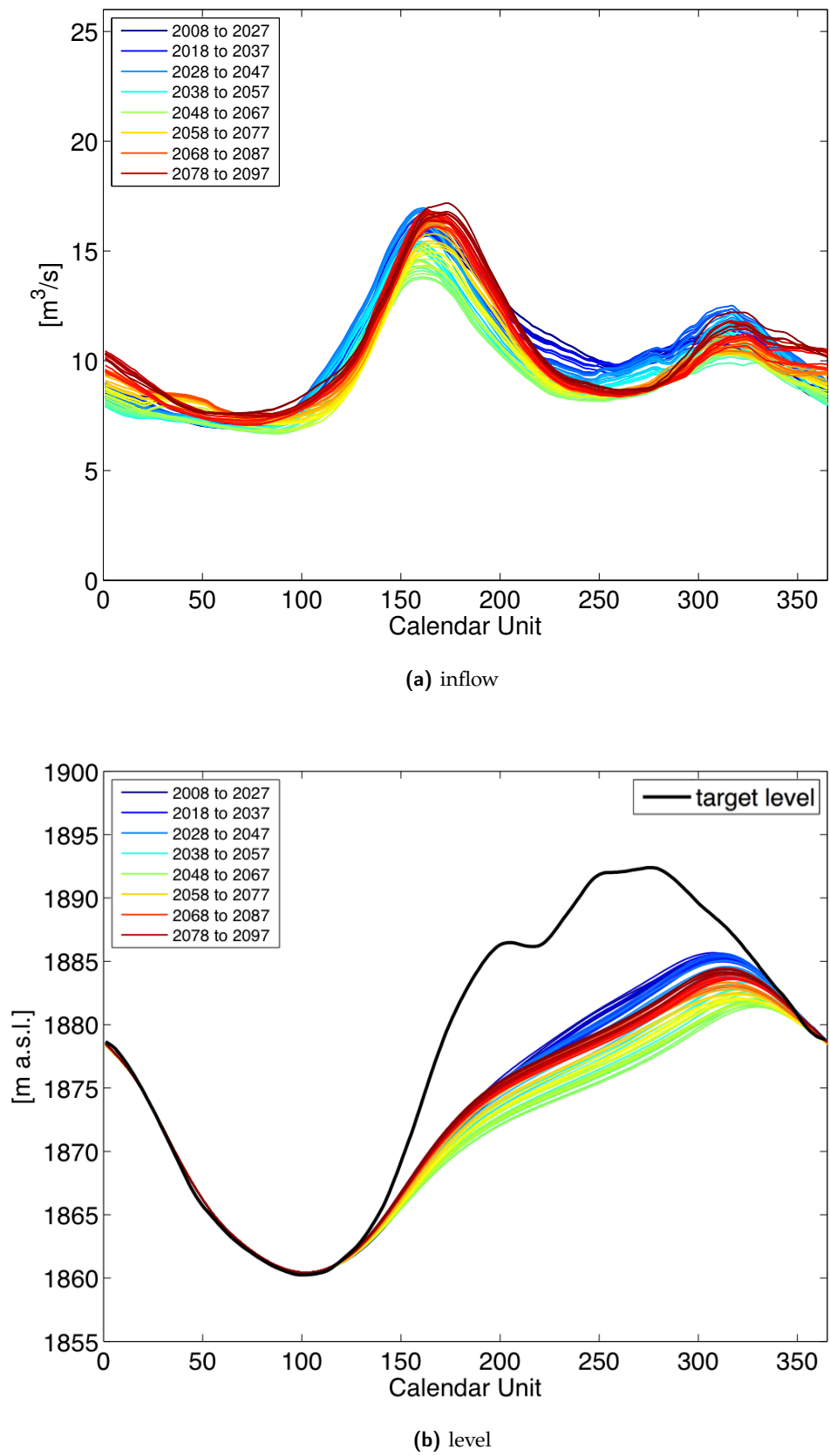


Figure 6.24: RACMO/ICHEC RCP4.5. MASH of A2A reservoir inflow and level. The target level adopted in the simulation is represented with a black line.

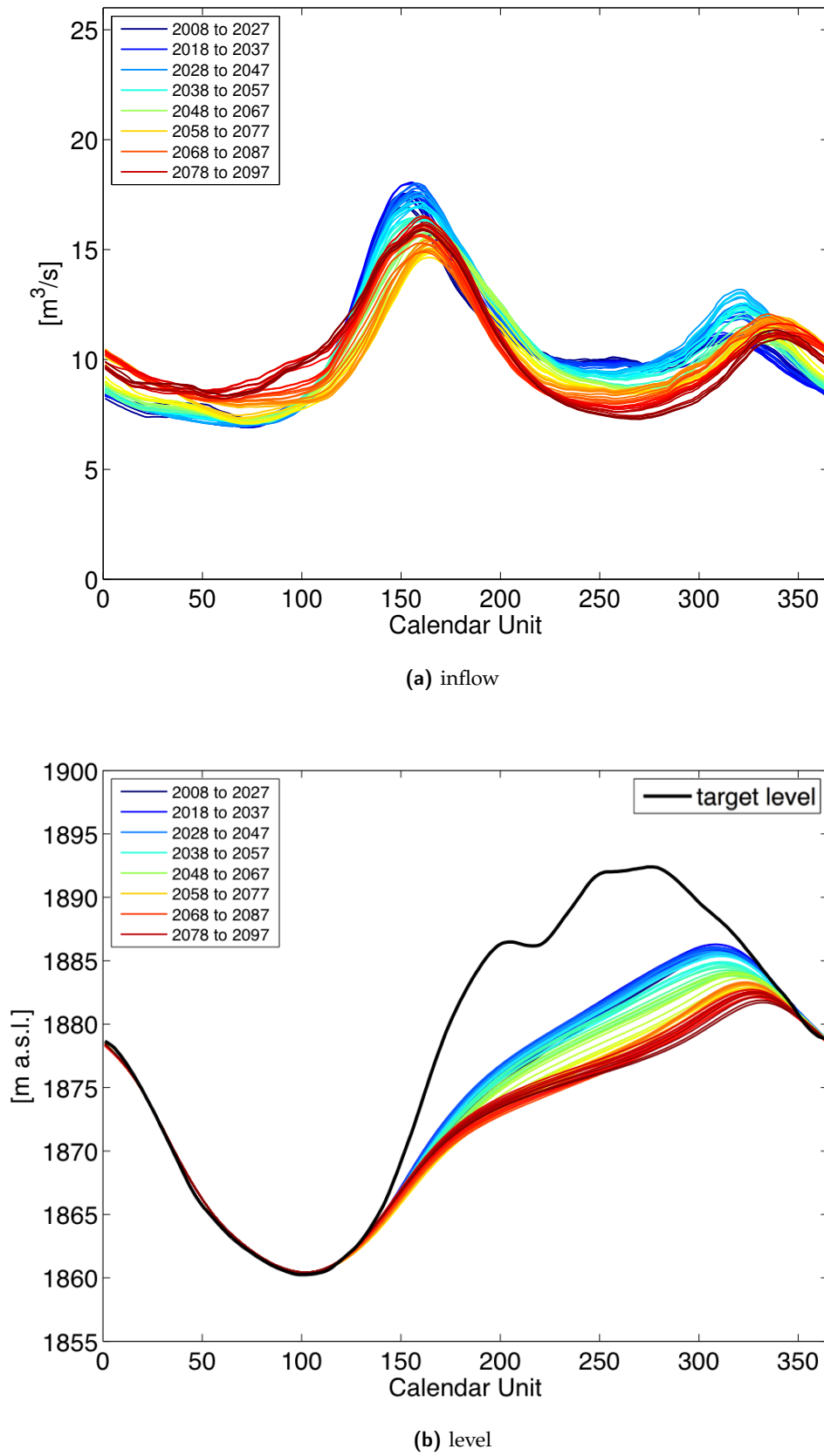


Figure 6.25: RACMO/ICHEC RCP8.5 MASH of A2A reservoir inflow and level. The target level adopted in the simulation is represented with a black line.

UNCERTAINTY CHARACTERIZATION

7.1 “CASCADE OF UNCERTAINTY” IN CLIMATE CHANGE IMPACT STUDIES

The aim of the majority of climate change impact studies is, implicitly or explicitly, to evaluate or design Policies, Plans, and Programs (PPPs) to reduce or mitigate those impacts. The design and implementation of those PPPs is generally a long and complex process due to political and economical reasons. The uncertainty related to climate change impact studies adds a further degree of complexity to decision making processes, which naturally would prefer certain predictions, rather than unclear estimations, in order to assess costs and benefits of an action (e.g., in the next century the river will reach a specific higher level, therefore we need to build new river banks, of that specific height, in order to avoid floods). Indeed, although the role of uncertainty is well addressed in literature, in most of the real applications the approach consists of ‘squeezing it out’ from the decision making process, as if the assumptions of deterministic environment were satisfied [Soncini-Sessa et al., 2007]. Already more than two decades ago Green [1992], quoting a work of Hogan and Jorgenson [1991], explains how the uncertainty in climate change impacts affects and delays the decision making process and how complex is implementing costly action on the basis of theoretical predictions of extremely uncertain and never-before experienced events. An important aspect of uncertainty is its location among other terms related to predictions. Foley [2010], adapting a scheme taken from Stirling [1998], tries to graphically define the concept of “uncertainty” between the ones of “risk” and “ignorance”, considering the knowledge about the outcomes and the knowledge about their likelihood. Figure 7.1 shows that, with less firm basis for probabilities and less knowledge about the outcomes of a system, scenario analysis should be carried out [Foley, 2010]. Thus, in the majority of climate change impact studies, where the outcomes are not clearly defined and the knowledge about their probability is low, “scenario-based” approaches, as the one used in this thesis and described in Chapter 2, are recommended.

The traditional workflow of climate change impact studies, described in Chapter 2, is composed by a chain of models. Each of them contains, to some extent, uncertain elements, which contribute to increase the global uncertainty. In Mitchell and Houlme [1999] the concept of the “cascade of uncertainty” is introduced. It is described as the ad-

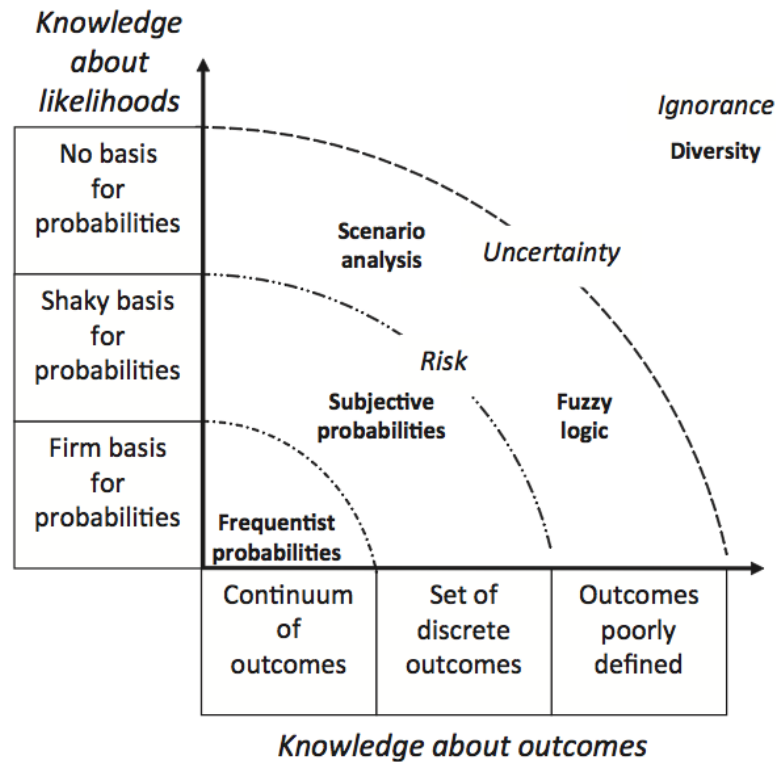


Figure 7.1: A scheme for defining ‘risk’, ‘uncertainty’ and ‘ignorance’, taken from Foley [2010]

ditive process that leads to a fast growing global uncertainty in the output of regional climate modelling.

This early “cascade” consists of three stages, schematized by triangles (Figure 7.2): the first represents the solar model and socio economic model, producing the magnitude of change in the external forcing; the second represents the climate model, producing the magnitude of climate change; the third represents the impact model, describing the magnitude of the environmental change. The basis of the triangles shows the raised uncertainty compared to the vertex, as shown in Figure 7.2.

More recently, Wilby and Dessai [2010], describe a similar concept: the “Envelope of Uncertainty” with an increased number of steps through which the uncertainty grows. Obviously, the advancements in the different research fields, in addition to a better understanding of the system, also lead to a more complex modelling chain, which produces a more detailed cascade of uncertainty. In this work we show a modified version of the original “cascade of uncertainty”, which fits to our analysis and case study but can be applied to other climate change impact studies in the field of water resources management. In the next sections the uncertainty sources related to the different components shown in Figure 7.3 are described in detail.

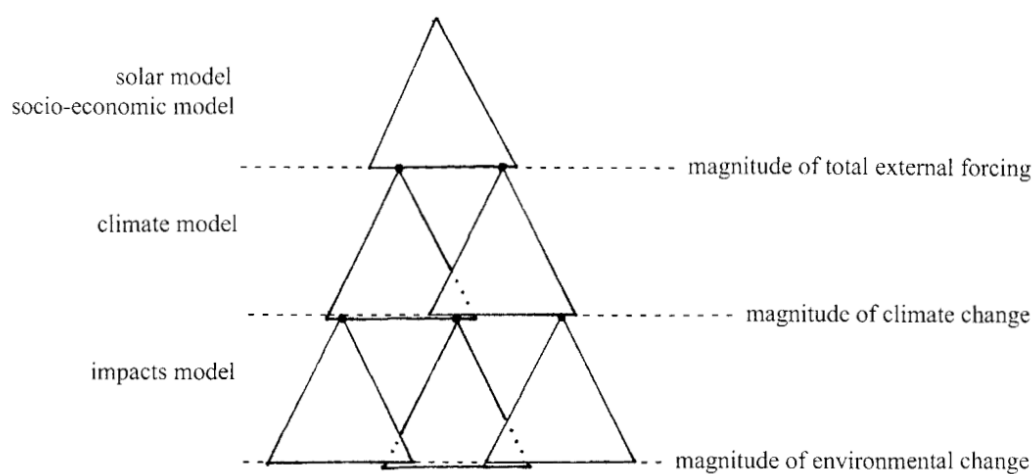


Figure 7.2: The "Cascade of Uncertainty", from Mitchell and Hulme [1999]

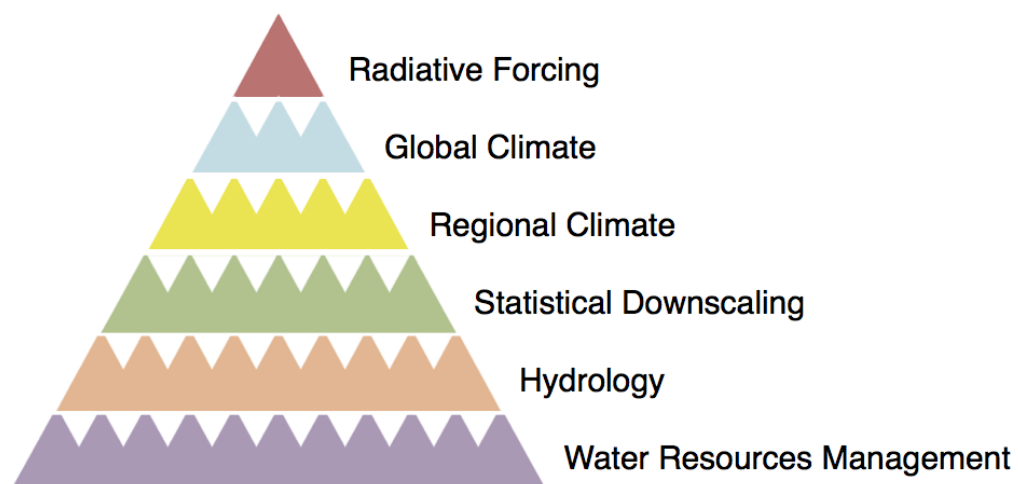


Figure 7.3: The cascade of uncertainty applied to the study case, adapted from Wilby and Dessai [2010]

7.1.1 *Uncertainty in Radiative Forcing Modelling*

The description of the radiative forcing and the resulting definition of the Representative Concentration Pathways are associated with many sources of uncertainty. The definition of an emission scenario, which is the cause of the increase in radiative forcing (see Chapter 2), involves the understanding of the population growth, the economic and social development and the future patterns of production and consumption of energy. In this context, the principal source of uncertainty stems from the unpredictability of anthropogenic GHGs emissions and their resultant atmospheric concentration [Foley, 2010]. The definition of radiative forcing scenarios, in addition to the emission scenarios (like the old SRES), implies also the complex description of the atmospheric GHGs concentrations and of the atmosphere chemistry [Moss et al., 2010]. Further important aspects and potential sources of uncertainty are the climate feedback and possible unexpected consequences [Foley, 2010], which can arise when GHGs emissions interfere with natural climate processes. One example can be the permafrost melting [Anisimov, 2007]. While it melts, methane and soil carbon contained in the Arctic and Siberian frozen soil are released, resulting in further global warming. This may obviously lead to a further thawing, amplifying the original signal as a positive feedback. It has been suggested that methane released from permafrost may have been the trigger for deglaciation at the end of the Marinoan ice age, approximately 635M years ago [Kennedy et al., 2008].

7.1.2 *Uncertainty in Global Climate Modelling*

In the global climate modelling and in the GCMs design, uncertainty arises from a limited understanding of the physical processes of the atmosphere that, combined with a coarse spatial resolution, leads to an inappropriate description of the interactions among atmosphere, oceans, cryosphere and land. Especially the parameterization of physical processes taking place at the small scale, for example cloud formation, is a highly crucial aspect [Murphy et al., 2004]. Clouds have a variety of effects on both the water balance and the radiation budget, which are determined by their height and type [Foley, 2010]. For instance, low and thick clouds, such as stratocumulus, have a cooling effect as they reflect back sunlight, while thin and high clouds such as cirrus, can constitute an extra forcing by trapping outgoing longwave radiation. All these different effects can not be reproduced in GCMs because they happen at a too low spatial resolution.

7.1.3 *Uncertainty in Regional Climate Modelling*

The sources of uncertainty related to Regional Climate Modelling and hence to the RCMs design are not dissimilar to the ones already described for GCMs. The main difference is the finer resolution, which allows RCMs to account for other aspects such as orography, land cover and small atmospheric feature. Since the climate systems have similarities with non-linear, chaotic systems [Foley, 2010], unpredictability can arise in two different ways, due to the concepts known in the literature as predictability of the first and of the second kind [Chu, 1998]. The first kind of predictability is related with initial conditions, and describes the amplification over time of errors in initial conditions. It represents one of the reasons why it is not possible to make accurate weather forecast beyond a week. The second kind of predictability is related to boundary conditions. The RCM domains have boundaries with the surrounding environment, and the model must consider the physical processes taking place also in this environment. Even though it has been less studied than the first kind of predictability, it has been argued that small variations to boundary conditions can also lead to large differences in the future behaviour [Chu, 1998]. For future projections, RCMs usually inherit both initial and boundary conditions from a parent GCM, with procedures known as nesting [Ding et al., 2006; Ju et al., 2007], or double-nesting [Im et al., 2006; Gao et al., 2006]. Since GCMs have already their own inherent flaws, RCM boundary conditions will always be a source of uncertainty.

7.1.4 *Uncertainty in Statistical Downscaling*

The choice of the downscaling procedure involves also a certain amount of uncertainty, arising from the quality of the available data and from the method employed. The historical climate observations needed for the statistical downscaling are often affected by measurement error. Moreover, the length of time series available might be too short to correctly describe the climate characteristics. Another source of uncertainty is related to the kind of relationship searched among the considered variables. This aspect depends on the downscaling procedure adopted. In this work, we use the Quantile Mapping technique, consisting in applying a correction function between the quantiles of observed and modelled values (Chapter 2).

7.1.5 *Uncertainty in Hydrological Modelling*

Although it has been argued that uncertainty related to the hydrological model is much smaller than the one related to climate projections [Teng et al., 2012], that step represents an important part of the modelling chain and uncertainty could arise in many different

ways. First, the uncertainty of a hydrological model could be related to its structure, which might not correctly represent the physical processes occurring among climate variables and streamflows. This is mainly the case of lumped and empirical rainfall-runoff models, but also physically-based and fully distributed hydrological models, as Topkapi-ETH (Chapter 2), can suffer of structural uncertainty [Finger et al., 2012]. A second source of uncertainty is represented by the parameters, since calibration is a critical step of hydrological modelling. A further aspect of the uncertainty in hydrological modelling, when studying Alpine areas, is related to the description of snow and ice in the catchment. It has been shown how glacier dynamics are crucial in determining changes in streamflow during the summer months [Finger et al., 2012], while in Jung et al. [2012] it is demonstrated that in snow-dominated catchments the uncertainty related to the hydrological model parameters is higher than elsewhere.

7.1.6 *Uncertainty in Water Resources Management*

Uncertainties in the description of the water management system could stem from the system model and from the manager behaviour. Regarding the system model, the structural error is quite small. The hydropower reservoir description provided in Topkapi-ETH, considering the scale of interest, is, for instance, quite accurate, if considering only the physical system. On the contrary, the sources of uncertainty regarding the water system manager behaviour could be several. If considering again the example of an Alpine hydropower reservoir, variations in the energy price or water demand will lead the reservoirs manager to change the behaviour as much as variations in the hydrological conditions [Anghileri, 2013]. This last aspect must be taken into account when carrying out analyses, which aim to explicitly consider the water resources management.

7.2 METHODS USED IN THE LITERATURE TO ADDRESS UNCERTAINTY

The problems related to uncertainty described in the previous section led to a deep research interest in the topic. The examined aspects are its general quantification, its relative partition among the different sources, and its relationship with the internal climate variability. The internal climate variability is shown by the natural fluctuations of the climate variables that arise also with no changes in the radiative forcing [Hawkins and Sutton, 2009]. It constitutes a further source of uncertainty that, if not explicitly taken into account, could be confused with climate change induced variations and mislead the results. Thus, the appreciation of the internal climate variability and its fluctuations are key matters for the decision making.

In the past, uncertainty has been tackled in several different ways, as the width and the complexity of the topic allow the use of many approaches. A climate model can perform well in representing one aspect of the climate, and lack skills in modelling another. Often climate models simulate accurately future seasonal trends, but do not give a clear description of changes in extreme events. The results of a study may vary a lot depending on the choice of the model and, in order to have robust and reliable findings, often a combination of different models, known as ensemble, can provide overall a higher reliability [Tebaldi and Knutti, 2007]. Ensemble methods are widespread in climate change studies and they can be distinguished in two categories: multi-model ensembles and perturbed physics ensembles. The multi-model ensemble approach consists in combining multiple model prediction together [Mitchell and Hulme, 1999]. Ideally, individual members of the ensemble should show high performances by themselves and correctly represent the climate. However, in reality, using multi-model ensembles can compensate single model weaknesses and errors. The multi-model ensemble approach can potentially generate misleading results, since often the members are chosen more due to their availability than for demonstrated quality [Allen and Stainforth, 2002]. Multi-model ensembles have also the strength to account for intermodal variability, representing it in the spread of the projections. The perturbed physics ensemble approach consists of several run of a single model, each perturbing the parameterization [Barnett et al., 2006]. Theoretically, in doing so, the uncertainty related to the model parameterization should be represented in the output spread. Compared to the multi-model ensembles, whose members are chosen on an opportunistic basis [Murphy et al., 2007], with perturbed physics ensembles the quantification of uncertainty should be more systematic [Foley, 2010]. The drawback is that this implies the subjective choice of the model to be used. This decision could be taken based on performance indicators, but the most skillful model in representing the current climate may not be as reliable under future conditions. While a perturbed physics approach can be used to quantify intra-model variability, it cannot characterize the inter-model variability as multi-model ensembles do.

In the last years, ensemble methods have been used in several works to tackle the problem of uncertainty in climate change impact studies. Hereafter, we present some of the most interesting recent findings, describing the methods that have been used to quantify and characterize uncertainty in climate change and water resources management studies.

Murphy et al. [2004] present an attempt to determine the range of climate changes based on a 53-members ensemble of the GCM HadAM3

obtained by varying the parameters. The parameters affected by the perturbation were the ones regarding the main processes described in the climate models such as: cloud formation, precipitation, convection, solar radiation, and land surface processes. The ensemble produced a range of climate changes much wider, in terms of climate variables probability distribution, than the ones predicted by methods based on individual simulations.

Horton et al. [2006] assess the hydrological response to climate change over 11 catchments in the Swiss Alps with a reservoir-based hydrological model. Nineteen combinations of three GCMs and nine RCMs are taken into account together with two SRES emission scenarios. The method used to assess the uncertainty among different sources is the analysis of the simulations output driven by a single GCM and different RCMs and vice versa. The main finding is that, besides the uncertainty induced by the choice of the emission scenario, the variability associated with the choice of the RCM is comparable to the one related to the choice of the GCM.

A sophisticated decomposition of the variance is applied by Deque et al. [2007] in order to quantify the uncertainty in climate variables associated to different sources over the European domain. Two SRES scenarios, ten RCMs and three GCMs are considered within the framework of the PRUDENCE project. With an algebraic method the variance is decomposed and then aggregated into the four main uncertainty sources: the choice of the SRES, the choice of the GCM, the choice of the RCM, and the choice of the ensemble member (as some models were available in different simulations). The results show that the main source of uncertainty is related to the GCM choice, but during the summer the used RCMs provide a comparable contribution of variability.

Hawkins and Sutton [2009] show an attempt of separating the sources of uncertainty over a time horizon, in order to highlight the potential to narrow uncertainty in climate predictions, namely the possibility to reduce the global uncertainty addressing properly further research effort. The three components of internal variability of the climate, model uncertainty and scenario uncertainty are separated proposing a method based on the fit of the projection with a fourth-order polynomial. The results of the analysis based on 15 GCMs and three SRES show that, although the emission scenario contribution will increase till the end of the century, the main source of uncertainty within the next decades is the one related to the climate model.

A comparison of the uncertainty caused by GCMs and hydrological modelling is presented by Teng et al. [2012] in Southeast Australia.

To assess the variability related to the 15 GCMs and the five lumped rainfall-runoff models taken into account, the relative variation between minimum and maximum values of annual and seasonal mean was calculated, fixing first the GCM and then the hydrological model. The results show that uncertainty caused by global climate modelling is expected to be much higher than the one generated by hydrological modelling.

Jung et al. [2012] assess the uncertainty related to two SRES, eight GCMs and four different parameterizations of the hydrological model on two different US catchments, one snow-dominated and one rainfall-dominated. The method used to assess the relative contribution of the single modelling component to global uncertainty is based on calculating the maximum variation in runoff among the different sources. The main finding is that in the snow-dominated catchment the uncertainty related to the hydrological model parameters is higher than in the other study case. This suggests that the importance of an accurate hydrological modelling increases in mountainous and snow-dominated areas.

Another attempt in quantifying the uncertainty in climate change impact on hydrology is presented by Finger et al. [2012], where seven RCMs are used to feed Topkapi-ETH coupled with a dynamical glacier description. To take into account the hydrological modelling uncertainty, ten parameterization and three glacier extents are considered. To examine the uncertainty of the three sources (climate projections, Topkapi-ETH parameterizations and glacier extents), an ANalysis Of VAriance (ANOVA) is carried out. The ANOVA is done monthly and over two time frames in the future (2037-2064 and 2071-2098). The results show that the uncertainty related to climate projections is higher during winter and spring, while during summer and autumn the hydrology and glaciers contribute to a higher variability. In the period 2071-2098 the uncertainty related to the hydrological model parameters increases, whereas the one related to the glacier extents becomes smaller.

7.3 NUMERICAL RESULTS

In order to take into account uncertainty, we consider the highest number of climate scenarios available at the moment the thesis started. In total we take into account 22 scenarios from the EURO-CORDEX project, comprising two RCPs, seven GCMs and five RCMs, as described in Chapter 4. We consider the climate scenarios only due to their availability and not for demonstrated skills, and, although this could result in misleading outcomes when working with multi-model ensemble [Allen and Stainforth, 2002], we assume them equally performing

through the rest of the analysis. The goal of this analysis is to provide an assessment of the uncertainty related to the choice of [RCP](#), [GCM](#) and [RCM](#) and to quantify the relative contribution of these three sources to the global uncertainty. Theoretically, a formal uncertainty analysis could be carried out only with a wider availability of scenarios and an equal distribution of [RCPs](#), [GCMs](#), and [RCMs](#) in the ensemble. Although that is not our case, as already seen in [Table 4.3](#) in [Chapter 4](#), we perform a brief uncertainty characterization using the scenarios available. This characterization is done both analyzing climate variables and hydrological variables, to examine how the uncertainty on climate reflects on hydrology. In order to do so, we use simple and reproducible methods, basing our choices on the literature outlined in the last paragraphs. First, comparing the mean of temperature and precipitation in a graph, we try to assess in a first approximation, from the spread of the values of increases and reductions in mean temperature and precipitation, which source of modelling ([RCP](#), [RCM](#), and [GCM](#)), is responsible for the highest variability in the output. Then, similarly to what has been done by [Hawkins and Sutton \[2009\]](#), we try to quantify how this uncertainty evolves with time. After that, we analyze the hydrological scenarios, showing graphs of cyclostationary streamflow means, letting vary only one modelling component, to assess the uncertainty associated to that source.

The [Figures 7.4](#), [7.5](#), [7.6](#), and [7.7](#) are intended to give to assess the variability related to different sources, considering the spread of the simulation outputs. Among the three considered sources of uncertainty ([RCP](#), [GCM](#), and [RCM](#)) we fix one of them in turn and compute the mean daily temperature and precipitation over the control and future scenario for each combination of the other two sources. We then plot the difference for temperature and the relative difference for precipitation between future scenario and control period. The wider the spread of the dots related to one source is, the higher is the uncertainty caused by that source. As the members of our multi-model ensemble are not equally distributed among the different sources ([Chapter 4](#), [Table 4.3](#)) and many model combinations are missing, we consider only one [GCM](#), one [RCM](#) (the ones with the largest number of simulations available) and the two [RCPs](#) to perform the analysis. [Figure 7.4](#) shows the 12 climate scenarios having [RCA4](#) as [RCM](#), thus representing the variability related to [RCP](#) and [GCM](#). Despite the uneven number of [GCMs](#) (six) and [RCPs](#) (two), we see how the outputs related to the different [GCMs](#) (different colors and highlighted by the yellow polygon) are more spread on the graph than the ones related to the [RCPs](#) (different symbols: triangles for [RCP4.5](#) and dots for [RCP8.5](#)). The eight climate scenarios having [ICHEC](#) as [GCM](#) are shown in [Figure 7.5](#). We see that the spread of the statistics related to different [RCMs](#) (different colors and highlighted by the blue poly-

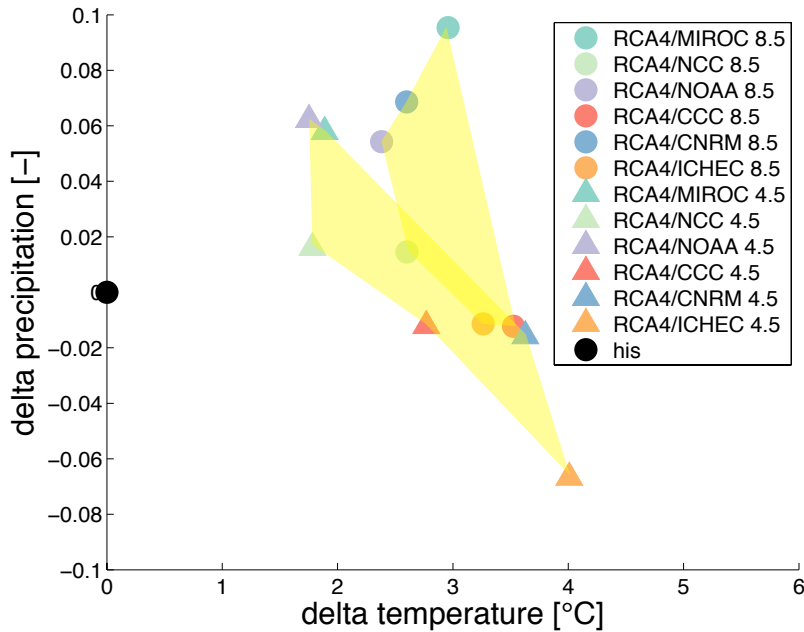


Figure 7.4: Uncertainty related to the choice of **GCM** and **RCP**

gon) is higher than the one with different symbols associated to the Representative Concentration Pathways. In Figures 7.6 and 7.7, nine scenarios, driven by the same **RCP** and having either the same **RCM** (RCA4) or **GCM** (ICHEC), are shown. Generally we might see that the variability induced by the choice of the **GCM**, represented by the spread of the dots (highlighted by the yellow polygon), is comparable to the one induced by the choice of the **RCM**, visible in the spread of the triangles (highlighted by the blue polygon). In both Figures we also see that the **RCM** RCA4 tends to predict an increase in the mean precipitation.

A further goal of this part of the analysis is to show how the relative contribution to the global uncertainty changes with time, following the general approach described in Hawkins and Sutton [2009], but using a slightly different methodology. Moreover, instead of concentrating on the uncertainty related to internal climate variability, general climate models and emission scenarios, we focus on radiative forcing scenarios, global climate modelling and regional climate modelling. In order to do so, we first calculate the mean of temperature and precipitation for the 22 climate scenarios over 19 five-year periods from 2006-2010 to 2096-2100. Then, we compute the Coefficient of Variation of the statistics just calculated among the climate scenarios with same **RCM** and **GCM**, but different **RCP**. The procedure is then repeated for the different modelling components: first calculating means and coefficients of variation for the models with same **RCP** and **RCM**, but different **GCM** and then calculating means and coeffi-

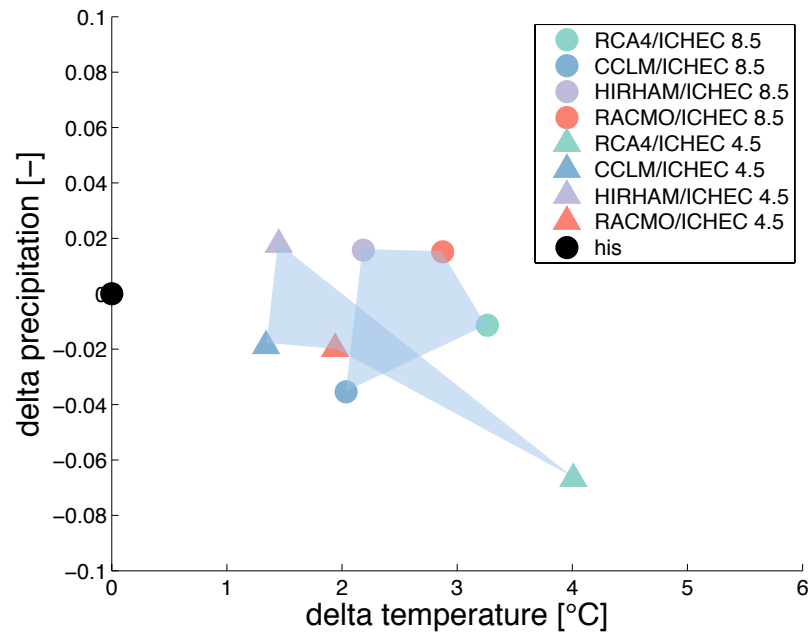


Figure 7.5: Uncertainty related to the choice of RCM and RCP

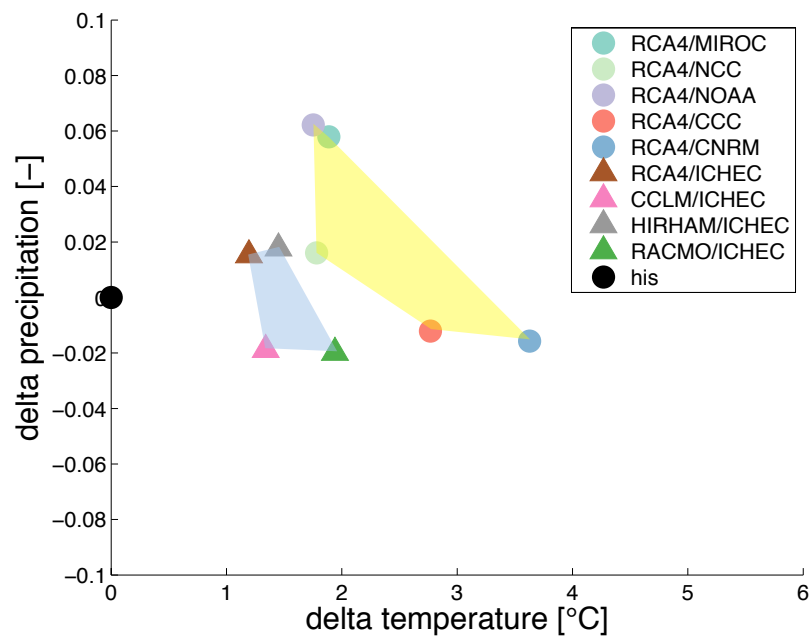


Figure 7.6: Uncertainty related to the choice of GCM and RCM fixing RCP4.5

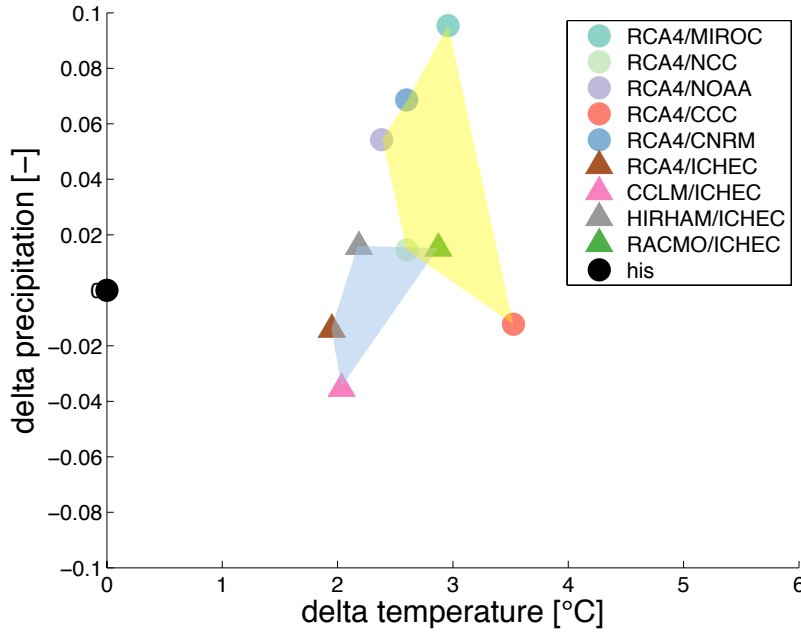


Figure 7.7: Uncertainty related to the choice of RCM and GCM fixing RCP8.5

coefficients of variation for the ones with same RCP and GCM, but different RCM. The Coefficient of Variation (CV) is chosen as non-dimensional and standardized measure, defined as the ratio between mean (μ) and standard deviation (σ).

$$CV = \frac{\sigma}{\mu}$$

The time series of the Coefficient of Variation related to the three components ($CV_t(\text{RCP})$, $CV_t(\text{GCM})$, and $CV_t(\text{RCM})$) are then normalized to unity in order to obtain the relative contribution to the global uncertainty. Then the obtained values are represented on the bar graphs shown in Figure 7.8 for temperature and 7.9 for precipitation. The employment of this method would assume that the three sources of uncertainty are independent from each other and this might not be correct, especially if considering RCM and GCM. Nevertheless, in a first approximation, we can consider this assumption valid and interpret the results shown in the two figures as a measure of the variability related to the three modelling components.

$$CV_{n_t}(\text{RCP}) = \frac{CV_t(\text{RCP})}{CV_t(\text{RCP}) + CV_t(\text{GCM}) + CV_t(\text{RCM})}$$

$$CV_{n_t}(\text{GCM}) = \frac{CV_t(\text{GCM})}{CV_t(\text{RCP}) + CV_t(\text{GCM}) + CV_t(\text{RCM})}$$

$$CV_{n_t}(\text{RCM}) = \frac{CV_t(\text{RCM})}{CV_t(\text{RCP}) + CV_t(\text{GCM}) + CV_t(\text{RCM})}$$

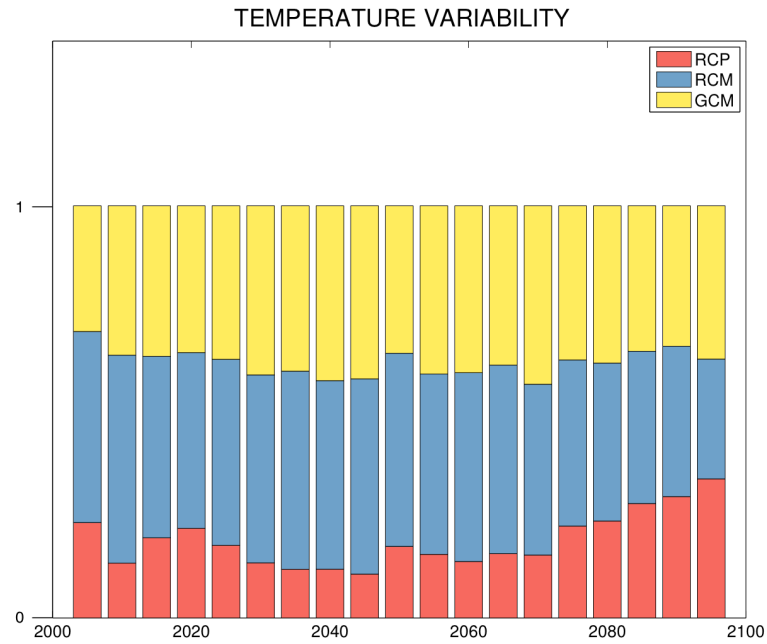


Figure 7.8: Temperature Uncertainty

Figure 7.8 shows that the uncertainty in temperature related to the choice of the GCM is comparable to the one related to the RCM choice. The choice of the RCP seems to have a lower impact at the beginning, but it grows with time after mid-century. The rising impact of the RCP choice is consistent with the definition of Representative Concentration Pathways in Figure 2.2, where we see how RCP4.5 and RCP8.5 begin to diverge considerably after the first half of the century. For the precipitation (Figure 7.9) the contribution to global uncertainty of the three modelling components has the same order of magnitude, and there is no shown growing trend in the RCP-related variability. The further step of this analysis is to examine how the uncertainty in climate variables reflects on the uncertainty of the hydrological future scenarios shown in Chapter 6. In order to do so, we follow a simple approach, similar to the one used to analyze the climate scenarios uncertainty. It is based on fixing two modelling components, letting the third one varying and analyzing the spread of the outputs to characterize the uncertainty. In this part of the work we wanted to examine the inter-annual variability. Therefore, we showed the cyclostationary mean of the streamflows at Fuentes over the future scenario, as computed in Chapter 6. Figures 7.10 and 7.11 show the outputs of combinations varying the RCP, while in Figures 7.12 and 7.13 the combinations with different GCM and RCM are represented. As already stated before, the unequal distribution of the available simulations in EURO-CORDEX (Table 4.3) and the considerably larger number of GCMs and RCMs, compared to the only two RCPs do not allow a for-

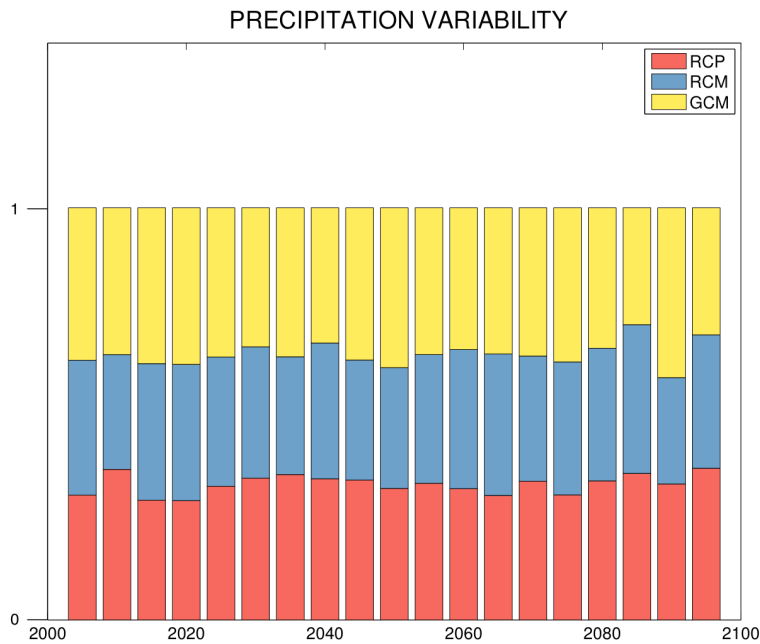


Figure 7.9: Precipitation Uncertainty

mal uncertainty analysis. Nevertheless, to a first approximation, we can see that the variability induced by different RCPs is lower than the one that might be induced by different climate models. Both global (Figure 7.12) and regional models (Figure 7.13) can produce considerably different seasonal hydrological patterns. Following a method used in Teng et al. [2012], we try to quantify this variability calculating the monthly percentage variation as the difference between the maximum and minimum values divided by the minimum. This analysis confirms that the choices of GCM and RCM play the most important role in terms of variability with an average variation of 39% for both components, while the minimum and maximum monthly variations were 21% and 68% and 19% and 60% respectively. On the contrary the RCP variability proves to be less significant, with a mean value of 10% and minimum and maximum monthly values of 7% and 16%.

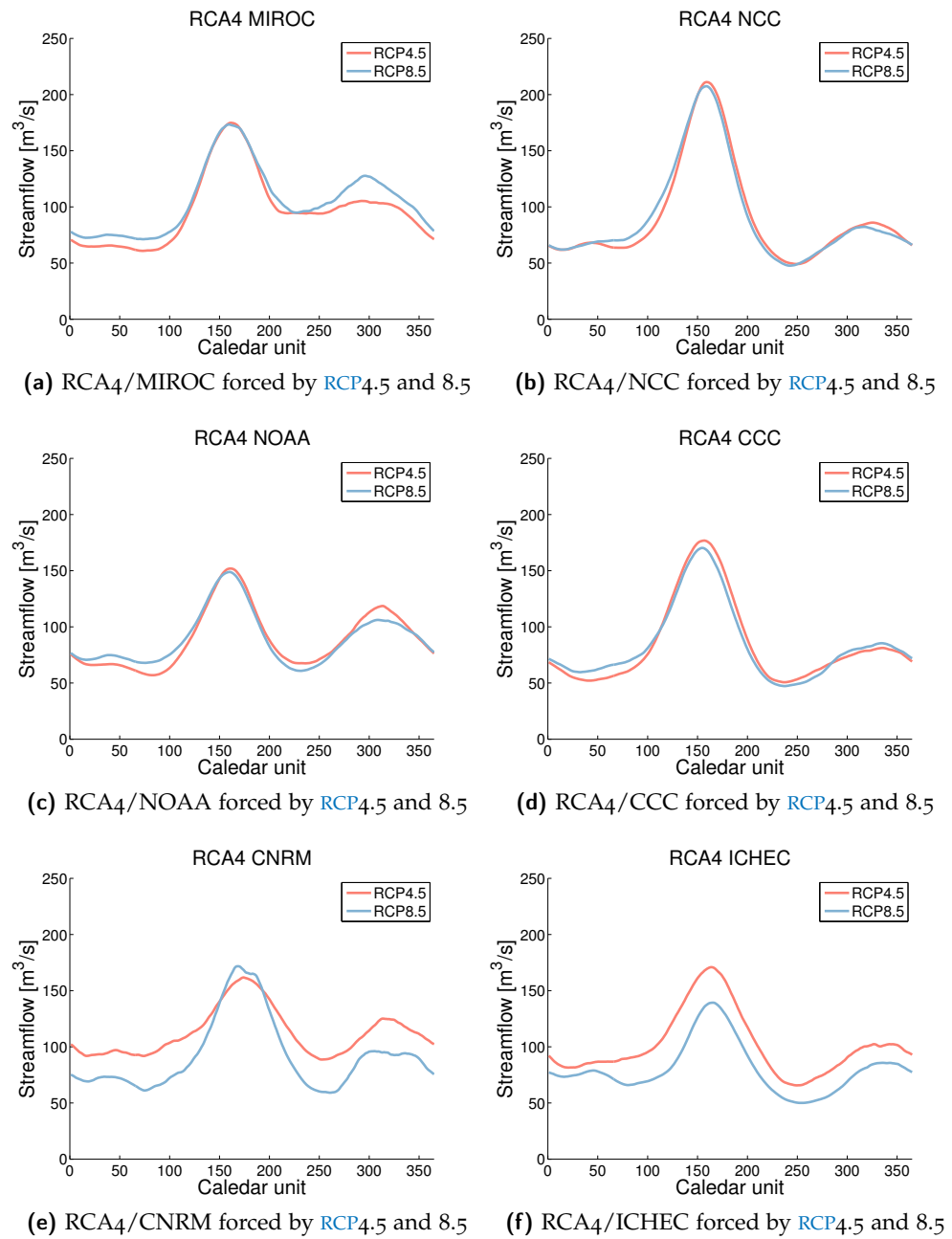


Figure 7.10: Mean trajectories simulated at Fuentes of the scenarios RCA4/MIROC, RCA4/NCC, RCA4/NOAA, RCA4/CCC, RCA4/CNRM, and RCA4/ICHEC forced by RCP4.5 and 8.5

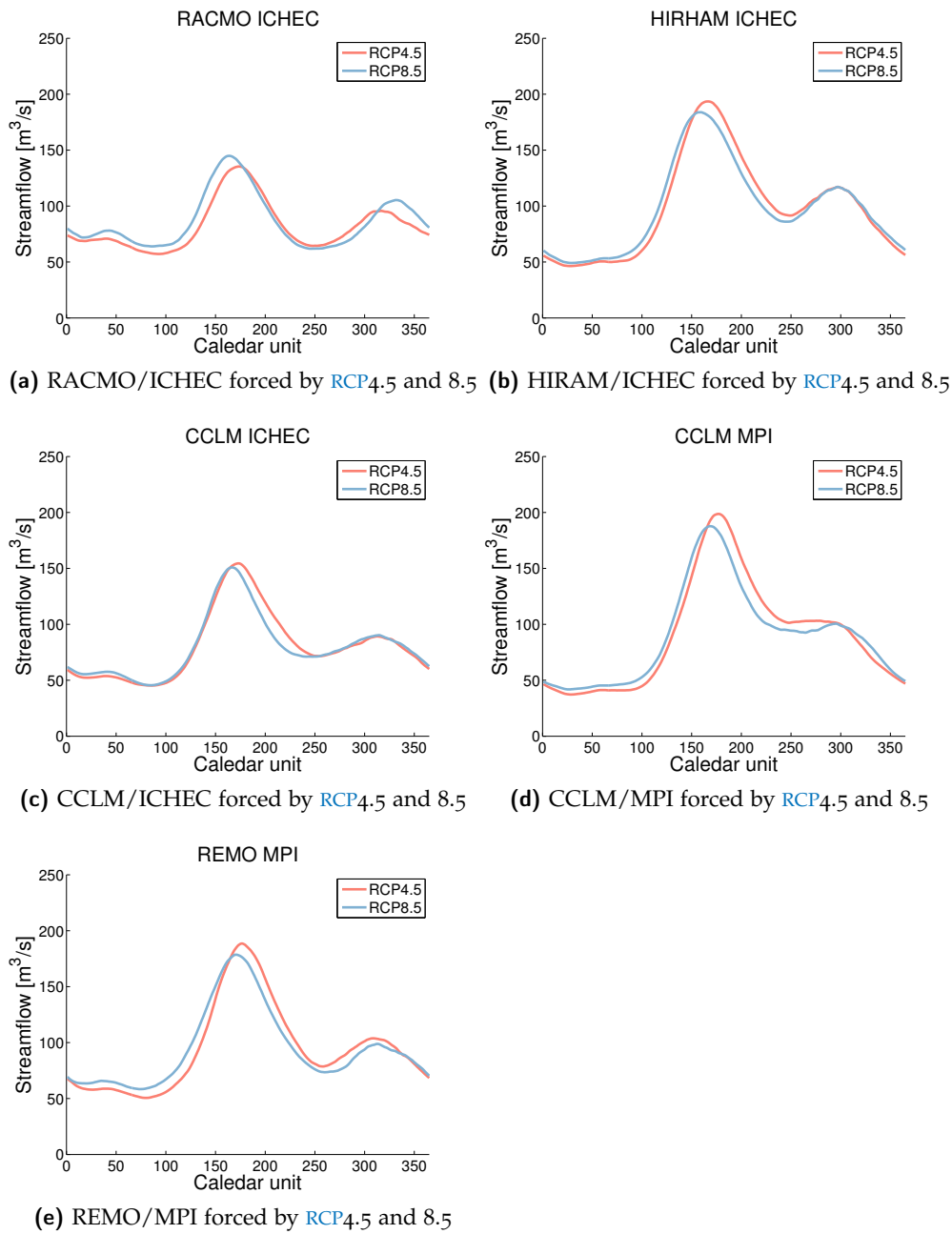
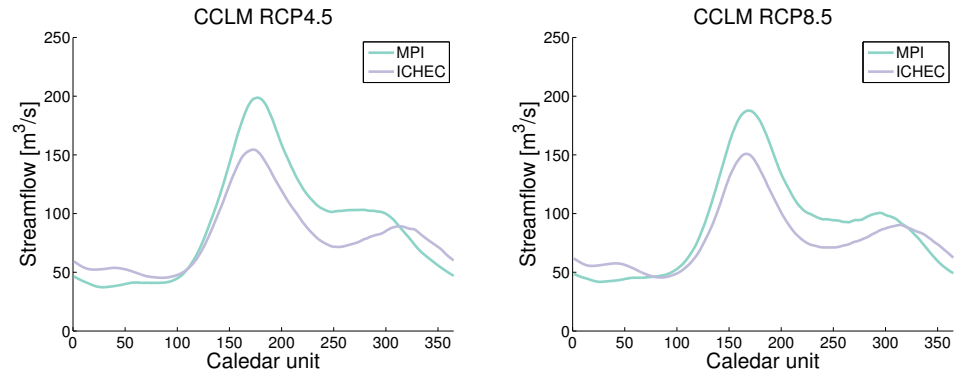
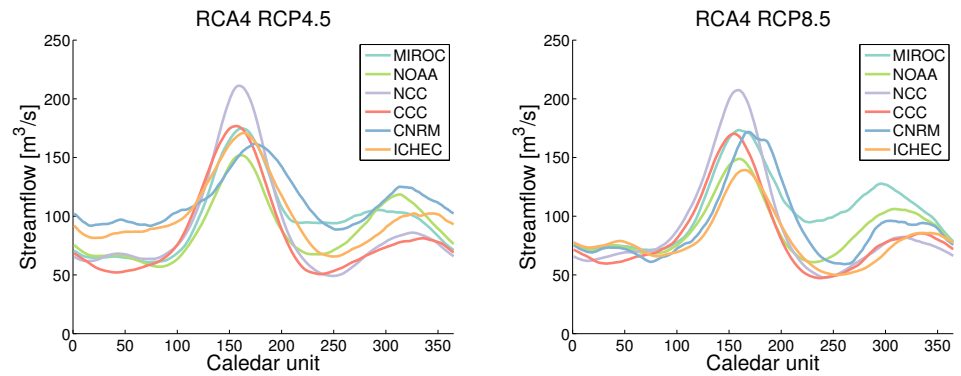


Figure 7.11: Mean trajectories simulated at Fuentes of the scenarios RACMO/ICHEC, HIRHAM/ICHEC, CCLM/ICHEC, CCLM/MPI, and REMO/MPI forced by RCP4.5 and 8.5



(a) CCLM/ICHEC and CCLM/MPI forced by RCP4.5 (b) CCLM/ICHEC and CCLM/MPI forced by RCP8.5



(c) RCA₄/MIROC, RCA₄/NOAA, RCA₄/CNRM, and RCA₄/ICHEC forced by RCP4.5 (d) RCA₄/MIROC, RCA₄/NCC, RCA₄/NOAA, RCA₄/CCC, RCA₄/CNRM, and RCA₄/ICHEC forced by RCP8.5

Figure 7.12: Mean trajectories simulated at Fuentes of the scenarios CCLM/ICHEC, CCLM/MPI, RCA₄/MIROC, RCA₄/NCC, RCA₄/NOAA, RCA₄/CCC, RCA₄/CNRM, and RCA₄/ICHEC forced by RCP4.5 and 8.5

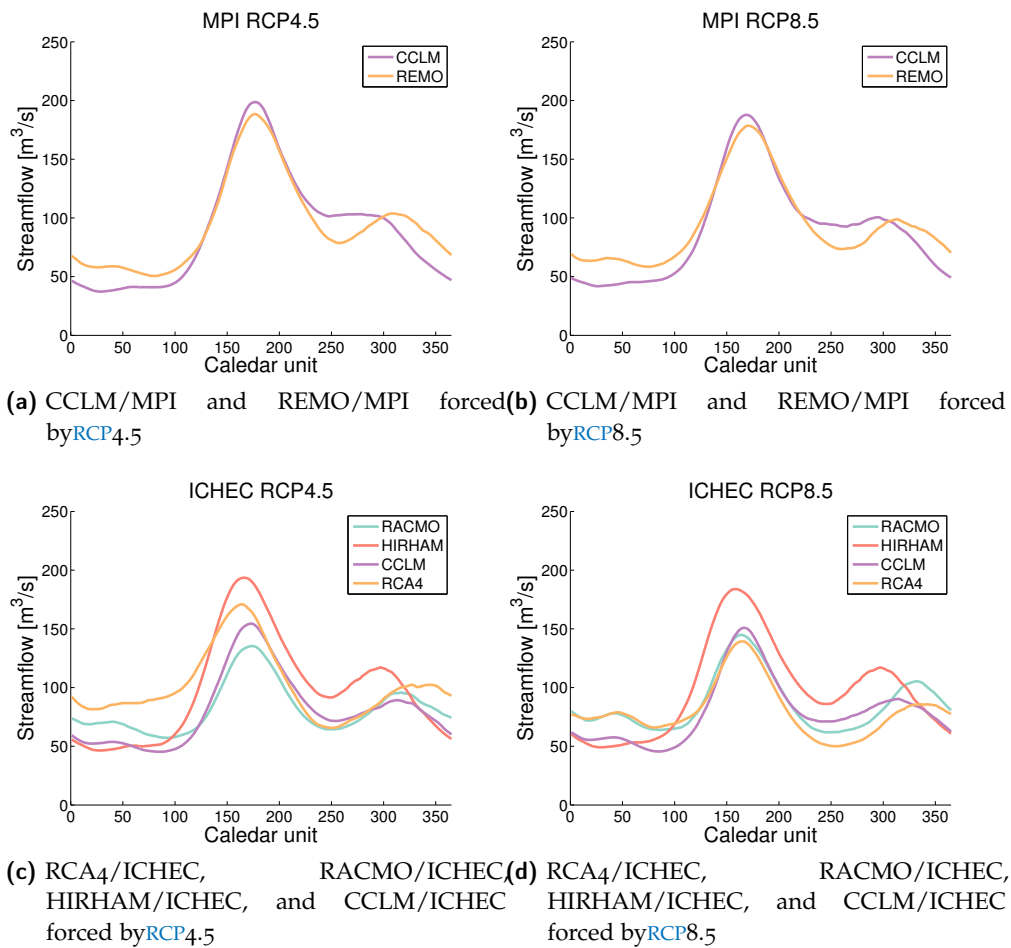


Figure 7.13: Mean trajectories simulated at Fuentes of the scenarios CCLM/MPI, REMO/MPI, RCA₄/ICHEC, RACMO/ICHEC, HIRHAM/ICHEC, and CCLM/ICHEC forced by RCP_{4.5} and 8.5

CONCLUSIONS

The objective of the thesis is to assess the impact of climate change on the hydrology of Alpine catchments and on the hydropower reservoirs. We focus on a case study in the Southern Alps: the Lake Como catchment, an area of 4762 Km², partly located in Switzerland and characterized by a dense hydropower network. The approach adopted is the one in literature often referred as “scenario-based”, or “top-down” approach. The “scenario-based” approach consists in the employment of a modelling chain, comprising the definition of GHGs emission scenarios, the global and regional climate modelling, the hydrological modelling and the modelling of the impact on the water resources management. The traditional weakness of this approach is the high uncertainty, which grows along the modelling chain. We tackle uncertainty taking into account a large number of climate scenarios and carrying out an uncertainty characterization in parallel with the “scenario-based” workflow.

The first part of the analysis is related to the climate change. We retrieve 22 climate scenarios from the EURO-CORDEX project including in total two different RCPs (RCP4.5 and RCP8.5), seven General Circulation Models (MPI, NOAA, NCC, CCC, ICHEC, MPI, MIROC), five Regional Circulation Models (REMO, RCA4, RACMO, HIRHAM, CCLM). Through a statistical analysis of the climate scenarios, we show that temperature would increase evenly over the domain of interest in the next century. Regarding precipitation, the climate models do not show the same changes in the mean yearly precipitation, but the majority of them shows a shift in the seasonal patterns, with drier summers and more rainy winters.

The next step of the analysis is the hydrological modelling via Topkapi-ETH, a physically-based and fully distributed model. The employment of a spatially distributed model is crucial to analyze the complex response of hydrology to climate change, allowing the detection of impacts on different areas and constituents of the river basin. In order to refine the spatial resolution of the climate scenarios we apply a statistical downscaling with the Quantile Mapping technique. We calibrate and validate Topkapi-ETH over the time horizon 1990-1999, focusing on the river section of Fuentes, located in proximity to the Lake Como. The final validation performance reached with the best parameterization shows R² values of 0.69, when computed on a daily basis, and 0.79 on a weekly basis. The analysis of the effects of climate change on the hydrology with the MASH tool shows similar trends with each climate scenario simulated: an increase in the

winter streamflow, a decrease in the summer streamflow and an earlier snowmelt peak. These behaviours are more pronounced when considering RCP8.5. The analysis of the glacier discharge shows a general decrease due to retreat, which seems to be more intense for glaciers located at lower elevations.

The last part of this work deals with the inflow to the Alpine reservoirs and the analysis of their seasonal storage. Topkapi-ETH allows taking into account reservoirs, and in our analysis we implement them forcing a “rule curve” as target level for reservoir operation. We focus on the main reservoir of the catchment, namely San Giacomo and Cancano. The MASH tool reveals how the seasonal changes of the inflow to the reservoir are qualitatively comparable to the ones registered at Fuentes. The main aspects are again a shift towards higher streamflows in winter, lower streamflows in summer and an earlier snowmelt peak. The seasonal shift influences the reservoir storages, by making it more difficult to reach the target level in summer, due to a considerably lower inflow in those months. The changes in the hydrological cycle will very likely induce hydropower companies to adopt new water management practices.

Finally, we carry out a brief uncertainty characterization. The characterization aims to assess the relative contribution to the global uncertainty of the three modelling components considered in the ensemble of climate scenarios: the RCP, the GCM and the RCM. Our findings show that the main source of uncertainty is related to the choice of the GCM, followed shortly by the one of the RCM and then by the one of the RCP, which has a lower impact at the beginning of the simulation horizon, but grows with time. Although based on several assumptions due to the limited number of climate scenarios available at the time of the analysis, our results are concordant with others shown in the literature.

Further research effort could be addressed to the implementation of more sophisticated operating policies, in order to better represent the behaviour of the reservoir manager. In this way, it could be better shown how changes in the reservoirs’ inflow induce changes in hydropower production, in terms of electricity produced and economic profit. The spatially distributed hydrological modelling, as well as the possibility to account for anthropogenic infrastructures in Topkapi-ETH, allows the analysis of the effect of possible mitigation measures in every single area of the catchment. This spatial analysis could ultimately be extended to other water-related activities besides hydropower production (e.g., flood protection, ecosystem conservation, and agriculture). Moreover, in order to extend the results of the uncertainty analysis, it would be important to rely on a higher number of simulations. This would allow a more comprehensive uncertainty analysis, that could be carried out with more sophisticated methods. Furthermore, it could be interesting to see the results of the RCP2.6,

the so-called “peak-and-decline” scenario, in order to estimate if and by how much lower [GHGs](#) emission at the end of the century could mitigate the effects of climate change on hydropower production.

BIBLIOGRAPHY

- [Allen and Stainforth, 2002] Allen, M. and Stainforth, D. (2002). Towards objective probabilistic climate forecasting. *Nature*, 419.
- [Anghileri, 2013] Anghileri, D. (2013). *Management of Multi-Purpose Reservoirs Under Climate Change: Impact Assessment and Adaptation Strategies*. PhD thesis, Politecnico di Milano, Department Elettronica, Informazione e Bioingegneria.
- [Anghileri et al., 2011] Anghileri, D., Pianosi, F., and Soncini-Sessa, R. (2011). A framework for the quantitative assessment of climate change impacts on water-related activities at the basin scale. *Hydrology and Earth System Science*, 15, 15.
- [Anghileri et al., 2014] Anghileri, D., Pianosi, F., and Soncini-Sessa, R. (2014). Trend detection in seasonal data: from hydrology to water resources. *Journal of Hydrology*, 511.
- [Anisimov, 2007] Anisimov, O. (2007). Potential feedback of thawing permafrost to the global climate system through methane emission. *Environmental Research Letters*, 2.
- [Barnett et al., 2006] Barnett, D., Brown, J., Murphy, J., Sexton, D., and Webb, M. (2006). Quantifying uncertainty in changes in extreme event frequency in response to doubled co2 using a large ensemble of gcm simulations. *Climate Dynamics*, 26.
- [Beniston, 2003] Beniston, M. (2003). Climatic change in mountain regions: a review of possible impacts. *Climatic Change*, 59.
- [Boe et al., 2007] Boe, J., Terray, L., Habetsb, F., and Martinc, E. (2007). Statistical and dynamical downscaling of the seine basin climate for hydro-meteorological studies. *International Journal of Climatology*, 27.
- [Carenzo et al., 2009] Carenzo, M., Pellicciotti, F., Rimkus, S., and Burlando, P. (2009). Assessing the transferability and robustness of an enhanced temperature-index glacier melt model. *Journal of Glaciology*, 55.
- [Chu, 1998] Chu, P. (1998). Two kinds of predictability in the lorenz system. *Journal of the Atmospheric Sciences*, 56.
- [Ciarapica and Todini, 2002] Ciarapica, L. and Todini, E. (2002). Topkapi: a model for the representation of the rainfall-runoff process at different scales. *Hydrolog. Proc.*, 16.

- [Clarke, 2007] Clarke (2007). Scenarios of greenhouse gas emissions and atmospheric concentrations. *Sub-report of Synthesis and Assessment Product, US Climate Change Science Program and the Subcommittee on Global Change Research, Department of Energy, Office of Biological and Environmental Research, Washington DC*, 1.
- [Corripio, 2003] Corripio, J. (2003). Vectorial algebra algorithms for calculating terrain parameters from dems and solar radiation modelling in mountainous terrain. *International Journal of Geographical Information*, 17.
- [Deque, 2007] Deque, M. (2007). Frequency of precipitation and temperature extremes over france in an anthropogenic scenario: Model results and statistical correction according to observed values. *Global and Planetary Change*, 57.
- [Deque et al., 2007] Deque, M., Rowell, D. P., Luethi, D., Giorgi, F., Christensen, J., Rockel, B., and Jacob, D. (2007). An intercomparison of regional climate simulations for europe: assessing uncertainties in model projections. *Climatic Change*, 81.
- [Ding et al., 2006] Ding, Y., Shi, X., Liu, Y., Liu, Y., Li, Q., and Qian, F. (2006). Multi-year simulations and experimental seasonal predictions for rainy seasons in china by using a nested regional climate model (regcm-ncc). part i: Sensitivity study. *Advances in Atmospheric Sciences*, 23.
- [Energiebundesamt, 2012] Energiebundesamt (2012). Schweizerische elektrizitätsstatistik 2012. Technical report, Schweizerische Eidgenossenschaft.
- [Farinotti et al., 2009] Farinotti, D., Huss, M., Bauder, A., and Funk, M. (2009). An estimate of the glacier ice volume in the swiss alps. *Global and Planetary Change*, 68.
- [Fatichi et al., 2013] Fatichi, S., Rimkus, S., Burlando, P., Bordoy, R., and Molnar, P. (2013). Elevational dependence of climate change impacts on water resources in an alpine catchment. *Hydrology and Earth System Science*, 10.
- [Finger et al., 2012] Finger, D., Heinrich, G., Gobiet, A., and A., B. (2012). Projections of future water resources and their uncertainty in a glacierized catchment in the swiss alps and the subsequent effects on hydropower production during the 21st century. *Water resources research*, 48.
- [Foley, 2010] Foley, A. (2010). Uncertainty in regional climate modelling: A review. *Progress in Physical Geography*, 1.
- [Fowler and Tebaldi, 2007] Fowler, H. J. and Blenkinsop, S. and Tebaldi, C. (2007). Linking climate change modelling to impacts

- studies: recent advances in downscaling techniques for hydrological modelling. *International Journal of Climatology*, 27.
- [Frei et al., 2006] Frei, C., Schoell, R., and Fukutome, S. (2006). Future change of precipitation extremes in europe: Intercomparison of scenarios from regional climate models. *Journal of Geophysical Research*, 111.
- [Frei et al., 1998] Frei, C., Schär, C., Lüthi, D., and Davies, H. (1998). Heavy precipitation processes in a warmer climate. *Geophysical Research Letters*, 25.
- [Fujino, 2006] Fujino, J. (2006). Multigas mitigation analysis on stabilization scenarios using aim global model. multigas mitigation and climate policy. *The Energy Journal*, 3.
- [Gao et al., 2006] Gao, X., Pal, j., and Giorgi, F. (2006). Projected changes in mean and extreme precipitation over the mediterranean region from a high resolution double nested rcm simulation. *Geophysical Research Letters*, 33.
- [Gaudard et al., 2014] Gaudard, L., Romerio, F., Dalla Valle, F., and Gorret, R. (2014). Climate change impacts on hydropower in the swiss and italian alps. *Science of the Total Environment*, 493.
- [Giacomelli et al., 2008] Giacomelli, P., Rossetti, A., and Brambilla, M. (2008). Adapting water allocation management to drought scenarios. *Natural Hazards Earth System Science*, 8.
- [Giorgi et al., 2009] Giorgi, F., Jones, C., and Asrar, G. (2009). Addressing climate information needs at the regional level: the cordex framework. *WMO Bulletin*, 58.
- [Gobiet et al., 2014] Gobiet, A., Sven Kotlarski, S., and Beniston, M. (2014). 21st century climate change in the european alps—a review. *Science of the Total Environment*, 493.
- [Green, 1992] Green, C. (1992). Economics and the green-house effect. *Climatic Change*, 22.
- [Gupta et al., 2009] Gupta, H., Kling, H., Yilmaz, K., and Martinez, G. (2009). Decomposition of the mean squared error and nse performance criteria: Implications for improving hydrological modelling. *Journal of Hydrology*, 377.
- [Haeberli and Beniston, 1998] Haeberli, W. and Beniston, M. (1998). Climate change and its impacts on glaciers and permafrost in the alps. *Ambio*, 27.
- [Hawkins and Sutton, 2009] Hawkins, E. and Sutton, R. (2009). The potential to narrow uncertainty in regional climate predictions. *American Meteorological Society*, 41.

- [Hay et al., 2000] Hay, L., Wilby, R., and Leavesley, G. (2000). A comparison of delta change downscaled gcm scenarios for three mountainous basins in the united states. *Journal of the American Water Resources Association*, 36.
- [Hijioka et al., 2008] Hijioka, Y., Matsuoka, Y., Nishimoto, H., and Masui, M. (2008). Global ghg emissions scenarios under ghg concentration stabilization targets. *Journal of Global Environmental Engineering*, 13.
- [Hogan and Jorgenson, 1991] Hogan, W. and Jorgenson, D. (1991). Productivity trends and the cost of reducing co2 emissions. *The Energy Journal*, 12.
- [Horton et al., 2006] Horton, P., Schaepli, B., Mezghani, A., Hingray, B., and Musy, A. (2006). Assessment of climate-change impacts on alpine discharge regimes with climate model uncertainty. *Hydrological Processes*, 20.
- [Im et al., 2006] Im, E., Park, E., Kwon, W., and Giorgi, F. (2006). Present climate simulation over korea with a regional climate model using a one-way double-nested system. *Theoretical and Applied Climatology*, 86.
- [IPCC, 2014] IPCC (2014). Climate change 2014. impacts, adaptation and vulnerability. part a: Global and sectoral aspects. *Fifth Assessment Report, WGII*.
- [Isotta et al., 2014] Isotta, F., Frei, C., and Weingartner, V. (2014). The climate of daily precipitation in the alps: development and analysis of a high-resolution grid dataset from pan-alpine rain-gauge data. *International Journal of Climatology*, 34.
- [Jacob et al., 2014] Jacob, D., Petersen, J., and Eggert, B. (2014). Euro-cordex: new high-resolution climate change projections for european impact research. *Regional Environmental Change*, 14.
- [Jansson et al., 2003] Jansson, P., Hock, R., and Schneider, T. (2003). The concept of glacier storage: a review. *Journal of Hydrology*, 282.
- [Ju et al., 2007] Ju, L., Wang, H., and Jiang, D. (2007). Simulation of the last glacial maximum climate over east asia with a regional climate model nested in a general circulation model. *Palaeogeography, Palaeoclimatology, Palaeoecology*, 248.
- [Jung et al., 2012] Jung, W., Moradkhani, H., and H., C. (2012). Uncertainty assessment of climate change impacts for hydrologically distinct river basins. *Journal of Hydrology*, 8.
- [Kennedy et al., 2008] Kennedy, M., Mrofka, D., and Von der Borch, C. (2008). Snowball earth termination by destabilization of equatorial permafrost methane clathrate. *Nature*, 453.

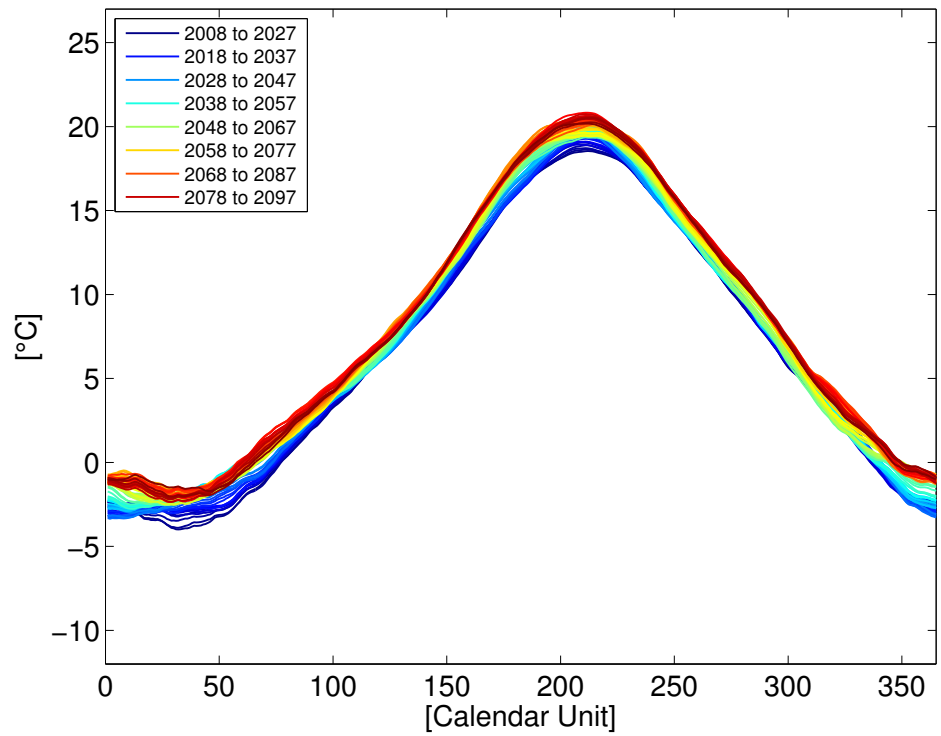
- [Legates and McCabe, 1999] Legates, D. and McCabe, G. (1999). Evaluating the use of goodness of fit measures in hydrologic and hydroclimatic model validation. *Water resources research*, 35.
- [Liu et al., 2005] Liu, Z., Martina, M. L. V., and Todini, E. (2005). Flood forecasting using a fully distributed model: application of the topkapi model to the upper xixian catchment. *Hydrology and Earth System Science*, 9.
- [Liu and Todini, 2002] Liu, Z. and Todini, E. (2002). Towards a comprehensive physically-based rainfall-runoff model. *Hydrology and Earth System Sciences*, 6.
- [Liu and Todini, 2006] Liu, Z. and Todini, E. (2006). Assessing the topkapi non-linear reservoir cascade approximation by means of a characteristic lines solution. *Hydrological Processes*, 19.
- [Mearns et al., 2003] Mearns, L., Giorgi, F., Whetton, P., Pabon, D., Hulme, M., and Lal, M. (2003). Guidelines for use of climate scenarios developed from regional climate model experiments. Technical report, IPCC.
- [Mitchell and Hulme, 1999] Mitchell, D. and Hulme, M. (1999). Predicting regional climate change: living with uncertainty. *Progress in Physical Geography*, 23.
- [Moss et al., 2010] Moss, R., Edmonds, J., Hibbard, K., and Manning, R. (2010). The next generation of scenarios for climate change research and assessment. *Nature*, 463.
- [Murphy et al., 2007] Murphy, J., Booth, B., Collins, M., Harris, G., D.M.H Sexton, D., and Webb, M. (2007). A methodology for probabilistic predictions of regional climate change from perturbed physics ensembles. *Philosophical Transactions of the Royal Society A: Mathematical, Physical and Engineering Sciences*, 365.
- [Murphy et al., 2004] Murphy, J. M., Sexton, D., and Barnett, D. (2004). Quantification of modelling uncertainties in a large ensemble of climate change simulations. *Nature*, 430.
- [Olsson et al., 2001] Olsson, J., Uvo, C., and Jinno, K. (2001). Statistical atmospheric downscaling of short-term extreme rainfall by neural networks. *Physics and Chemistry of the Earth*, 26.
- [Pellicciotti et al., 2005] Pellicciotti, F., Brock, B., Strasser, U., Burlando, P., and Funk, M. (2005). An enhanced temperature-index glacier melt model including the shortwave radiation balance: development and testing for haut glacier d'arolla, switzerland. *Journal of Glaciology*, 51.

- [Priestley and Taylor, 1972] Priestley, C. and Taylor, R. (1972). On the assessment of surface heat flux and evaporation using large-scale parameters. *Monthly Weather Review*.
- [Riahi et al., 2007] Riahi, K., Gruebler, A., and Nakicenovic, N. (2007). Scenarios of long-term socio-economic and environmental development under climate stabilization. *Technological Forecasting and Social Change*, 74.
- [Smith and Wigley, 2006] Smith, S. and Wigley, L. (2006). Multi-gas forcing stabilization with the minicam. multigas mitigation and climate policy. *The Energy Journal*, 3.
- [Soncini-Sessa et al., 2007] Soncini-Sessa, R., Castelletti, A., and Weber, E. (2007). *Integrated and Participatory Water Resources Management: Theory*, volume 1A.
- [Stirling, 1998] Stirling, A. (1998). On the economics and analysis of diversity. *SPRU*.
- [Tebaldi and Knutti, 2007] Tebaldi, C. and Knutti, R. (2007). The use of the multi-model ensemble in probabilistic climate projections. *Philosophical Transactions of the Royal Society A: Mathematical, Physical and Engineering Sciences*, 365.
- [Teng et al., 2012] Teng, J., Vaze, J., and Chiew, F. (2012). Estimating the relative uncertainties sourced from gcms and hydrological models in modeling climate change impact on runoff. *Journal of Hydrometeorology*, 13.
- [Terna, 2012] Terna (2012). Dati generali. Technical report, Terna Group.
- [van Vuuren et al., 2007] van Vuuren, D., den Elzen, M., Lucas, P., Eickhout, B., Strengers, B., and van Ruijven, B. (2007). Stabilizing greenhouse gas concentrations at low levels: an assessment of reduction strategies and costs. *Climate Change*, 81.
- [Von Storch, 1995] Von Storch, H. (1995). Inconsistencies at the interface of climate impact studies and global climate research. *Meteorologische Zeitschrift*, 4.
- [Wilby and Dessai, 2010] Wilby, L. and Dessai, S. (2010). Robust adaptation to climate change. *Weather*, 65.
- [Wilby et al., 2004] Wilby, R., Charles, S., Zorita, E., Timbal, B., and Mearns, L. (2004). Guidelines for use of climate scenarios developed from statistical downscaling methods. Technical report, IPCC.

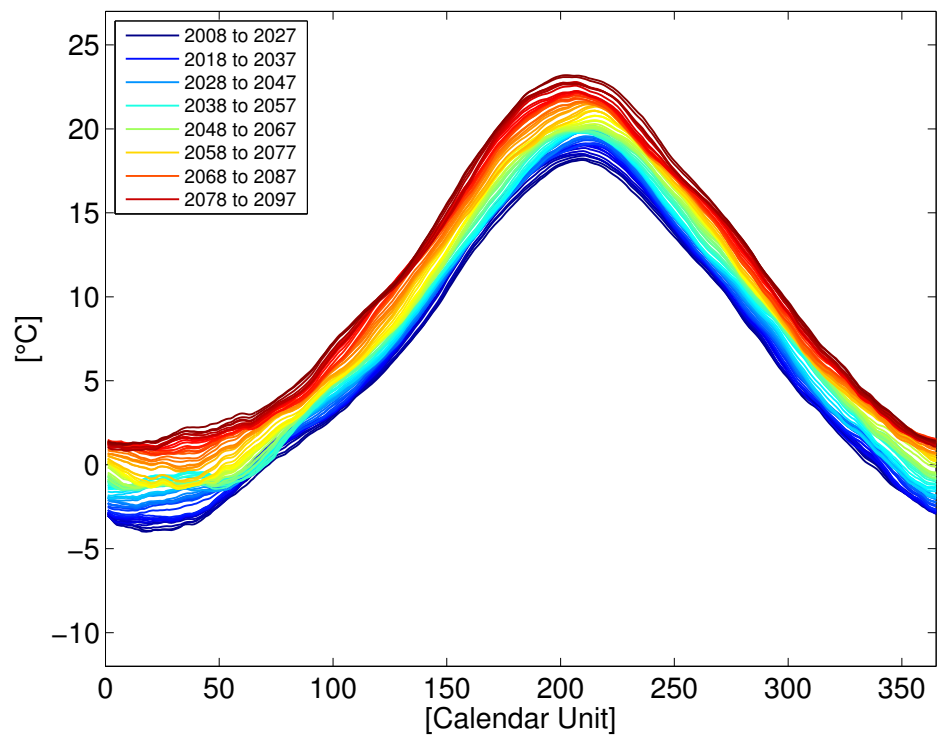
- [Wilks and Wilby, 1999] Wilks, D. and Wilby, R. (1999). The weather generation game: a review of stochastic weather models. *Progress in Physical Geography*, 23.
- [Zierl and Bugmann, 2005] Zierl, B. and Bugmann, H. (2005). Global change impacts on hydrological processes in alpine catchments. *Water Resources Research*, 41.
- [Zorita, 1999] Zorita, E. and Von Storch, H. (1999). The analog method as a simple statistical downscaling technique: Comparison with more complicated methods. *Journal of Climate*, 12.



CLIMATE SCENARIOS MASH

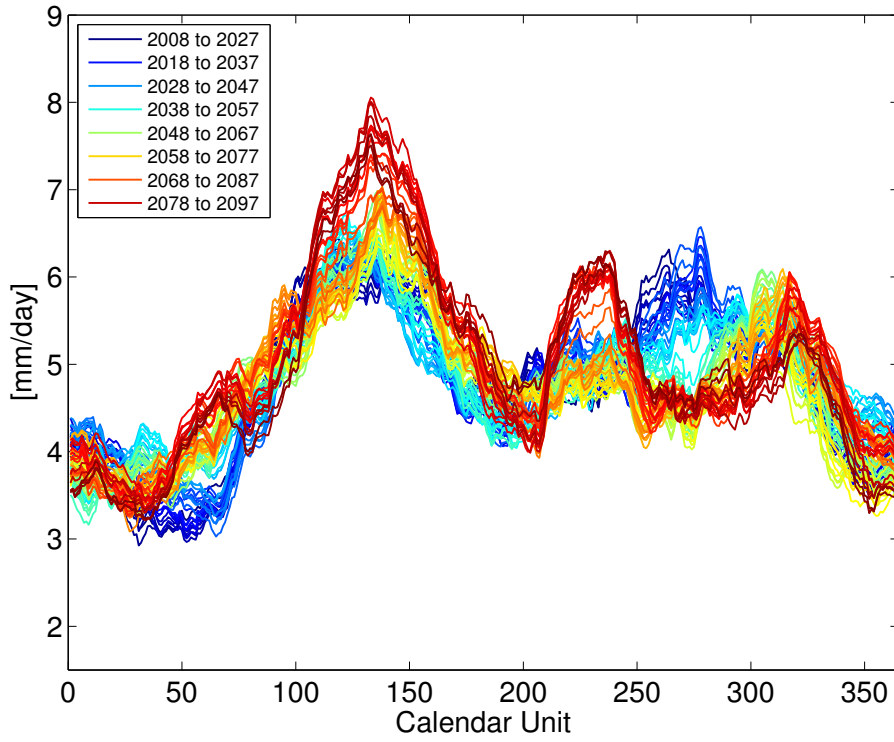


(a) RCP_{4.5}

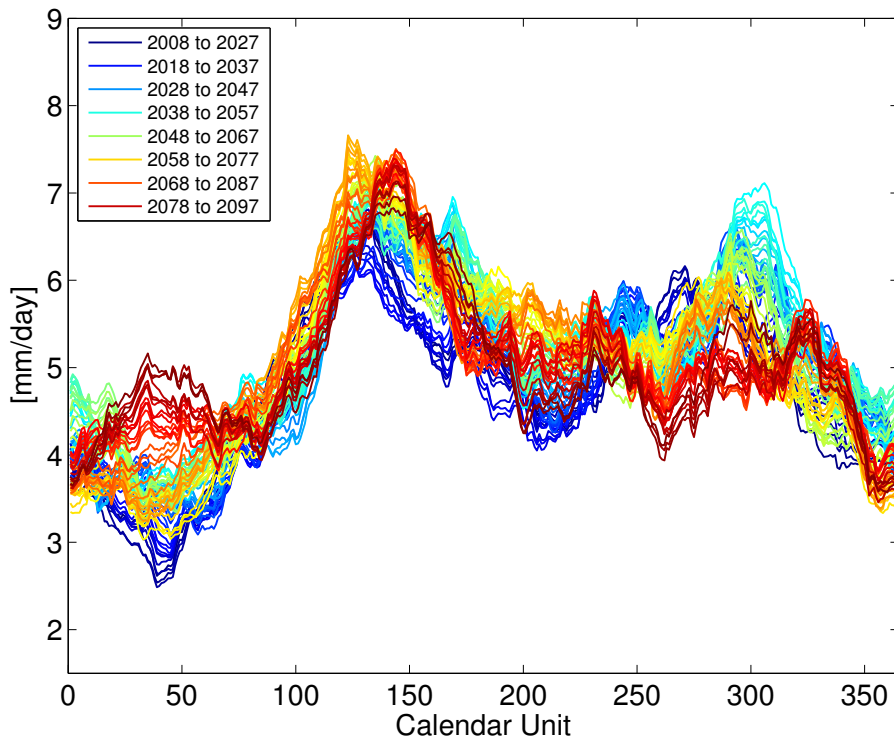


(b) RCP_{8.5}

Figure A.1: Temperature MASH of RCA₄/MIROC

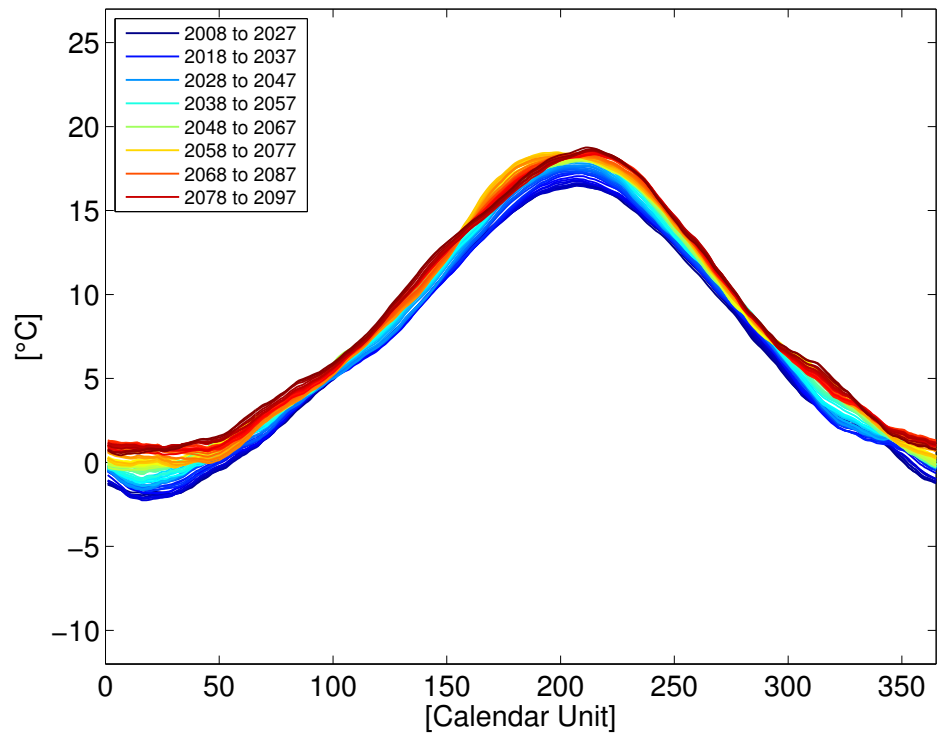


(a) RCP4.5

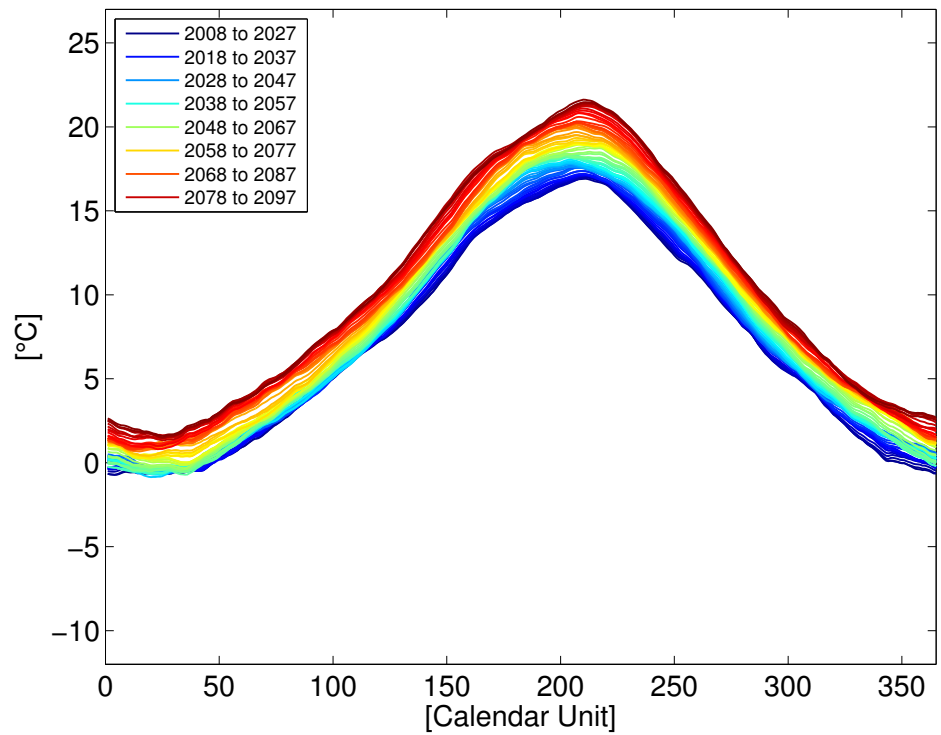


(b) RCP8.5

Figure A.2: Precipitation MASH of RCA4/MIROC

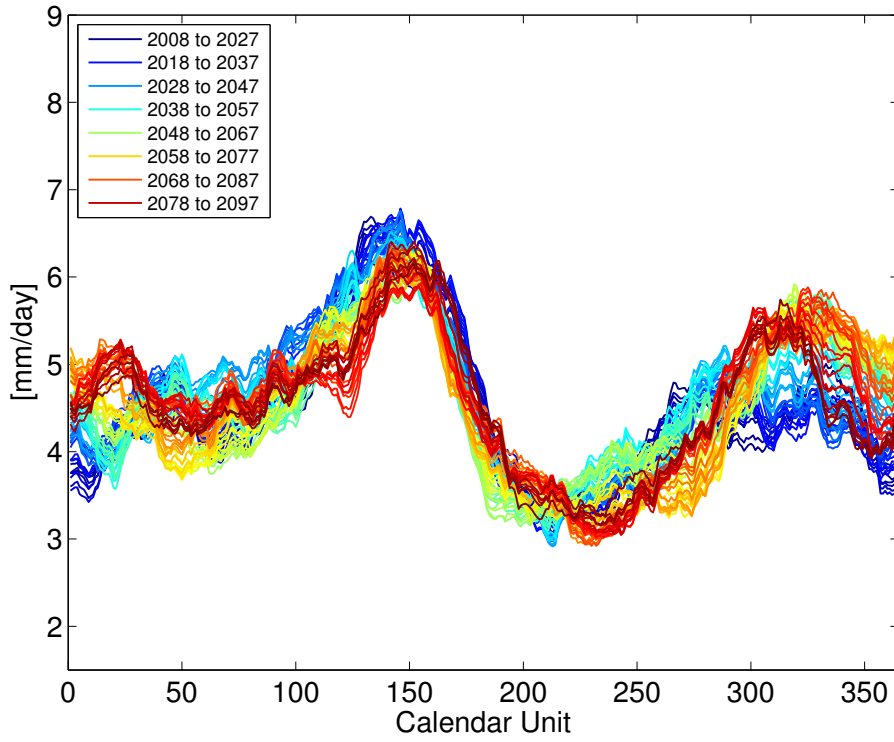


(a) RCP_{4.5}

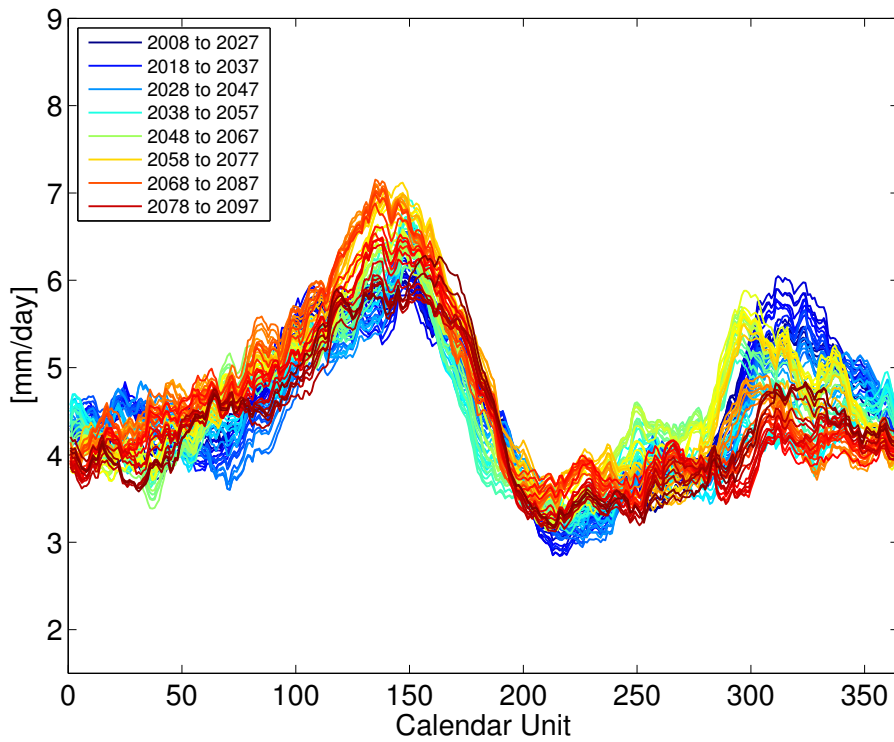


(b) RCP_{8.5}

Figure A.3: Temperature MASH of RCA4/NCC

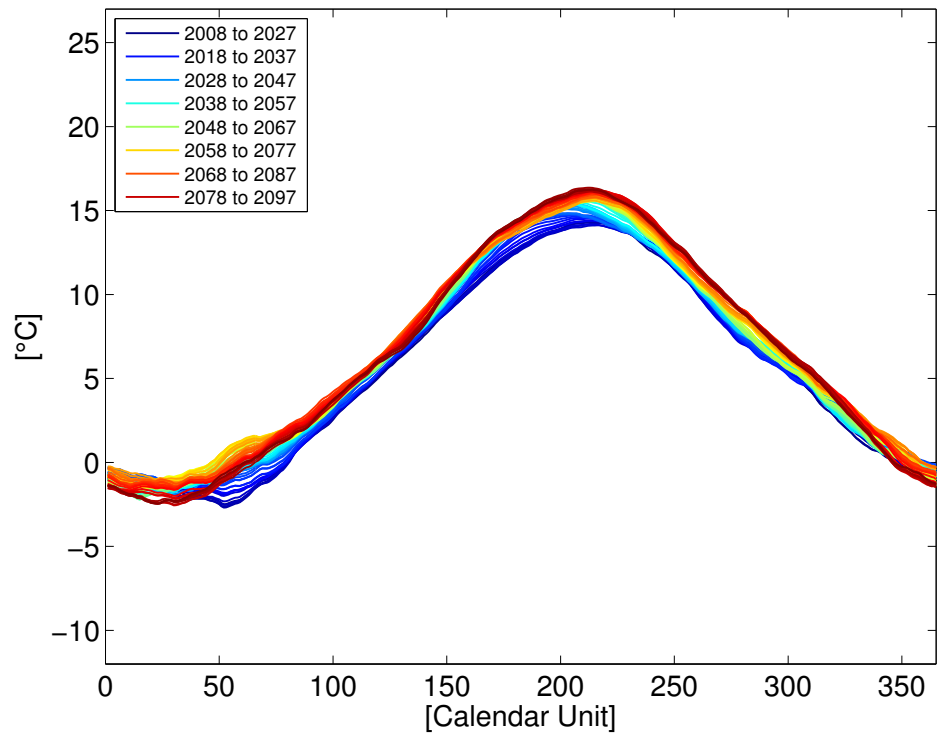


(a) RCP4.5

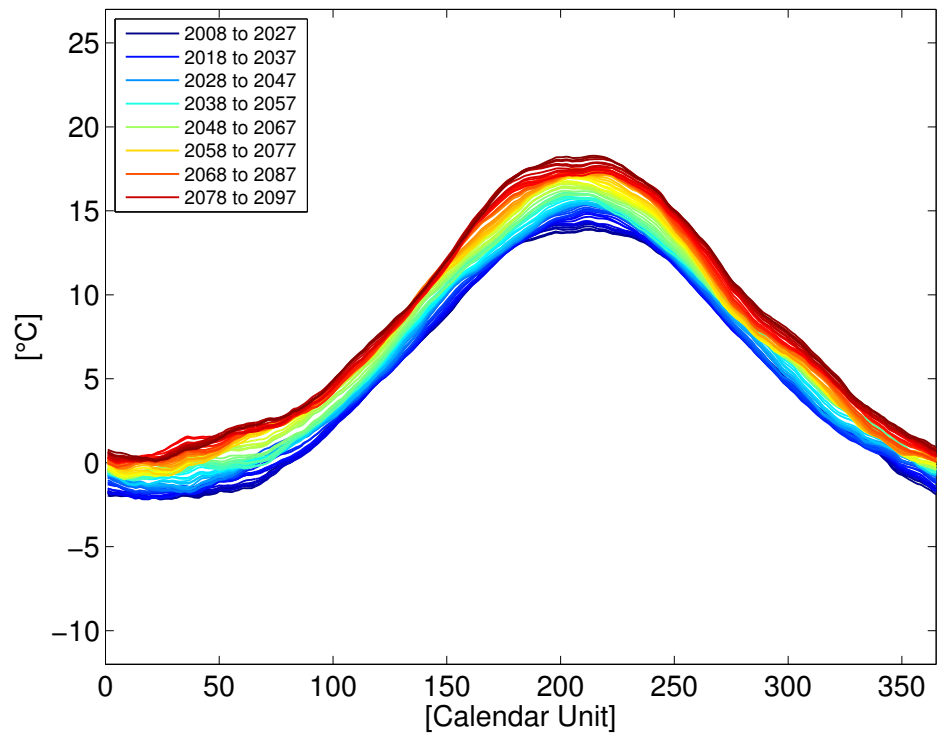


(b) RCP8.5

Figure A.4: Precipitation MASH of RCA4/NCC

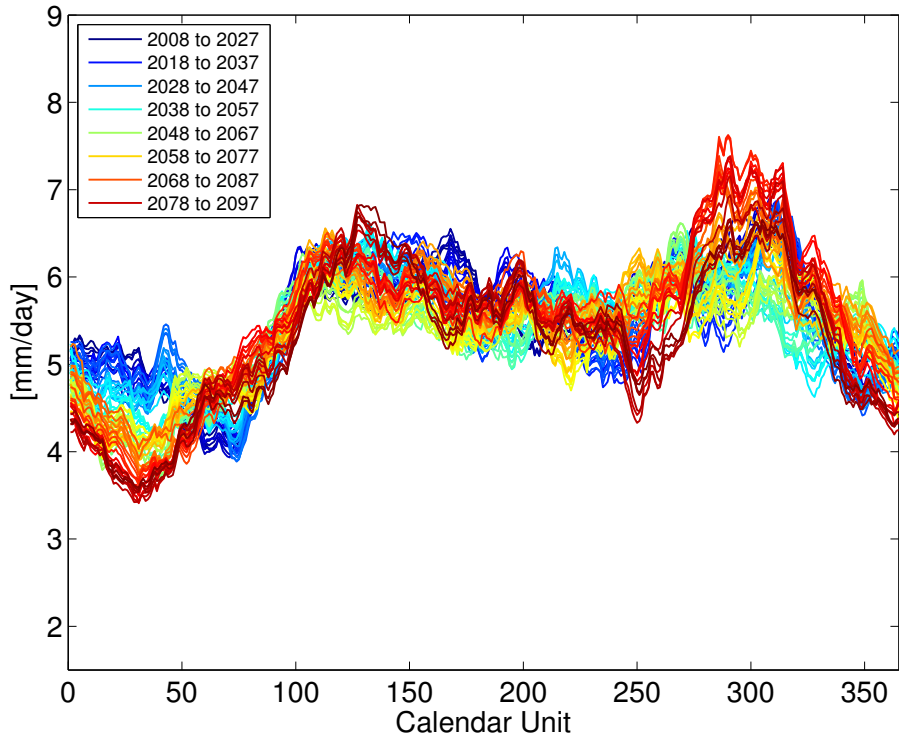


(a) RCP4.5

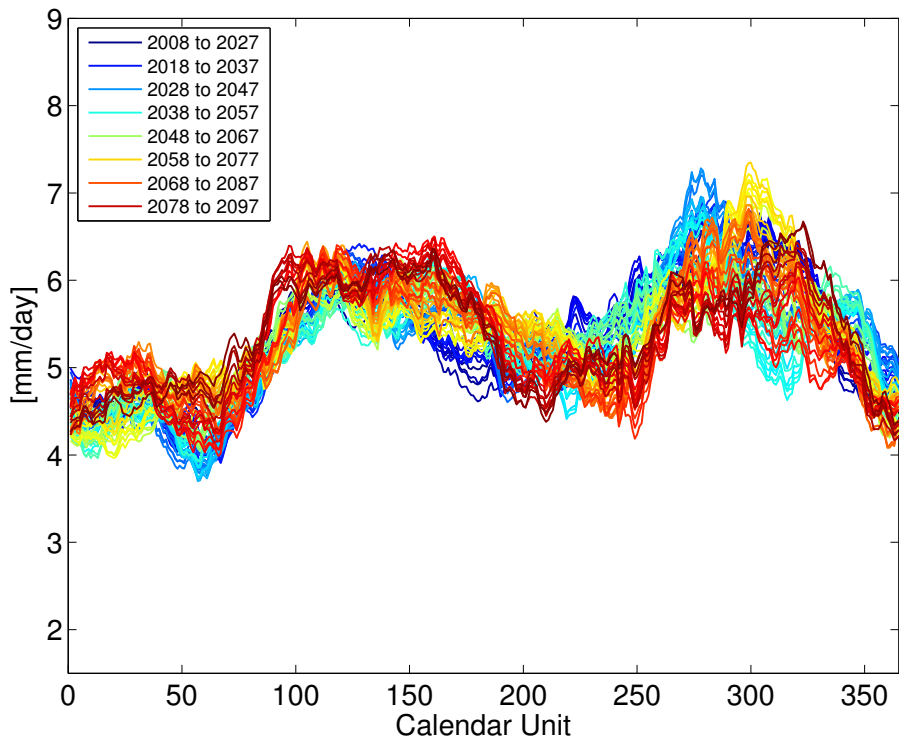


(b) RCP8.5

Figure A.5: Temperature MASH of RCA4/NOAA

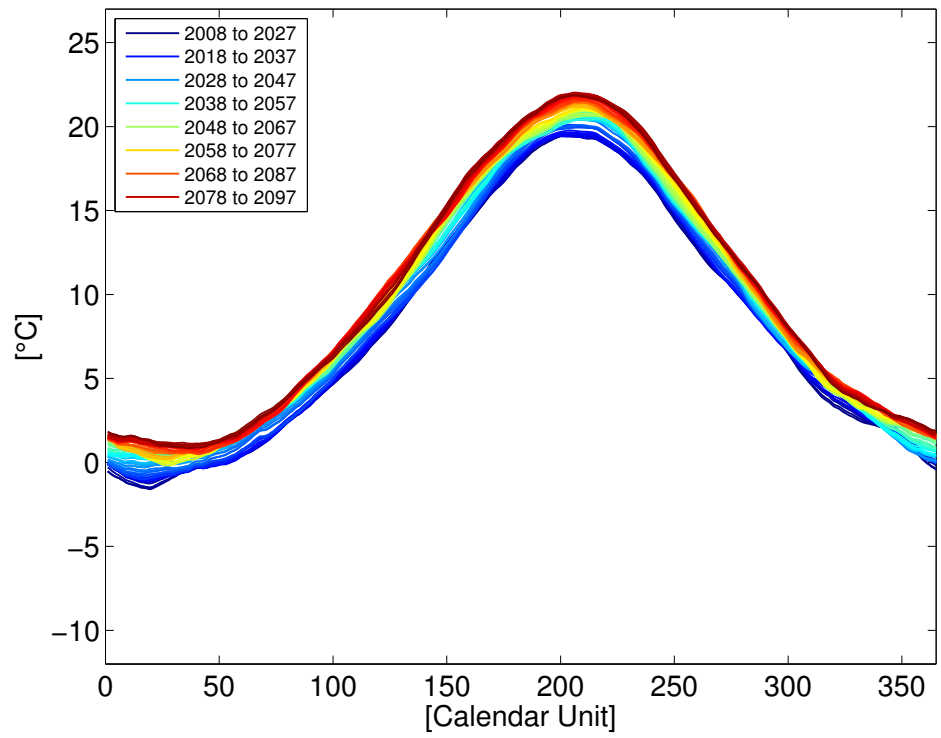


(a) RCP4.5

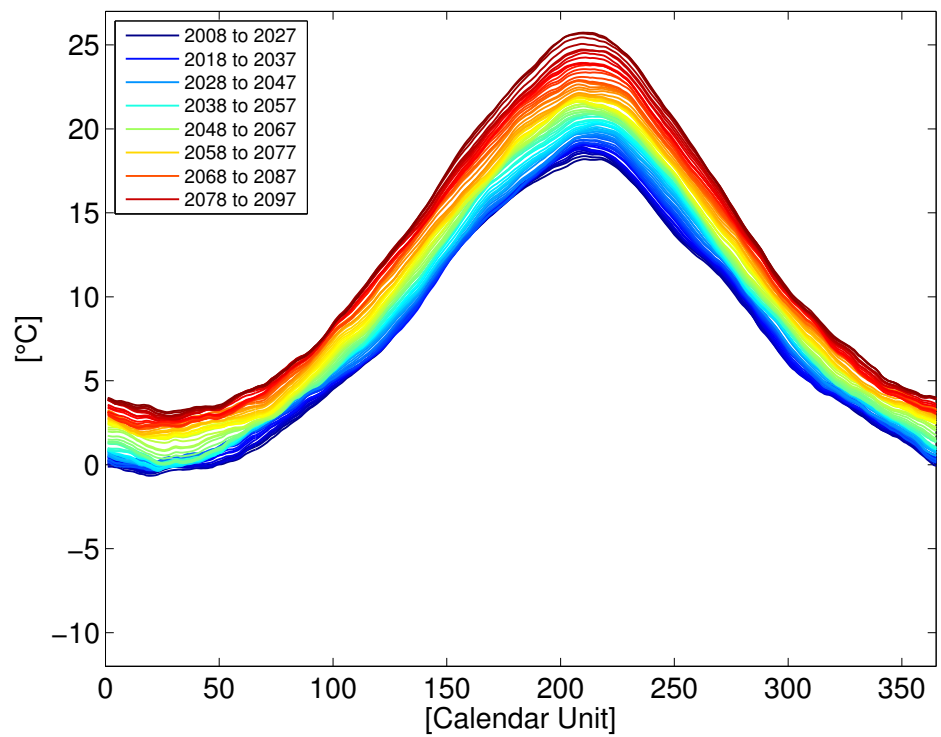


(b) RCP8.5

Figure A.6: Precipitation MASH of RCA4/NOAA

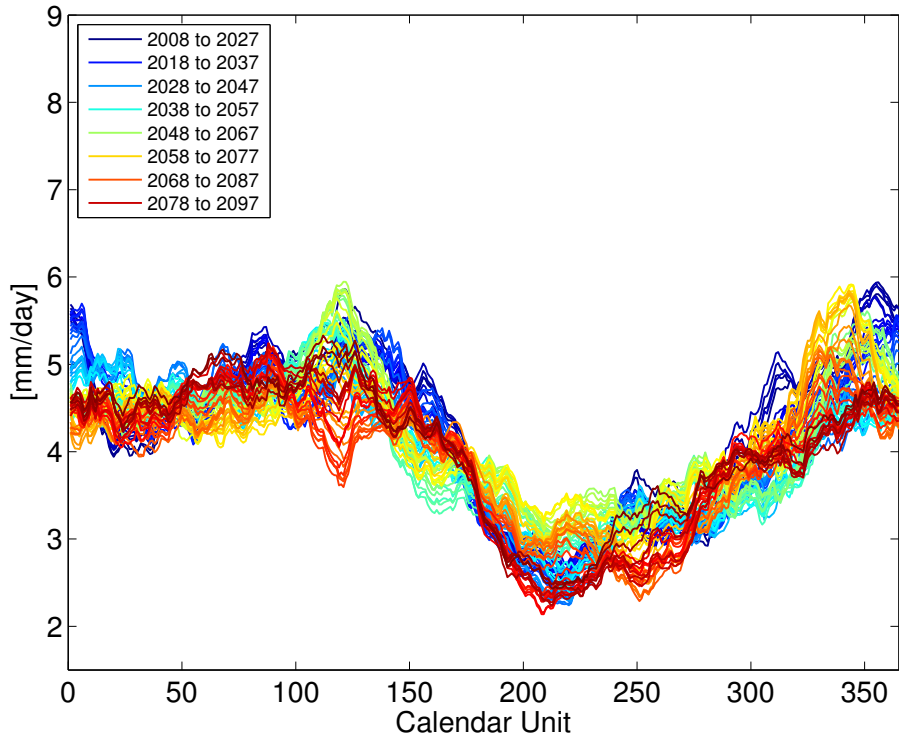


(a) RCP_{4.5}

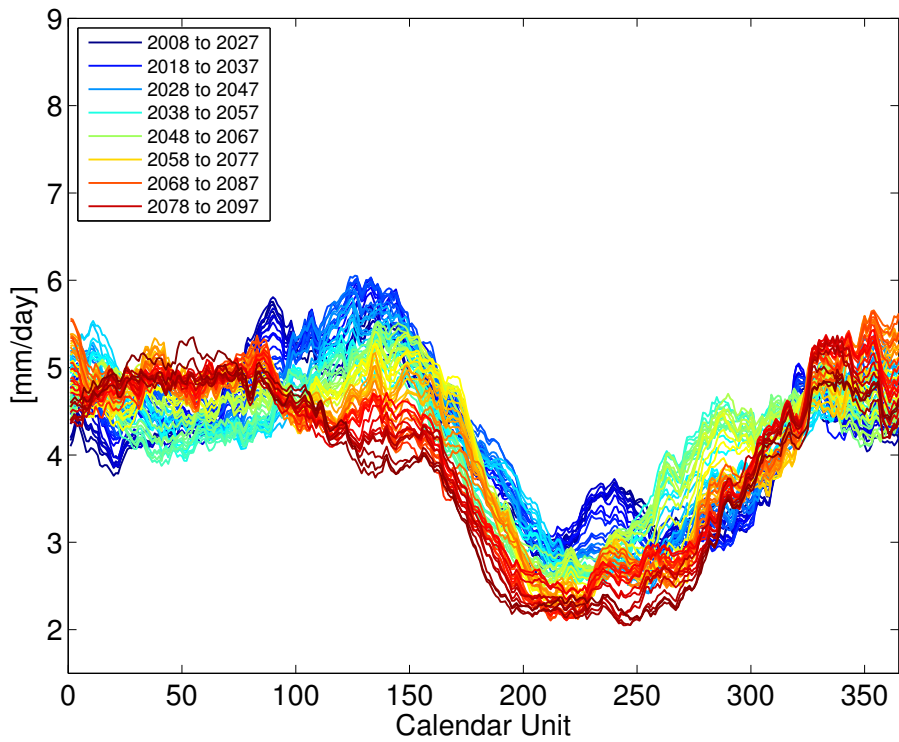


(b) RCP_{8.5}

Figure A.7: Temperature MASH of RCA₄/CCC

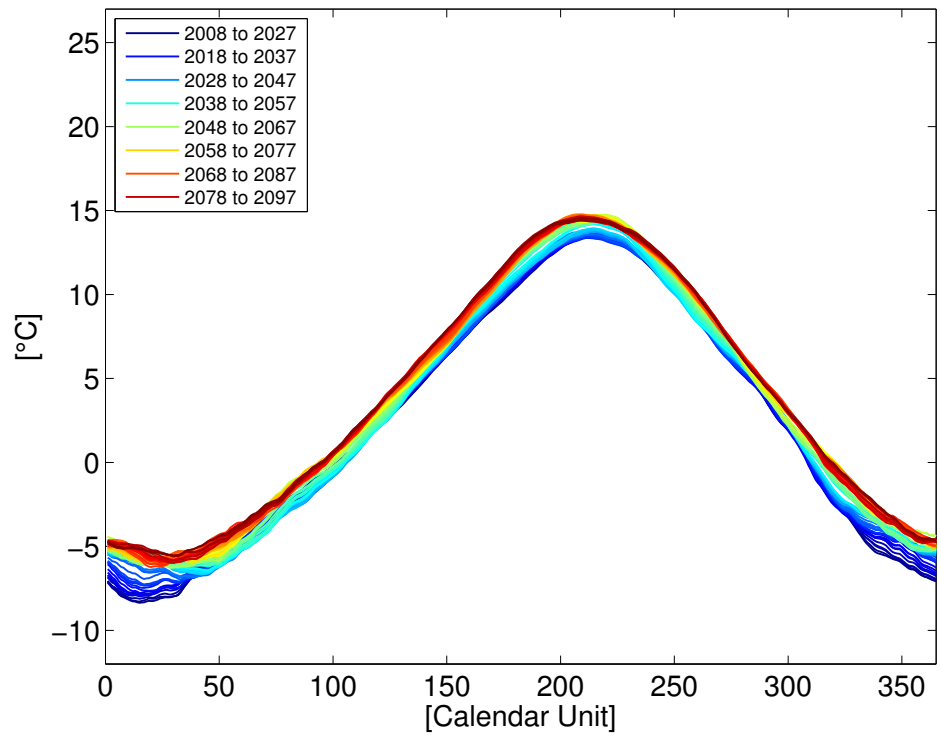


(a) RCP4.5

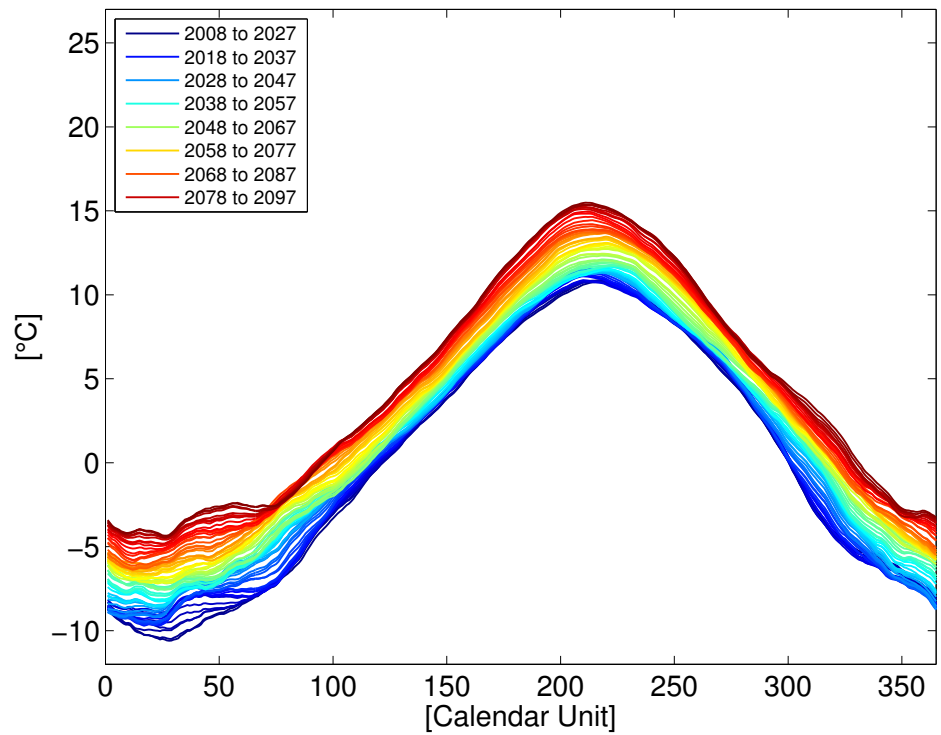


(b) RCP8.5

Figure A.8: Precipitation MASH of RCA4/CCC

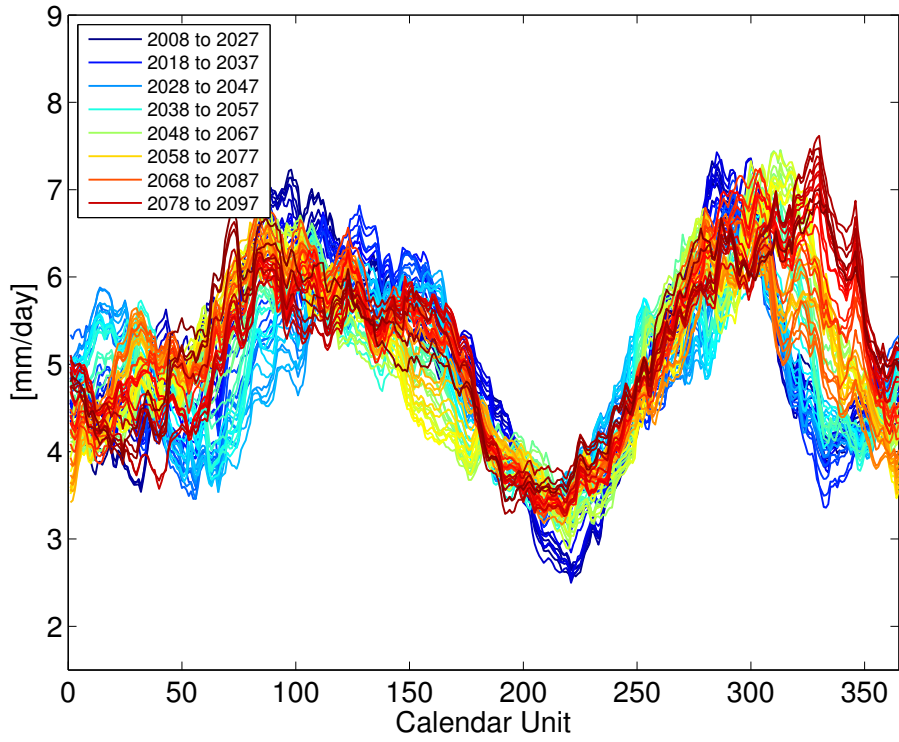


(a) RCP4.5

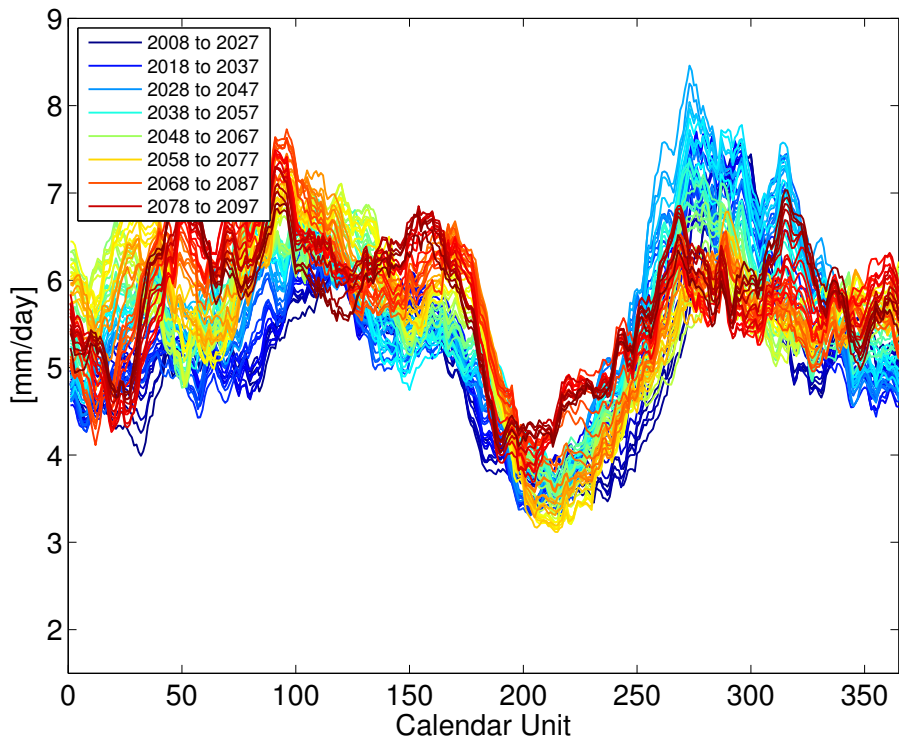


(b) RCP8.5

Figure A.9: Temperature MASH of RCA4/CNRM

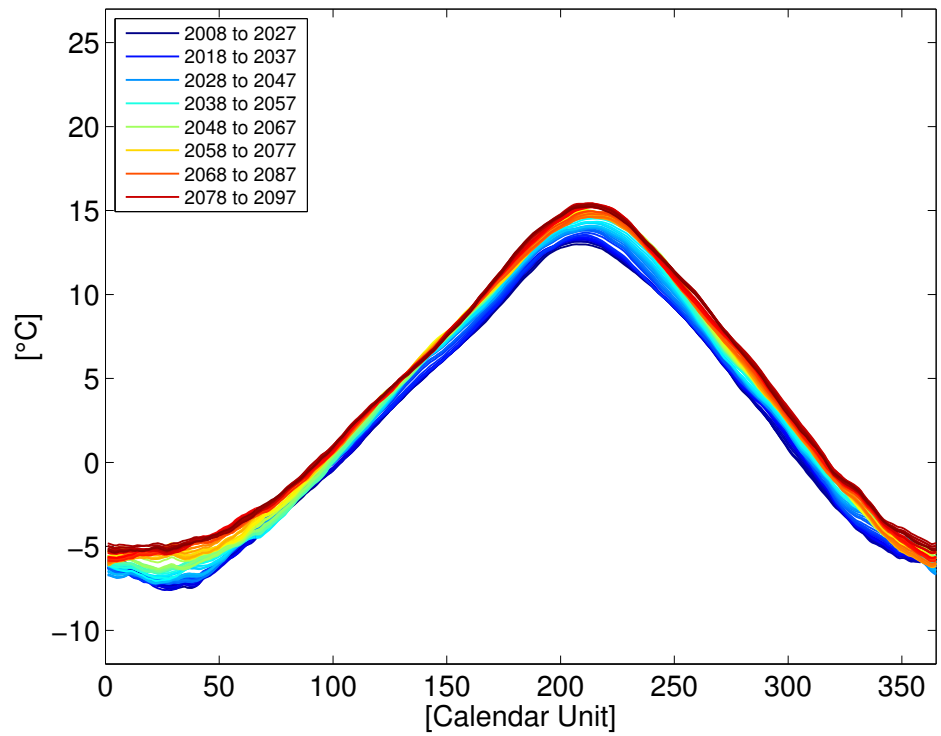


(a) RCP4.5

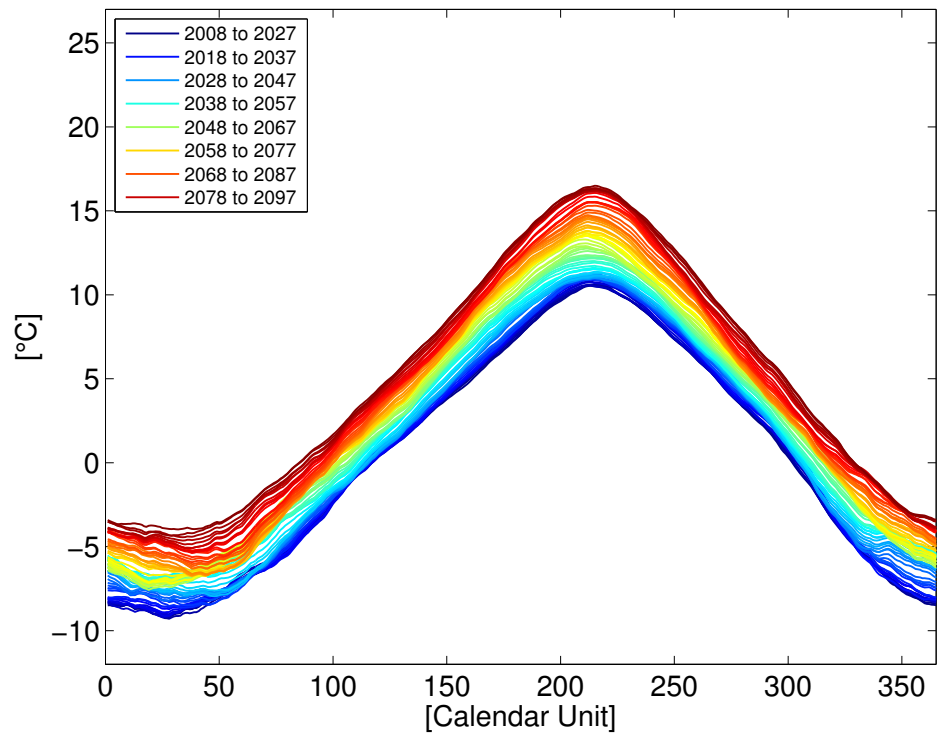


(b) RCP8.5

Figure A.10: Precipitation MASH of RCA₄/CNRM

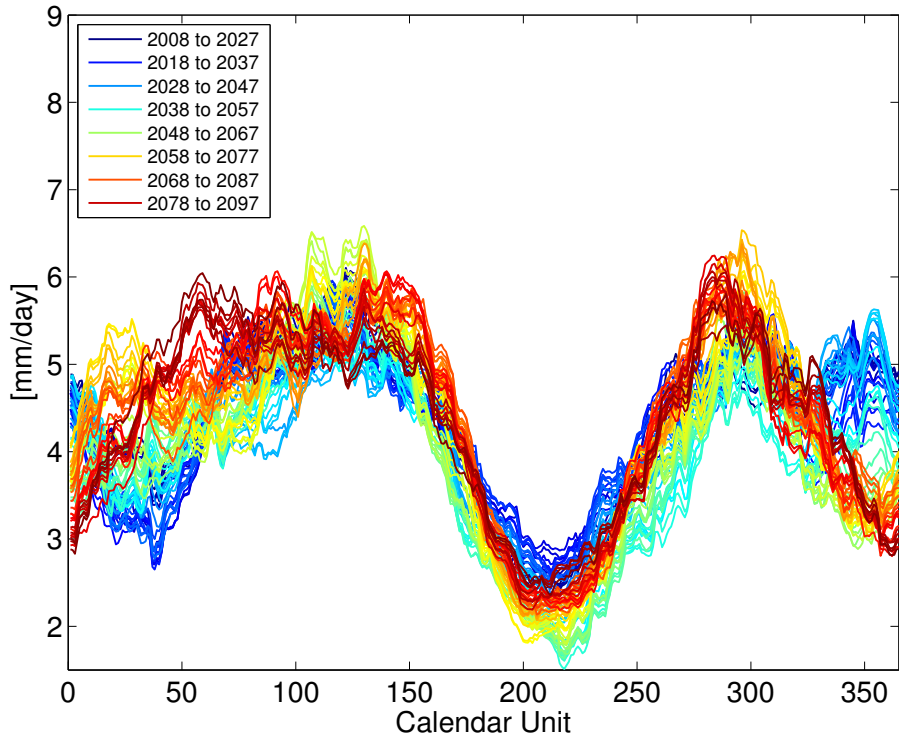


(a) RCP_{4.5}

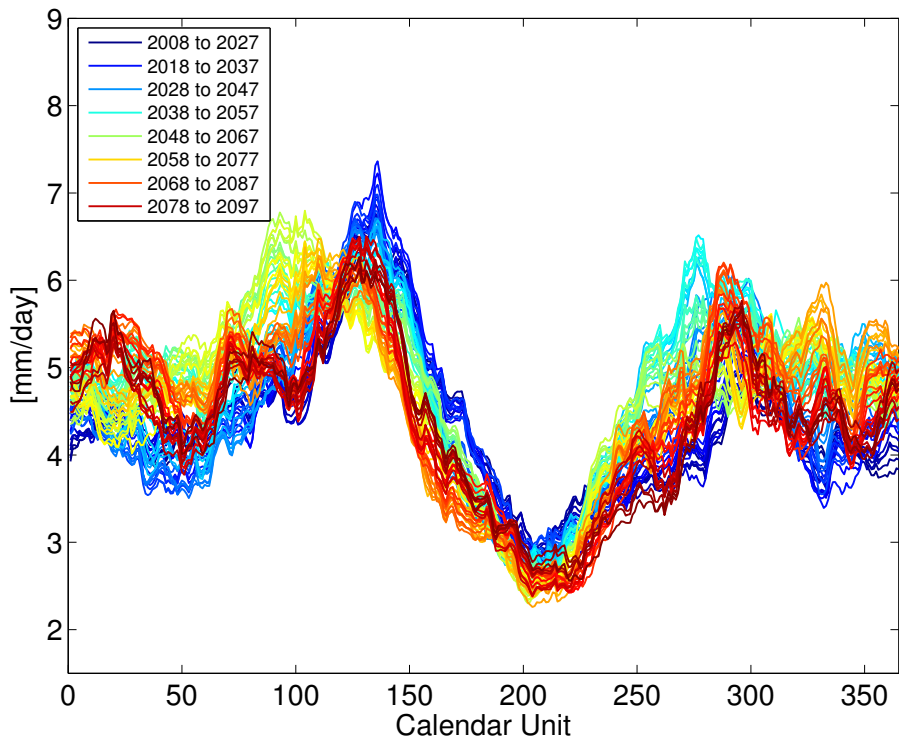


(b) RCP_{8.5}

Figure A.11: Temperature MASH of RCA₄/ICHEC

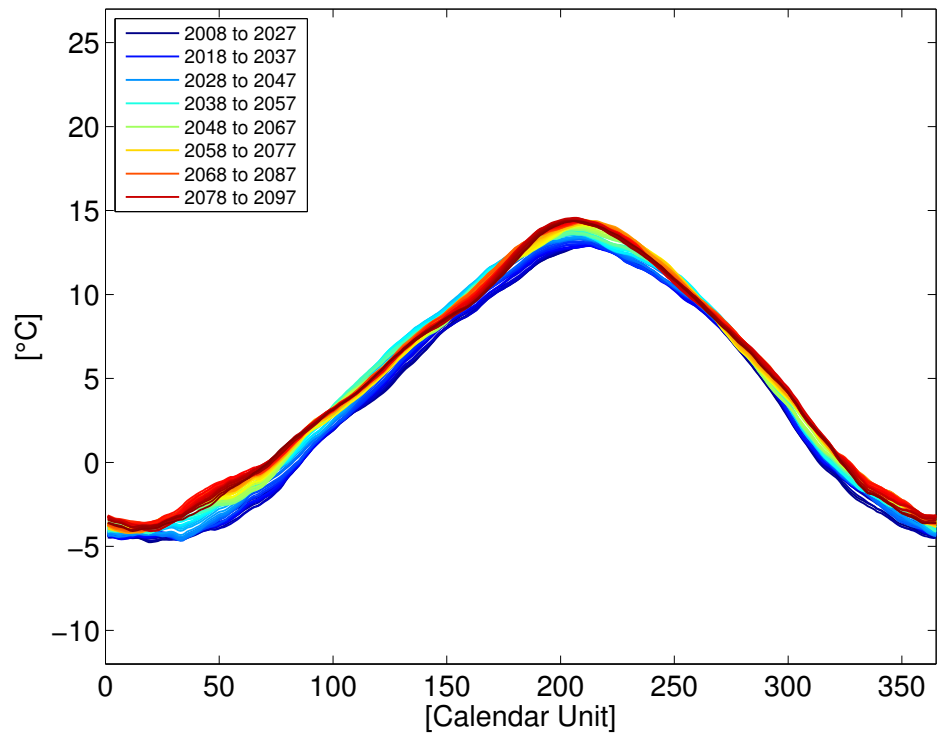


(a) RCP4.5

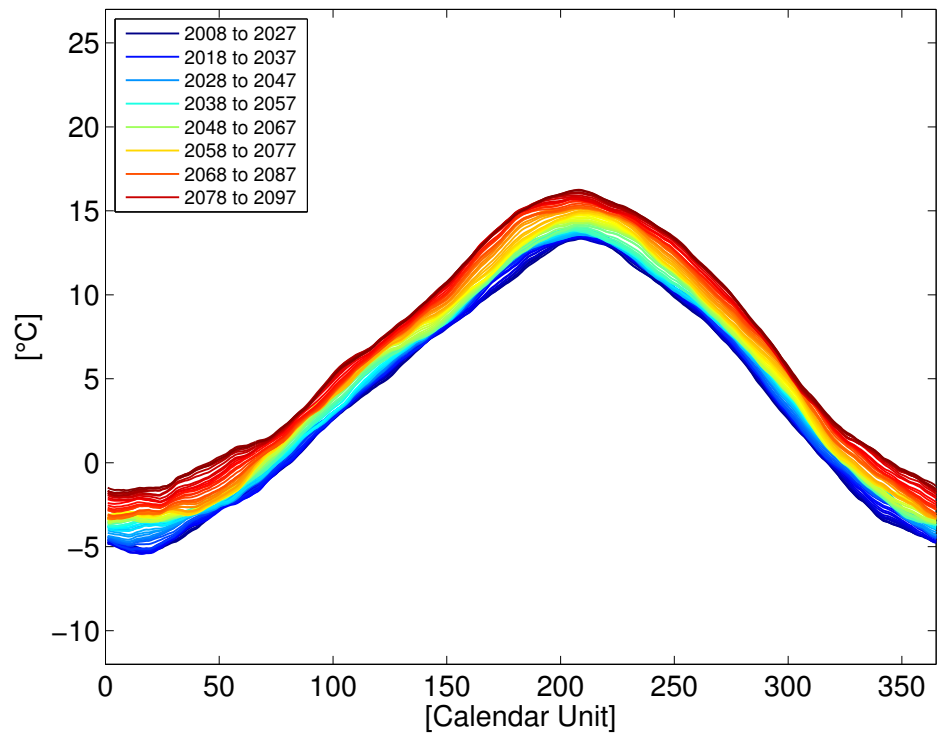


(b) RCP8.5

Figure A.12: Precipitation MASH of RCA4/ICHEC

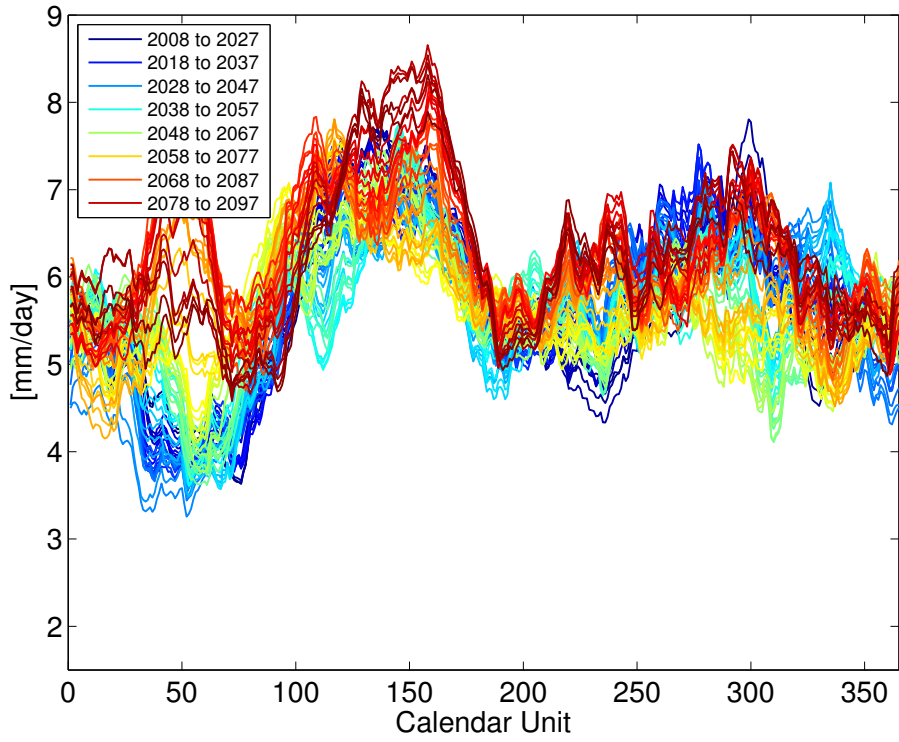


(a) RCP4.5

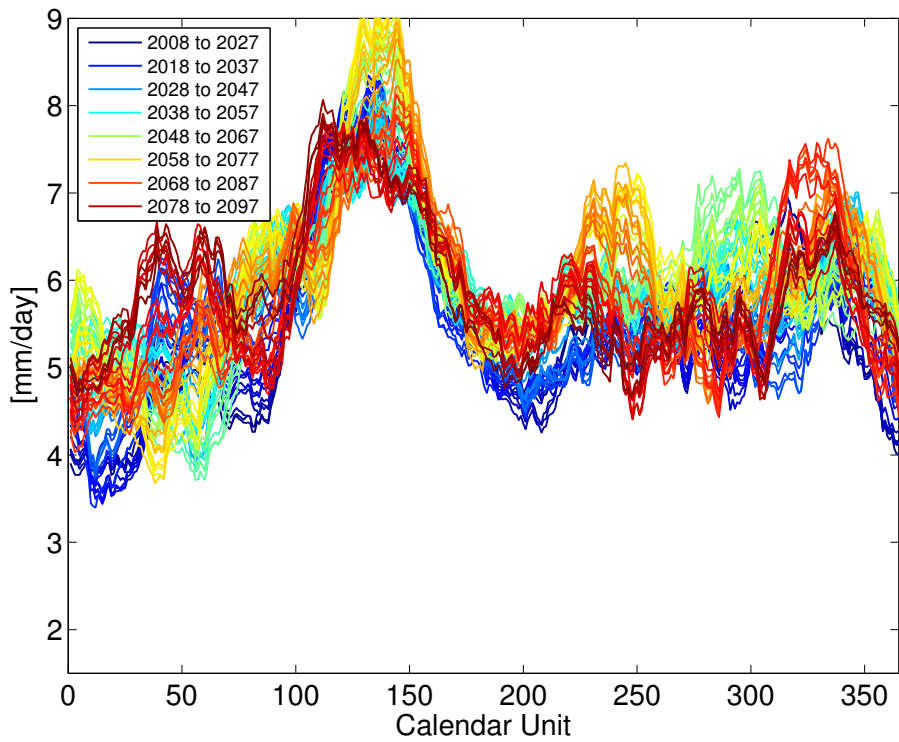


(b) RCP8.5

Figure A.13: Temperature MASH of HIRHAM/ICHEC

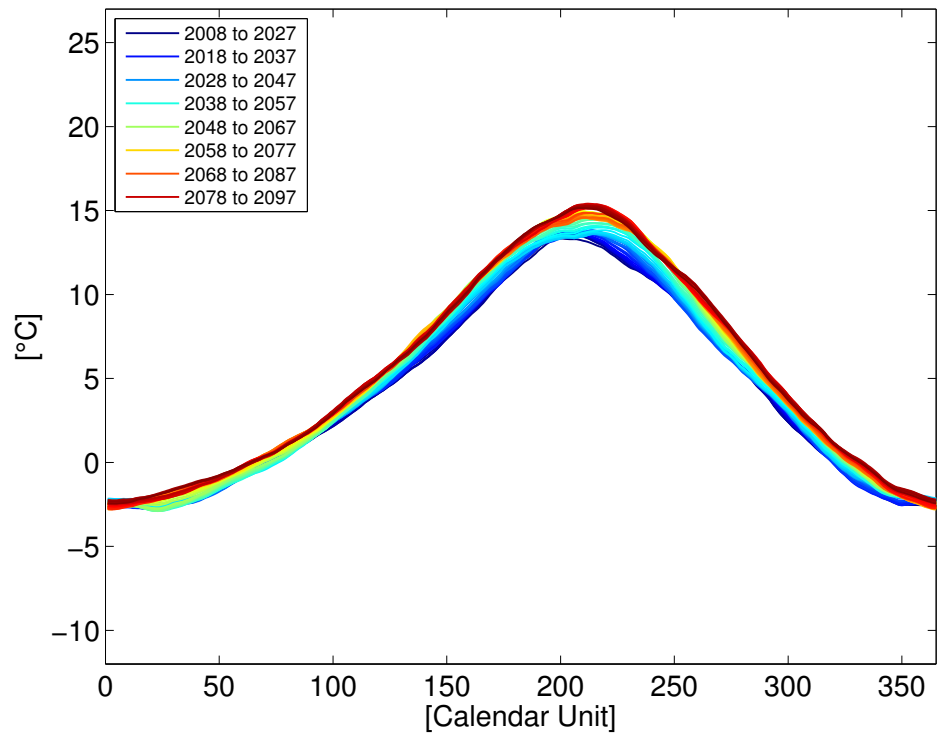


(a) RCP4.5

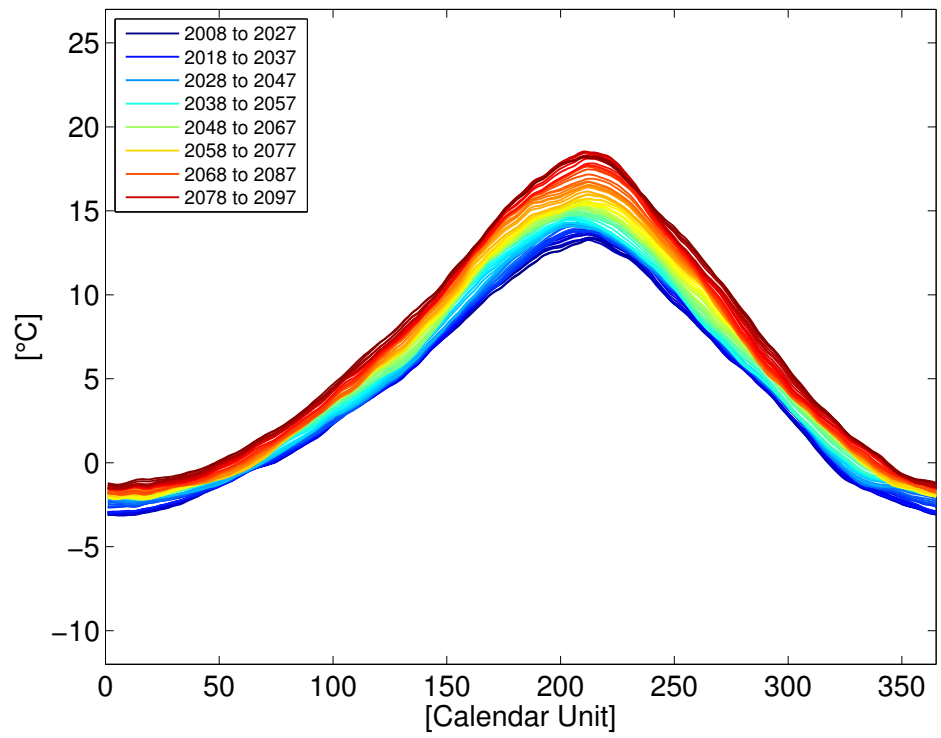


(b) RCP8.5

Figure A.14: Precipitation MASH of HIRAM/ICHEC

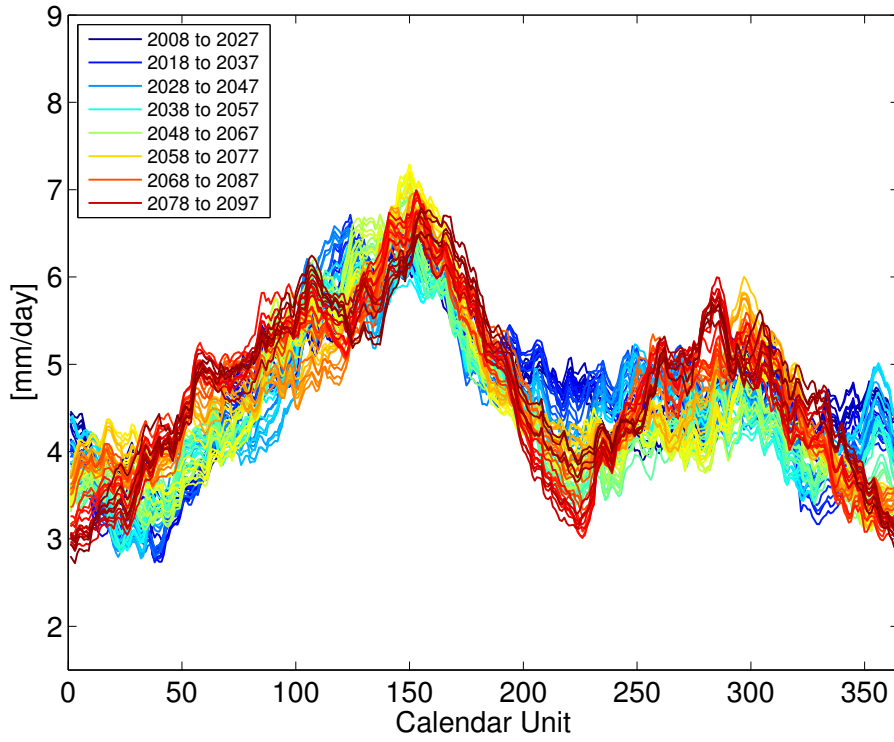


(a) RCP4.5

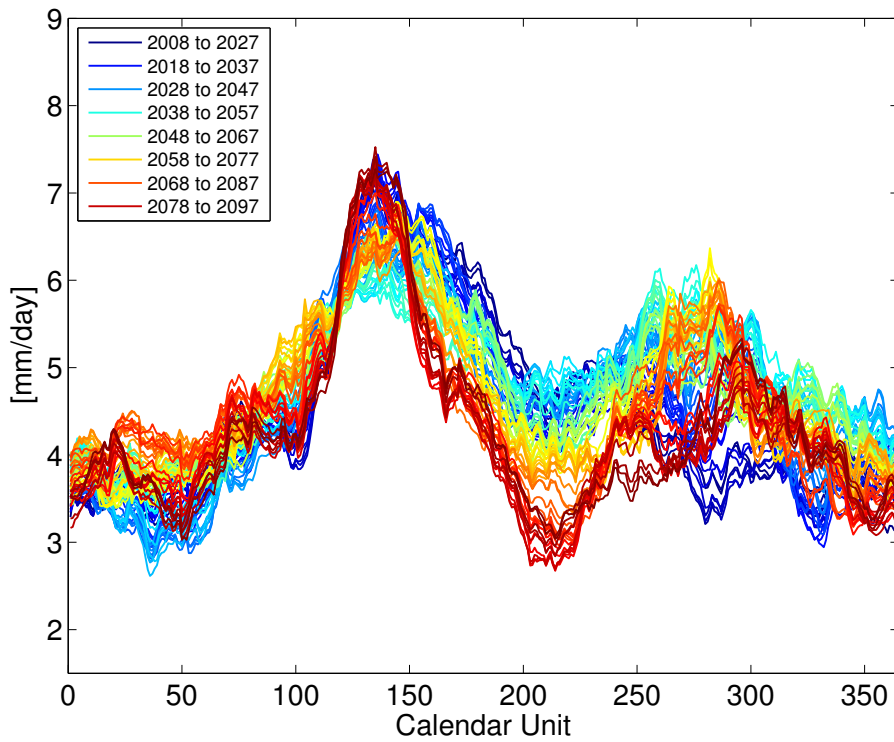


(b) RCP8.5

Figure A.15: Temperature MASH of CCLM/ICHEC

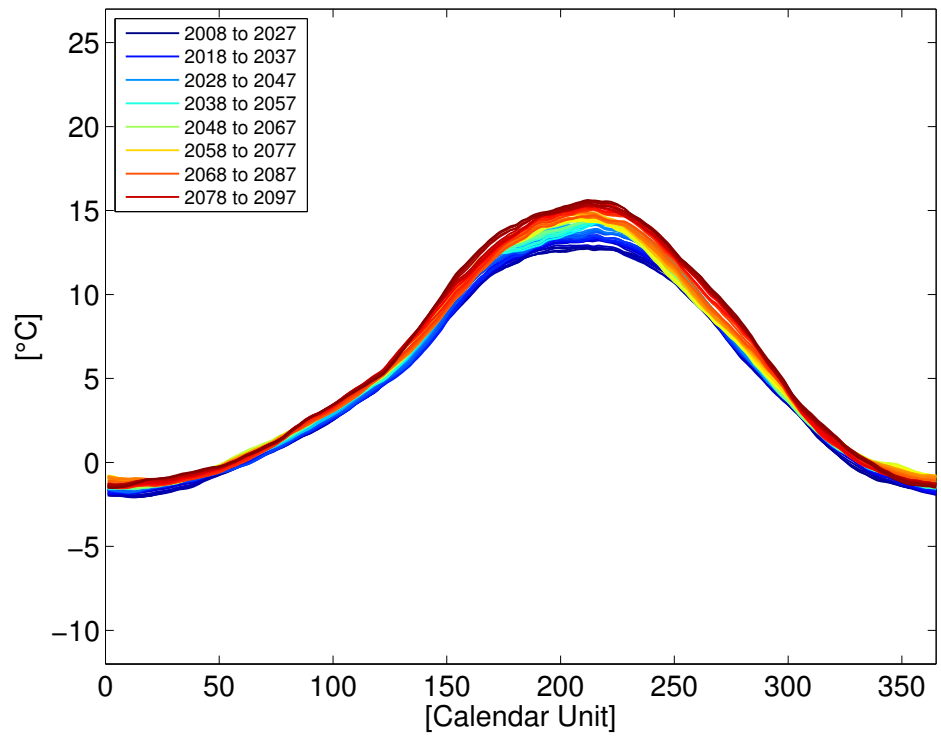


(a) RCP4.5

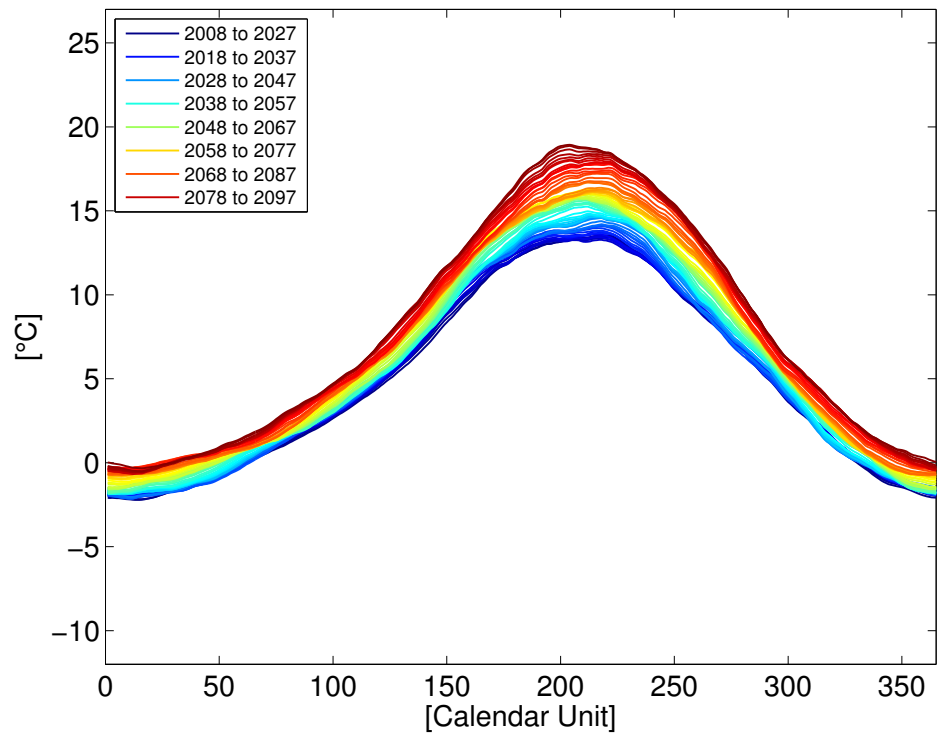


(b) RCP8.5

Figure A.16: Precipitation MASH of CCLM/ICHEC

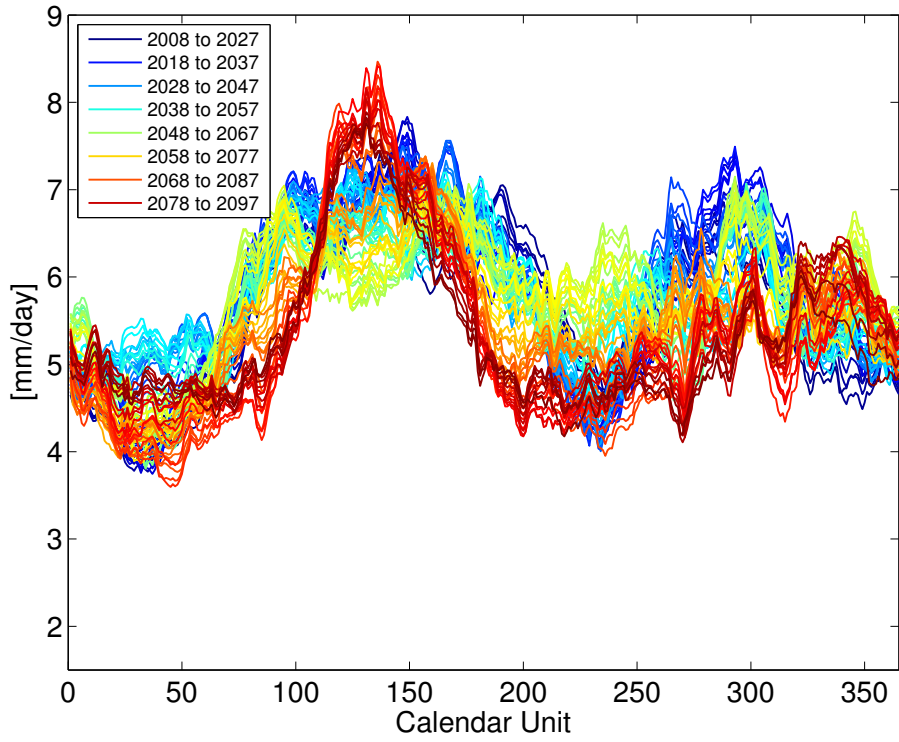


(a) RCP4.5

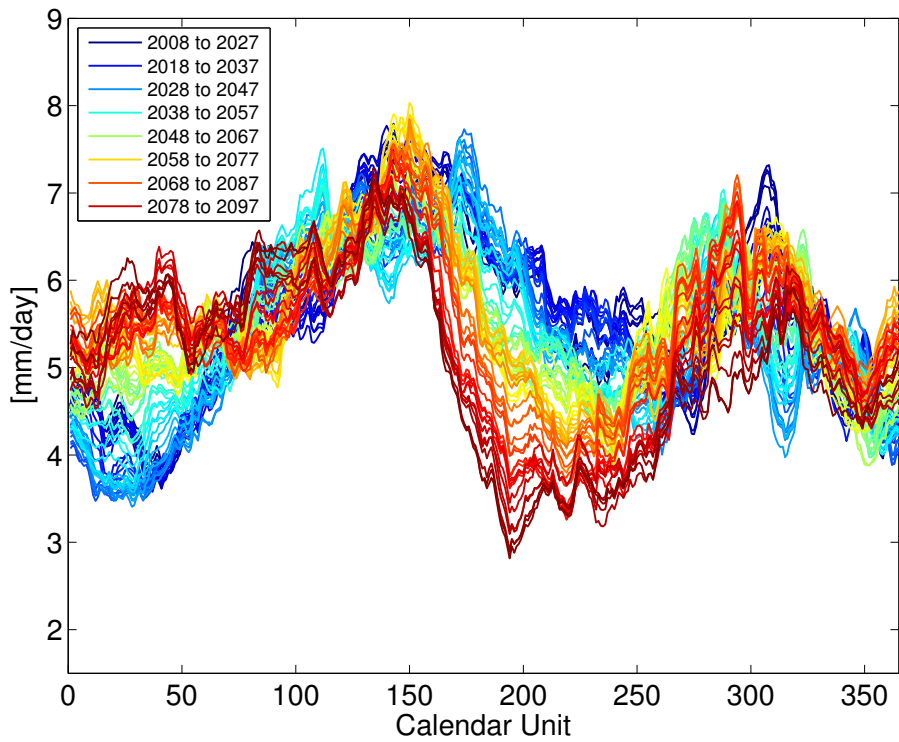


(b) RCP8.5

Figure A.17: Temperature MASH of CCLM/MPI



(a) RCP4.5

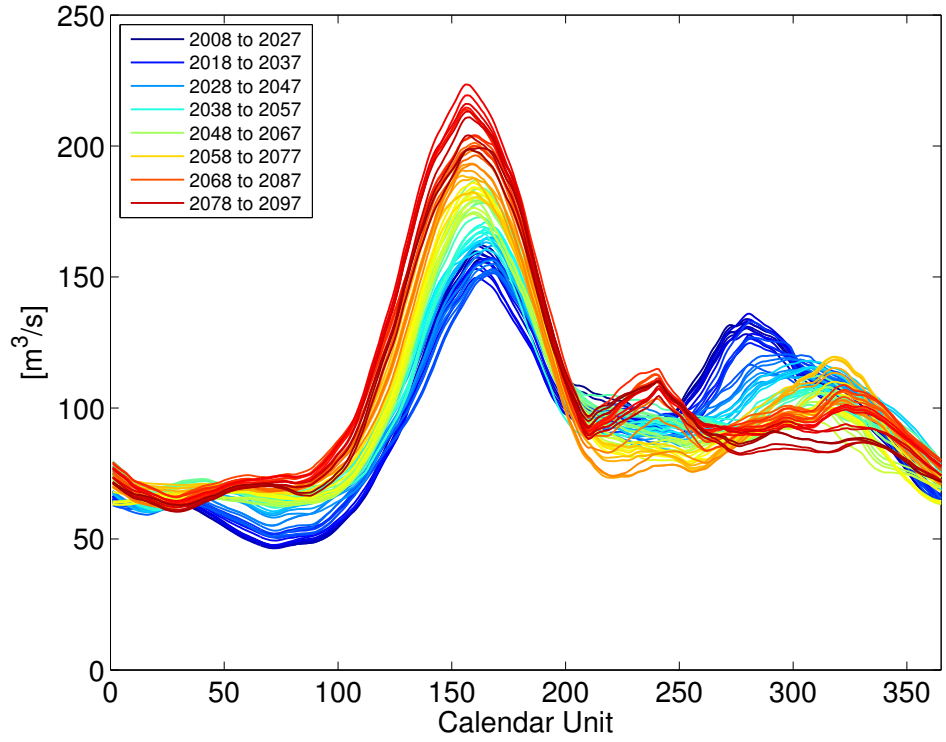


(b) RCP8.5

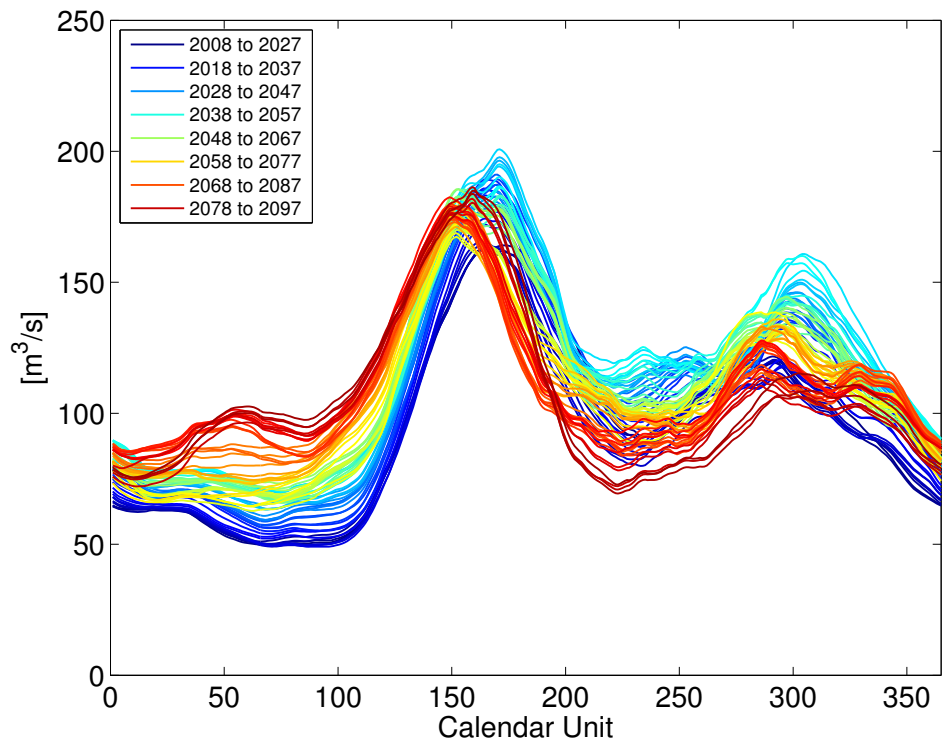
Figure A.18: Precipitation MASH of CCLM/MPI

B

HYDROLOGICAL SCENARIOS MASH

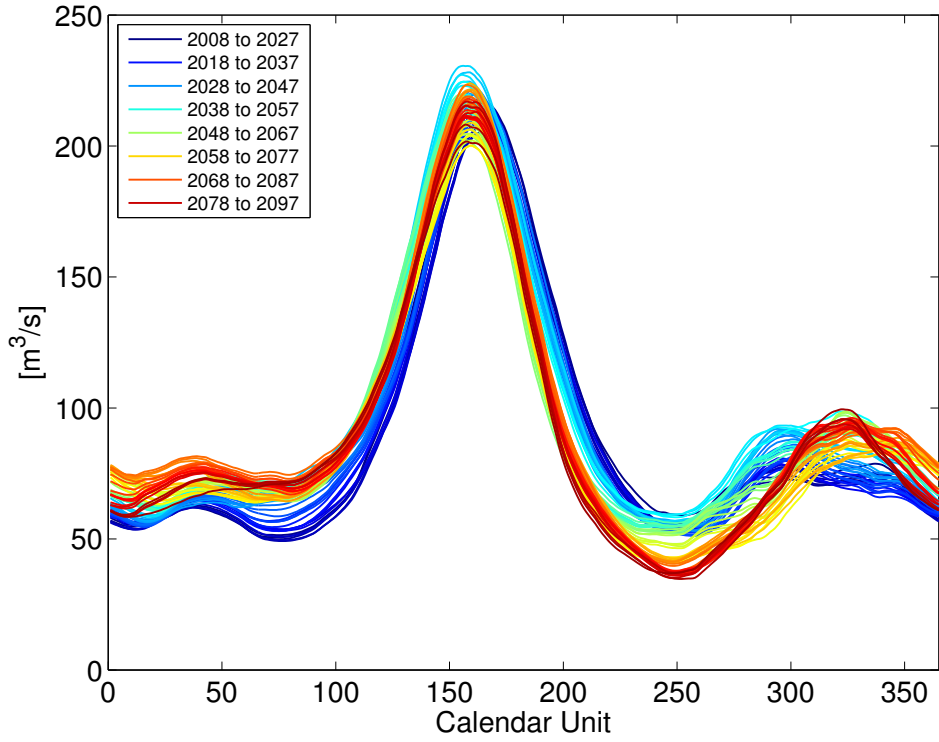


(a) RCP4.5

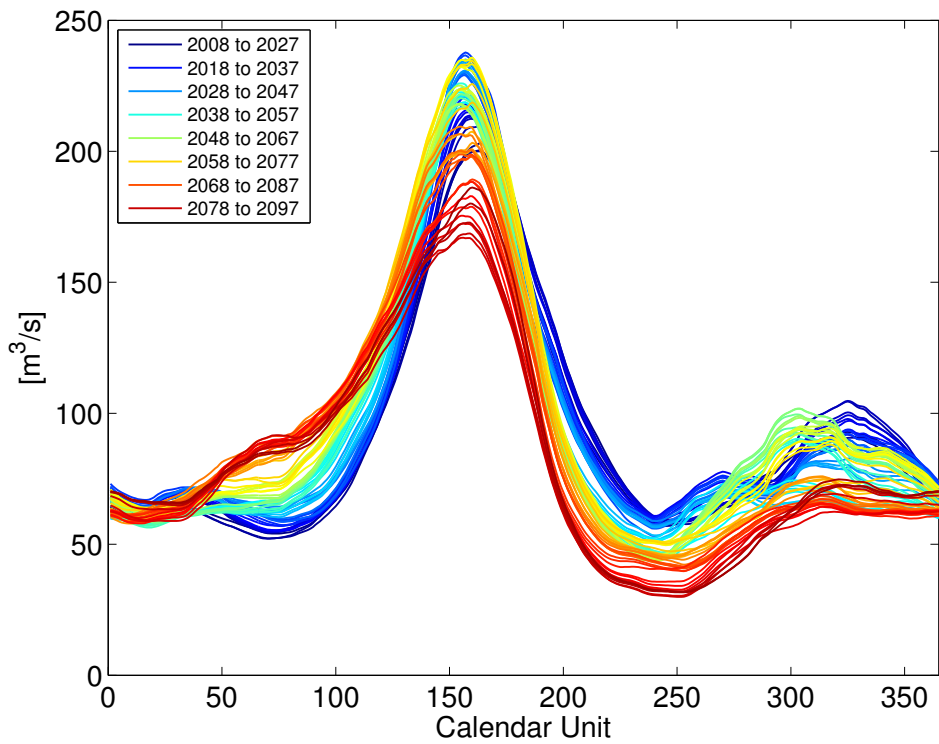


(b) RCP8.5

Figure B.1: RCA4/MIROC, Fuentes streamflow

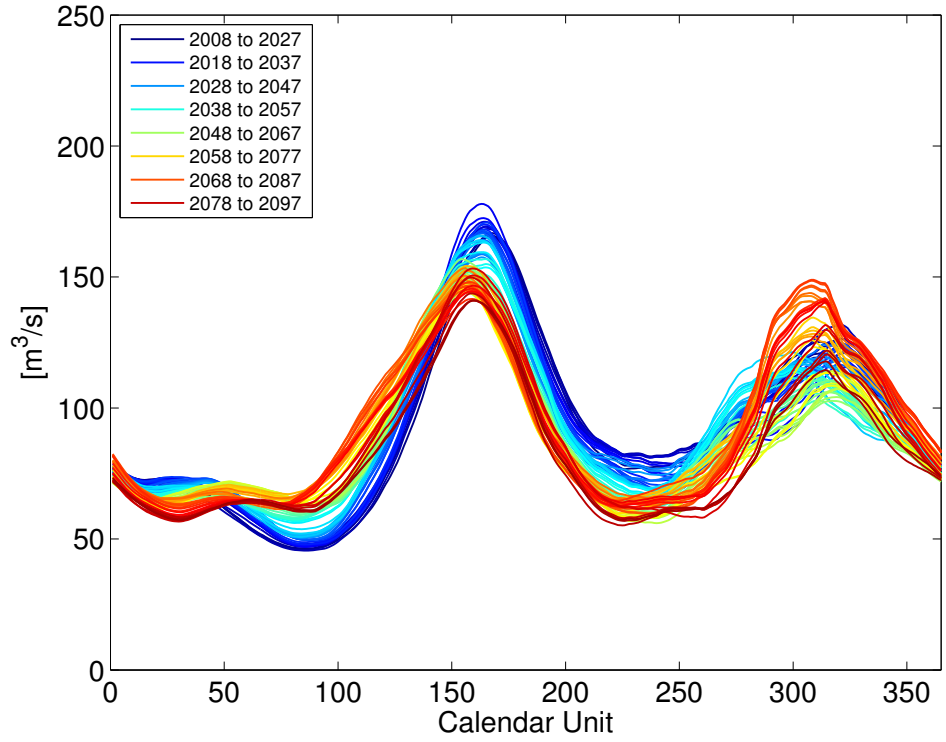


(a) RCP4.5

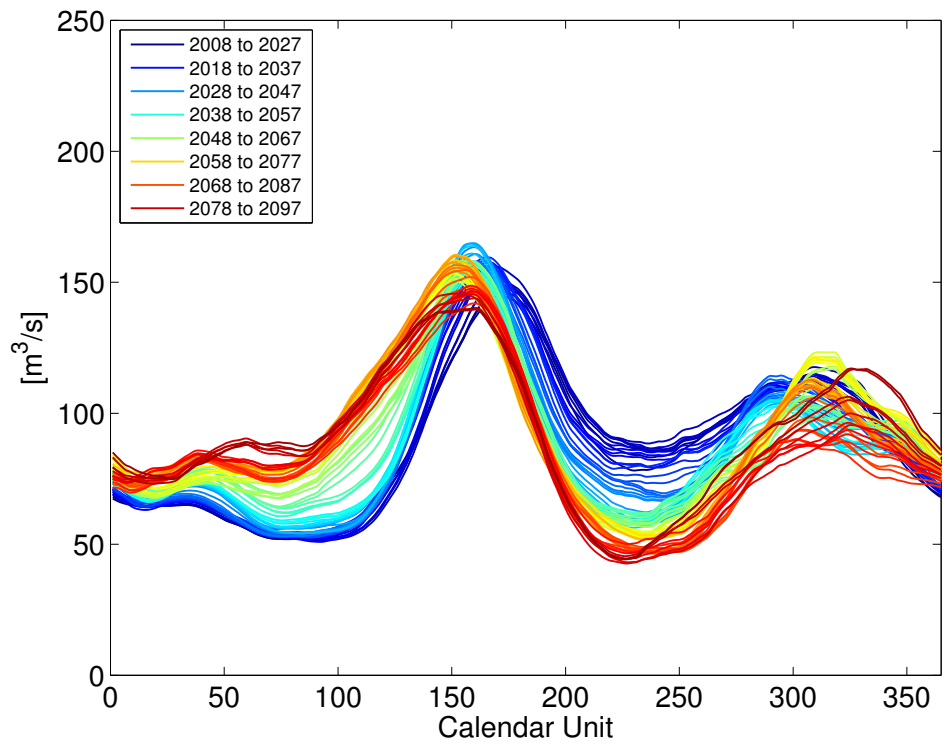


(b) RCP8.5

Figure B.2: RCA₄/NCC, Fuentes streamflow

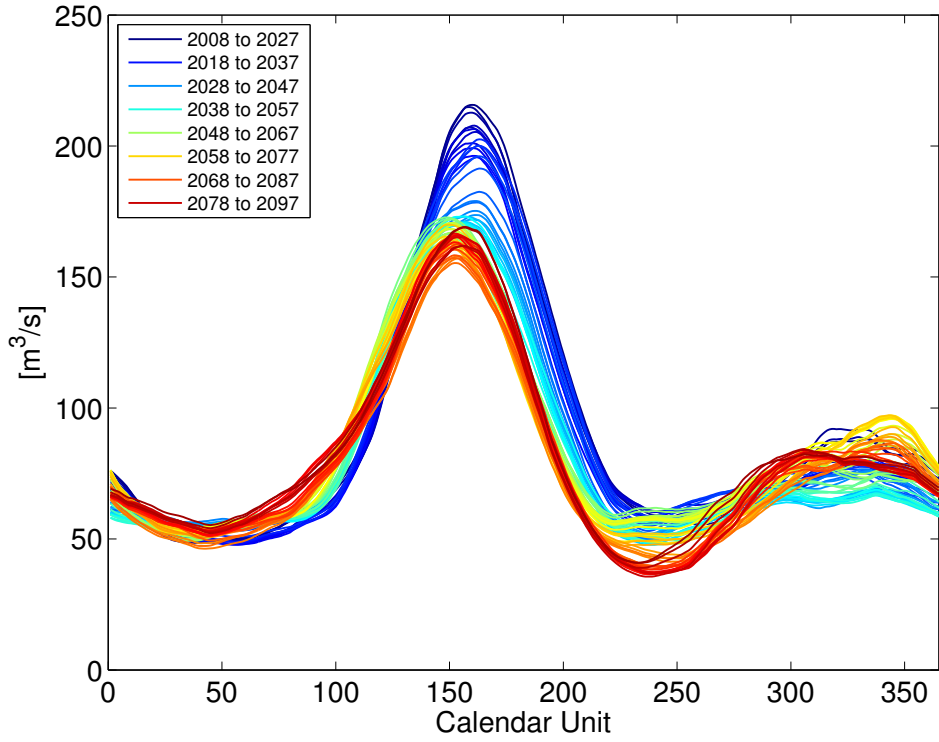


(a) RCP4.5

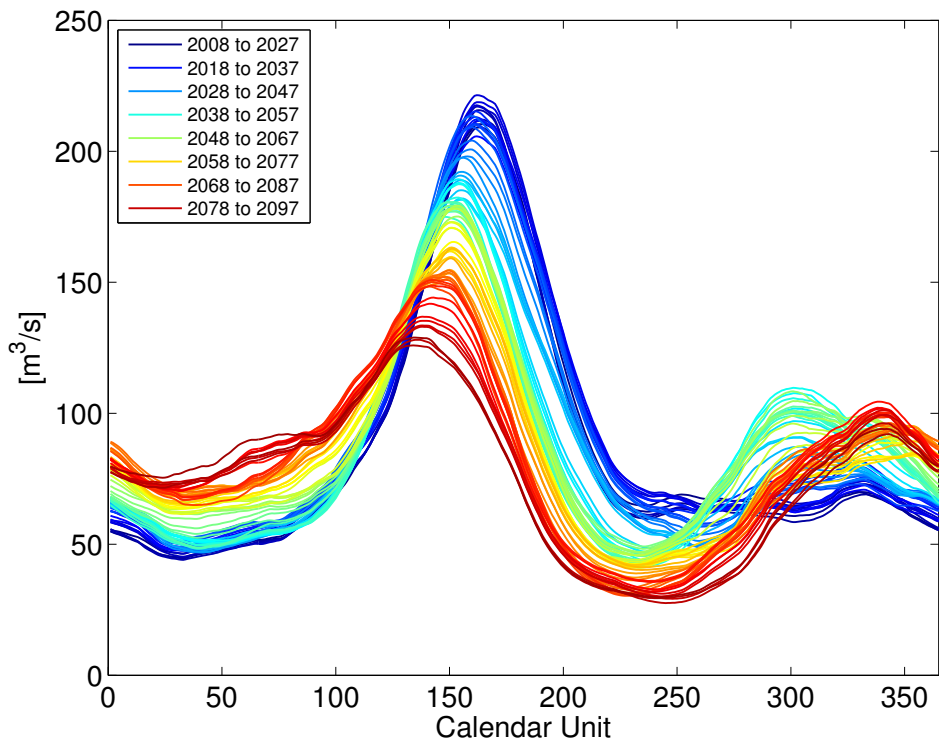


(b) RCP8.5

Figure B.3: RCA₄/NOAA, Fuentes streamflow

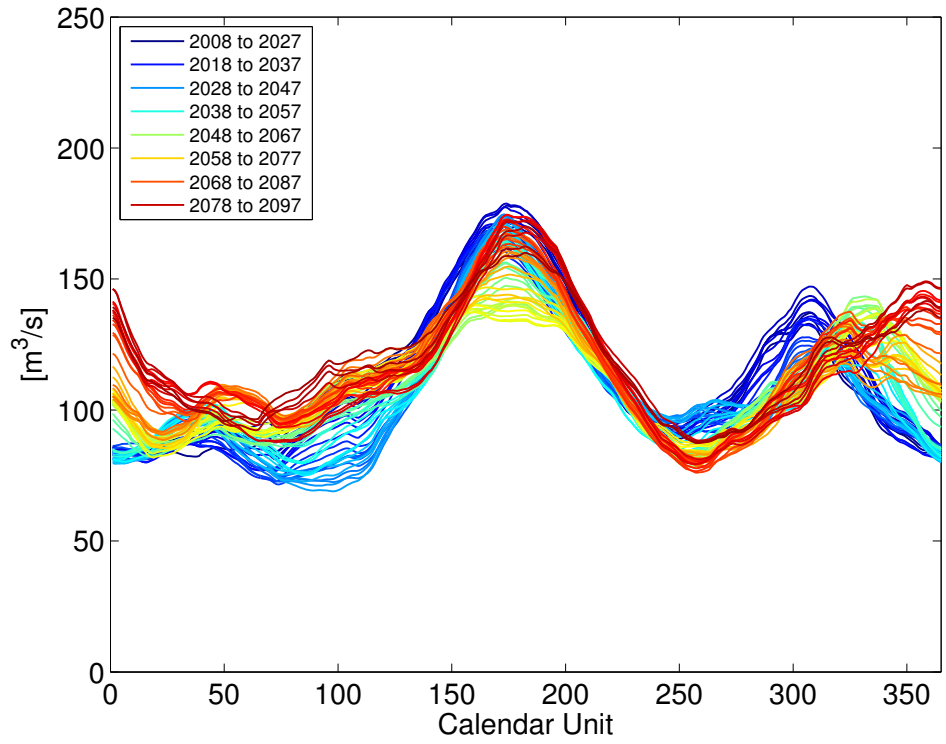


(a) RCP4.5

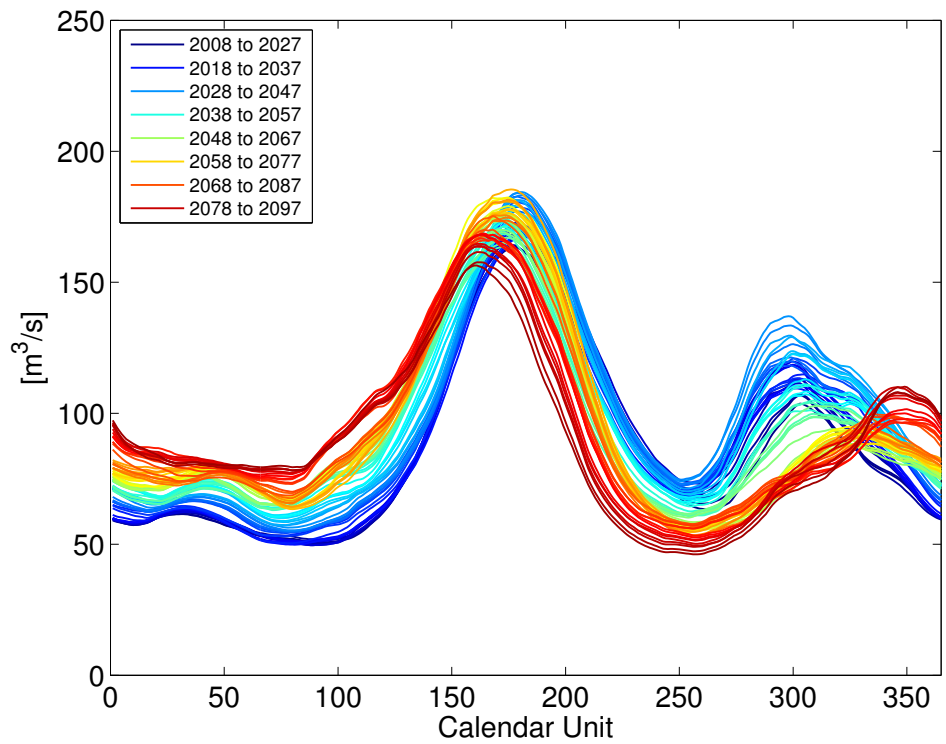


(b) RCP8.5

Figure B.4: RCA4/CCC, Fuentes streamflow

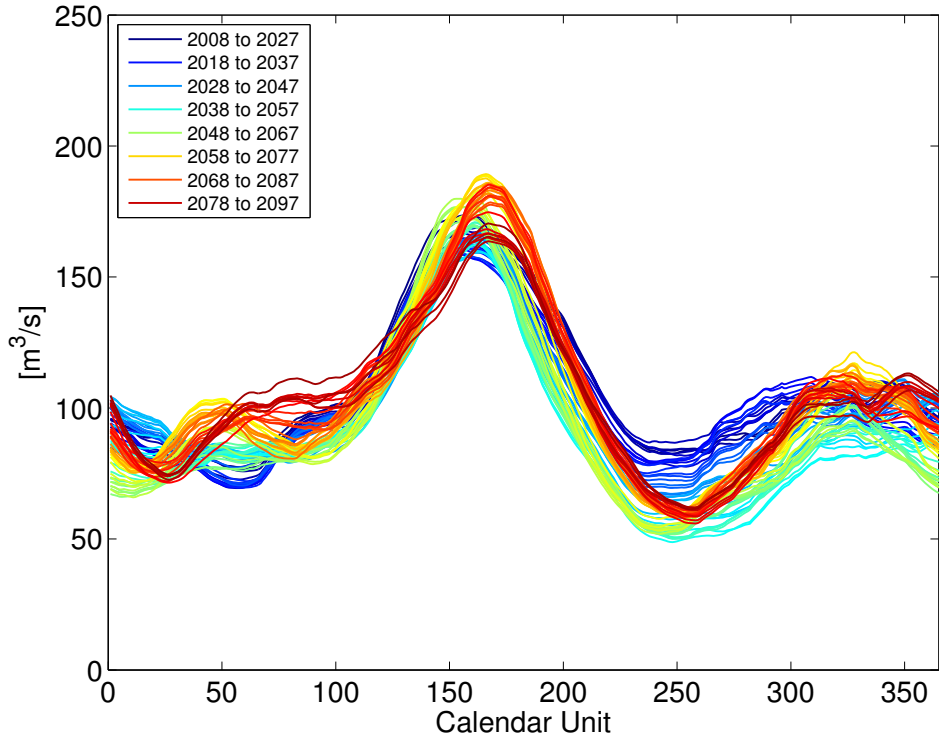


(a) RCP4.5

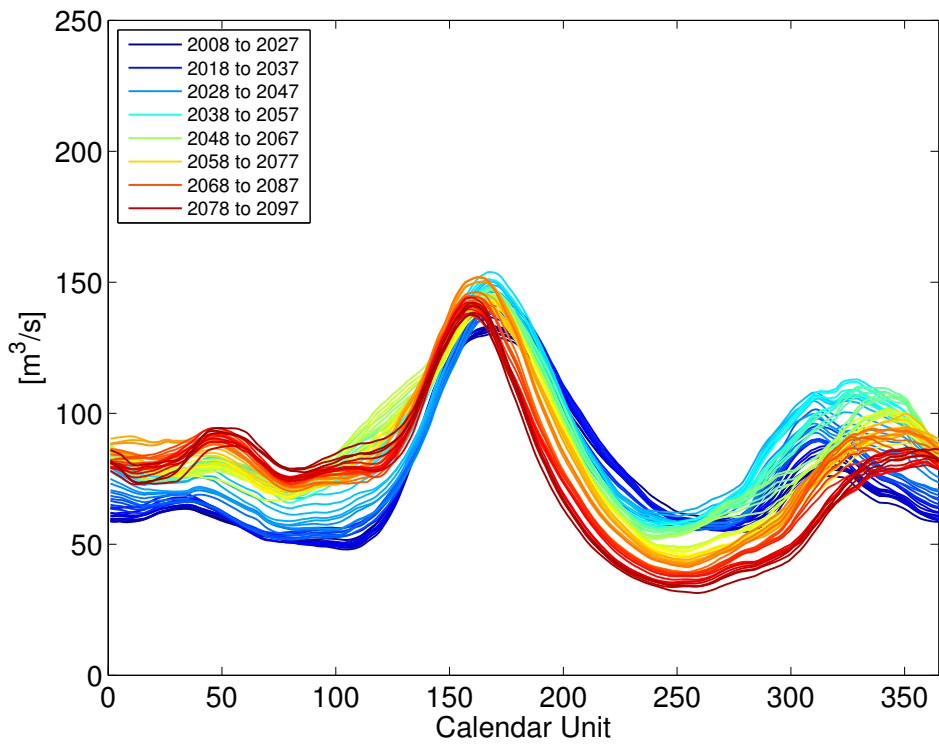


(b) RCP8.5

Figure B.5: RCA₄/CNRM, Fuentes streamflow

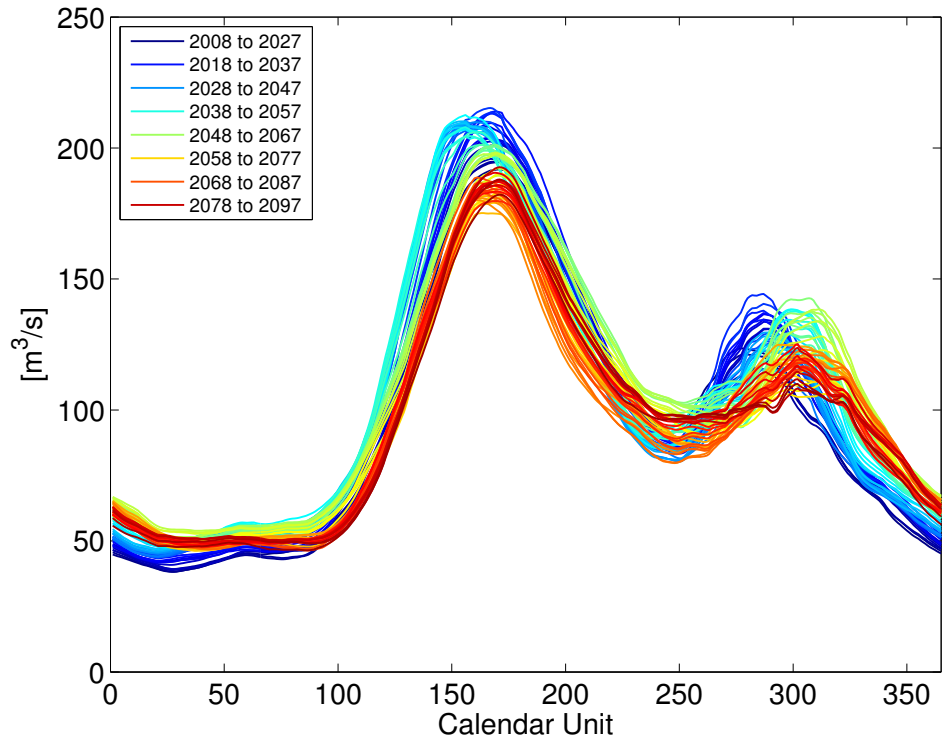


(a) RCP4.5

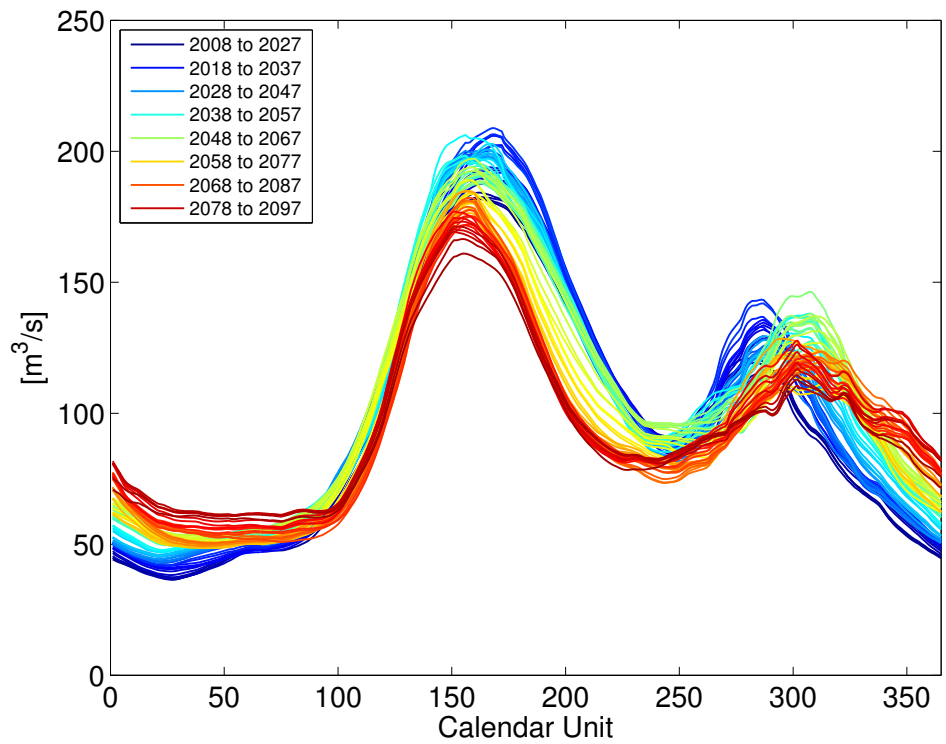


(b) RCP8.5

Figure B.6: RCA4/ICHEC, Fuentes streamflow

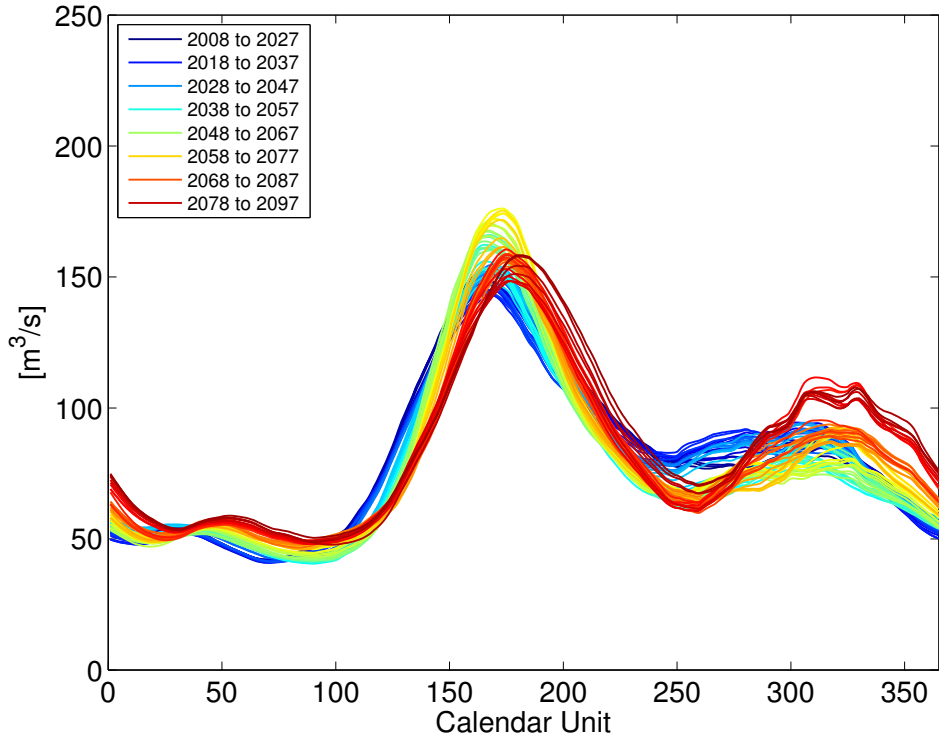


(a) RCP4.5

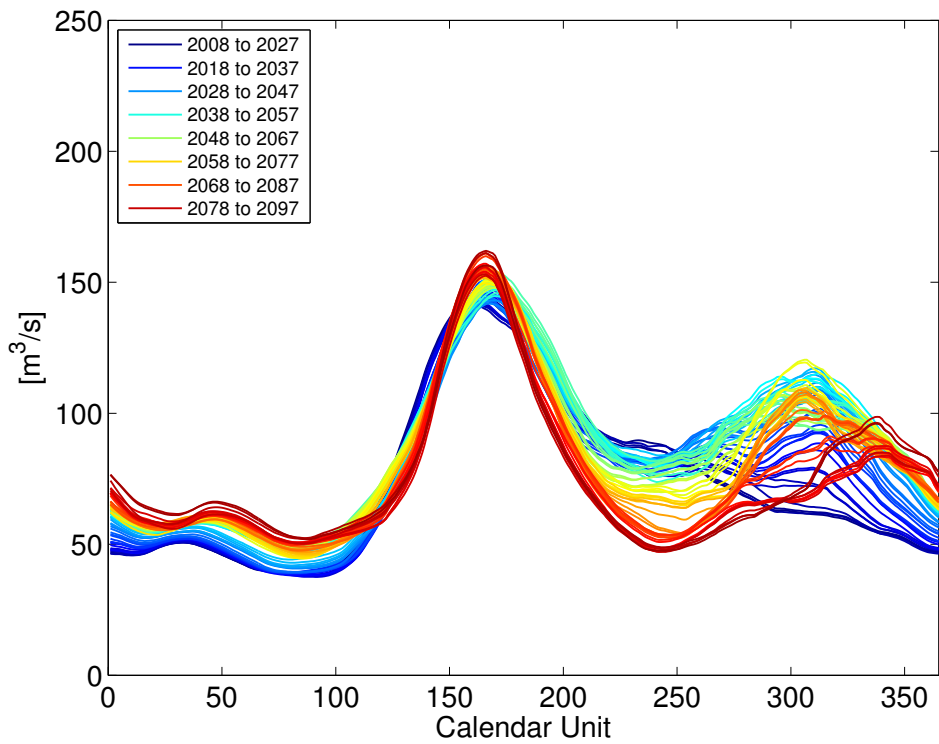


(b) RCP8.5

Figure B.7: HIRHAM/ICHEC, Fuentes streamflow

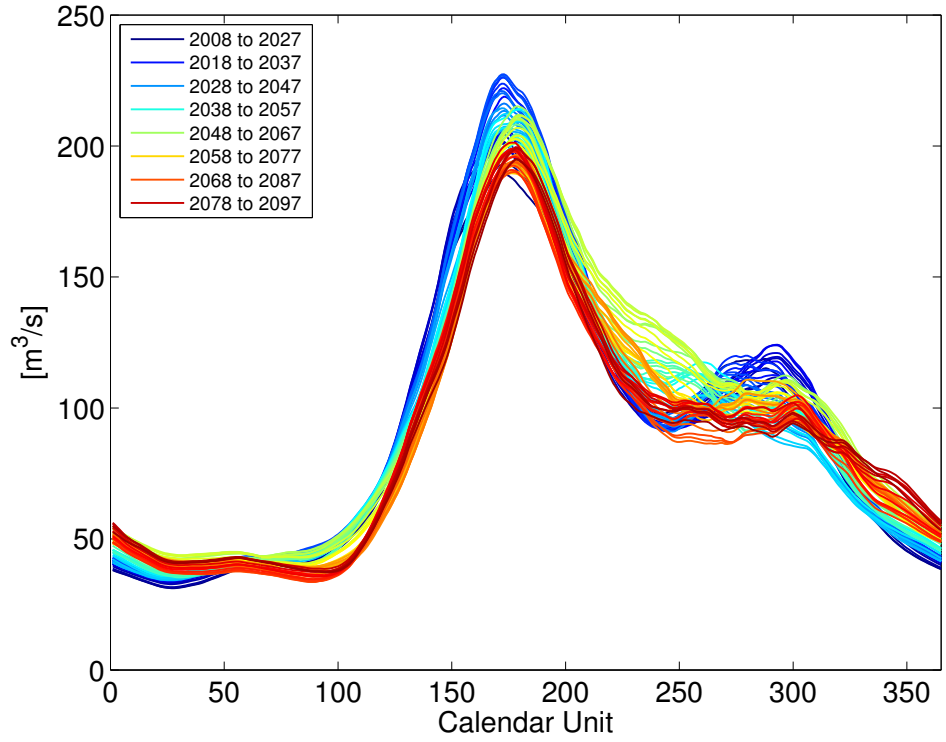


(a) RCP4.5

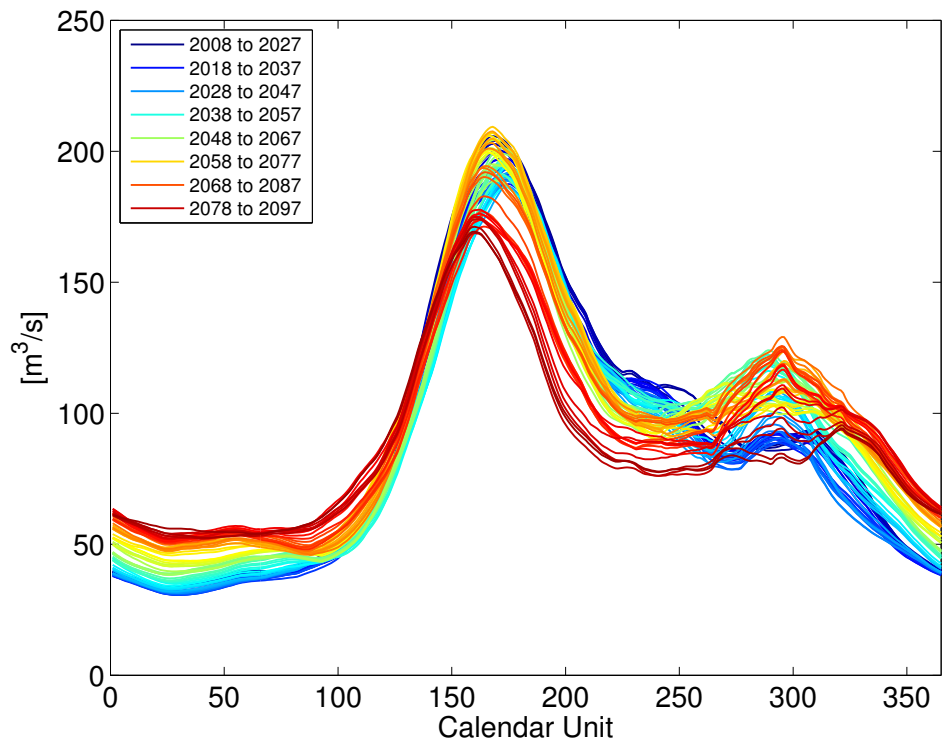


(b) RCP8.5

Figure B.8: CCLM/ICHEC, Fuentes streamflow



(a) RCP4.5



(b) RCP8.5

Figure B.9: CCLM/MPI, Fuentes streamflow